SIMPLE MODELS OF QUANTUM CHAOS: SPECTRUM AND EIGENFUNCTIONS

Felix M. IZRAILEV

Institute of Nuclear Physics, 630090 Novosibirsk, USSR

Contents:

Abstract:

The statistical properties of so-called quantum chaos are considered on the basis of the well-known model of a kicked rotator. Attention is paid mainly to the quasienergy spectrum and the structure of the eigenfunctions in the case of strong classical chaos. The influence of quantum localization effects on the statistics of the spectrum is examined for a model with a finite number of states. Both cases of maximal and of intermediate quantum chaos are studied in dependence on the degree of localization. The possible relation to other physical models is also discussed.

SIMPLE MODELS OF QUANTUM CHAOS: SPECTRUM AND EIGENFUNCTIONS

Felix M. IZRAILEV

Institute of Nuclear Physics, 630090 Novosibirsk, USSR

NORTH-HOLLAND

1. Introduction

In this paper the statistical properties of so-called quantum chaos are discussed on the basis of the relatively simple model of a kicked rotator. This model was for the first time introduced in [CCFI79] as a quantum analog of "the standard mapping" [C79]. The latter is known to be the basic model for the study of the conditions under which dynamical chaos appears; it also serves as a good model for the investigation of the statistical properties of strong chaotic motion. Unlike classical chaos, in the kicked rotator model dynamical chaos was found to have some specific features which are closely related to the quantum nature of the model. In particular, the so-called "quantum suppression of classical chaos" has been discovered in [CCFI79], which has some relevance to Anderson localization in solid state models with disorder [FGP82]. The model of the kicked rotator turned out to be very rich, reflecting many general features of quantum chaos. In fact, like the standard mapping in the classical theory of dynamical chaos, it is the basic model for understanding the concept of quantum chaos.

The aim of this paper is threefold. First, this is an attempt to collect all the most important results on the kicked rotator model, which are distributed now in many journals and preprints, some of them not easily available. Second, it seems to be productive, at present, to discuss the old and new data for the kicked rotator, in the light of the modern understanding of the general problem of quantum chaos. Third, since the statistical properties of the quasienergy spectrum and quasienergy functions are not so well studied as those of autonomous systems, this paper may be regarded as a review of the main results and problems of quantum chaos in its application to the spectral statistics and the eigenfunction structure of periodically driven systems (see also [CM89]). Also, new results are presented which may have relevance to more realistic models, in particular, to solid state models.

As a result, the present paper is not a review of general problems of quantum chaos and can be regarded only as a supplement to the known books and reviews. To study the current state of quantum chaos theory, the reader is referred to the literature given in the text. Recently, a number of very good reviews have appeared on this subject (see, e.g., [E88] and [E88a]). Also, the reviews [CIS81, CIS88] may be useful for understanding the concept of the quantum suppression of classical chaos. The application to the specific problem of the microwave ionization of hydrogen atoms is thoroughly discussed in [DKS83, CCGS87, CGS88]. There are also reviews on the applications of quantum chaos in other fields (see, e.g., [BG84, BW88] and references in [E88a, E88]). The best collection of references on the subject of quantum chaos, together with its different applications, is contained in [E88].

2. Quantum chaos in the kicked rotator model

2.1. Classical model: standard mapping

Let us first consider the classical counterpart of our main model and discuss briefly its properties. The classical model is represented by the Hamiltonian

$$H = p^2/2I + \varepsilon_0 \cos \theta \, \delta_T(t) , \tag{2.1.1}$$

which describes a pendulum in a kicked gravitational field. Here p is the angular momentum (action), θ is the angular displacement (phase), I is the moment of inertia of the pendulum and ε_0 is the kick

strength (perturbation). In what follows we use the dimensionless variable $I = 1$. The time dependence of the external field in (2.1.1) is given by a periodic delta function,

$$\delta_T(t) \equiv \sum_{\tilde{i}=-\infty}^{\infty} \delta(t - \tilde{i}T) ,$$

(2.1.2)

with T being the period of the kicks. Such a form of the perturbation allows us to go from the differential equations of motion to a mapping, which is much more convenient for numerical analysis. It turns out that in spite of the specific form of the perturbation the model (2.1.1) reveals the general properties of nonlinear systems with the Hamiltonian

$$H = H_0(p) + V(\theta)f(t) , \quad f(t + T) = f(t) .$$

(2.1.3)

Here H_0 stands for the unperturbed (integrable) part, while the perturbation, generally nonlinear, is periodic in time and has many resonant harmonics with unperturbed motion.

Starting from the Hamiltonian (2.1.1) one can get the equations of motion and then, integrating over one period T it is easy to obtain the mapping for p and θ,

$$p_{\tilde{i}+1} = p_{\tilde{i}} + \varepsilon_0 \sin \theta_{\tilde{i}} , \qquad \theta_{\tilde{i}+1} = \{\theta_{\tilde{i}} + Tp_{\tilde{i}+1}\} ,$$

(2.1.4)

where $p_{\tilde{i}}$ and $\theta_{\tilde{i}}$ are the values of the momentum and of the phase just after the $\tilde{i}$th delta function "kick". Here the brackets indicate that the phase θ is taken modulo 2π. Also, here $\tilde{i}$ is the dimensionless time; in what follows, we often use the same notation t both for the time t and for the normalized time, $\tilde{t} = t/T$. At first glance, the motion of the model (2.1.4) seems to depend on two parameters: kick strength ε_0 and period T (apart from the initial conditions p_0, θ_0). Nevertheless, as can be seen from the rescaling of the momentum p by $P = pT$, only the parameter $K = \varepsilon_0 T$ is essential for the behaviour of the model. Then, in the new variables P and θ we have the so-called "standard mapping" in its standard form (see, e.g., [C79, LL83]),

$$P_{t+1} = P_t + K \sin \theta_t , \qquad \theta_{t+1} = \{\theta_t + P_{t+1}\} ,$$

(2.1.5)

which is also known as the "Chirikov–Taylor mapping".

Having a long history (see [T69, F72, C79]), the mapping (2.1.5) is a cornerstone of the modern physical theory of dynamical chaos. Moreover, it is used as a test model for polishing the new approaches in the description of the transition from quasiperiodic to chaotic motion as well as the statistical properties of fully developed chaos. It should be noted that, in spite of its apparent simple form, the standard mapping can be used as a good model of some real physical systems. For example, it describes the motion of a charged particle in a magnetic trap (see, e.g., [C79]). But most important is that the standard mapping can be used to describe (for small K) the motion of a generic Hamiltonian system in the case where only one isolated nonlinear resonance can be taken into account while other resonances are regarded as a perturbation.

The properties of this mapping have been thoroughly investigated and this was a good reason to start with the study of its quantum analog [CIS81, CCFI79] as the main model for the investigation of the quantum counterpart of classical chaos (see next section).

We now recall the most essential properties of the model (2.1.5) (see [C79, LL83]). As far as the

perturbation in (2.1.5) is periodic in θ, the phase space of the system is a cylinder, therefore allowing an unbounded motion in momentum P. In addition, it turns out that the phase space is also periodic in P with period 2π. The latter property simplifies very much the investigation and makes it possible to restrict oneself to studying the structure of the phase space on the square $0 \le P$, $\theta < 2\pi$. For this reason the model (2.1.5) sometimes is called "uniform model".

Without perturbation ($K = 0$) all trajectories of the motion can be represented in phase space by the straight lines $P = \text{const.}$ (which are so-called "unperturbed tori" in the terminology of KAM theory [K54, A63, M62]; see also [AA68]). With increasing perturbation ($K > 0$) some of these lines start to bend; meanwhile those trajectories which correspond to special (resonant) values of P turn out to be destroyed. At the same time, new invariant curves appear which correspond to nonlinear resonances of different harmonics of the perturbation. In parallel, in the vicinity of these resonances small regions arise with a new type of motion, so-called "stochastic" or "chaotic" motion. Nevertheless, for a sufficiently small perturbation, all chaotic trajectories are restricted in momentum P by the non-destroyed (nonresonant) tori. This situation is known as "global stability" of the motion.

Finally, when the perturbation K exceeds some critical value K_{cr}, the last invariant nonresonant curve is destroyed and the motion becomes unbounded in momentum (if the initial conditions P_0, θ_0 do not belong to the remnants of resonant tori or, in other words, if the starting point of this trjectory is not inside a region with quasiperiodic motion). There are different approaches to find out this critical value (see [C79, LL83]); according to [G79] $K_{cr} \approx 0.9716$.

With further increase of $K > K_{cr}$ the regions of phase space with regular quasiperiodic motion ("stable regions") decrease and become too small to take care of their influence on the motion of the system. Indeed, it has been estimated [CI73, C79] that the total area of these regions is exponentially small for generic values of $K \gg 1$. Therefore, the motion of the system for $K \gg 1$ turns out to be, practically, fully chaotic and reveals strong statistical properties such as local instability, mixing, fast decay of the correlations and has a positive Kolmogorov–Sinai entropy (see the reviews [C79, LL83, Z85, SUZ89]). Numerical data show [C79] that even for a not very large value $K \gtrsim 5$ our model (2.1.5) has all these properties and can be treated as completely chaotic.

One of the properties of our model (2.1.5), the most important in view of future comparison with the quantum model, is the diffusive character of the motion in momentum P. This diffusion takes place both for individual trajectories and for sets of trajectories initially localized in some region of phase space. The time dependence of the momentum (in the number of kicks) can be expressed from (2.1.5) as

$$(P_t - P_0)^2 = K^2 \sum_{j,m}^{t-1} (\sin \theta_j \sin \theta_m) , \qquad (2.1.6)$$

where θ_j, θ_m are the phases taken at different times. It is seen that in the case of fast decay of correlations between these phases the increase of the momentum is of a diffusive form. Indeed, numerical data give excellent agreement with a diffusion law for $K \gg 1$. As an example we can take a large number of trajectories with initial momentum $P_0 = 0$ and phases θ_0 uniformly distributed in $(0, 2\pi)$. Then, the mean square of the momentum, averaged over all trajectories, grows linearly in time,

$$\langle P_t^2 \rangle \approx \tfrac{1}{2} K^2 \tilde{t} . \qquad (2.1.7)$$

The same result appears when the average is performed over many sections of the individual trajectory

(normalizing P to zero at the beginning of each segment). It was also numerically found that the momentum distribution itself has a time-dependent Gaussian form

$$f(P) = \frac{1}{K\sqrt{\pi \tilde{t}}} \exp(-P^2/K^2\tilde{t}) , \tag{2.1.8}$$

as would be expected from the central limit theorem provided the phases θ_j, θ_m in (2.1.6) are regarded as statistically independent.

The diffusion coefficient $D_{cl}(K)$ for the model (2.1.5) was found to be an oscillating function of K for $K > 4.5$ (with decreasing amplitude of the oscillation for $K \gg 1$, see [RW80, RRW81]). In the case of K slightly above the critical value $(K - K_{cr} \ll 1)$ another law holds [C79, MMP84, DF85, CS86]. As a result, the combined expression for $D_{cl}(K)$ can be given as

$$D_{cl}(K) \equiv \langle (\Delta P)^2 \rangle / \tilde{t} \approx \begin{cases} \frac{1}{2}K^2\{1 - 2J_2(K)[1 - J_2(K)]\} , & K \ge 4.5 , \\ \\ 0.30(K - K_{cr})^3 , & K_{cr} < K < 4.5 , \end{cases} \tag{2.1.9}$$

where $J_2(K)$ is a Bessel function and the time $\tilde{t}$ is measured in the number of kicks. It turns out that for $K \approx 5$ the diffusion coefficient D_{cl} is close to the limiting $(K \to \infty)$ value $K^2/2$, and this is why in numerical experiments the value $K = 5$ is often used. Correspondingly, for the diffusion in momentum p [see eq. (2.1.4)] we get the coefficient

$$D_p = \langle (\Delta p)^2 \rangle / \tilde{t} = D_{cl} / T^2 , \tag{2.1.10}$$

with $D_p \approx \varepsilon_0^2/2$ for $K \gg 1$. Therefore, the energy growth for our model (2.1.1) in a diffusive regime $(K \gg 1)$ can be approximately represented as

$$\Delta E_{cl}(\tilde{t}) = E_{cl}(\tilde{t}) - E_{cl}(0) \approx \frac{1}{2} D_p \tilde{t} \approx \frac{1}{4} \varepsilon_0^2 \tilde{t} . \tag{2.1.11}$$

2.2. Quantum suppression of classical diffusion

It is now natural to put the question of the influence of quantum effects on the dynamical chaos which appears in the model (2.1.5) under strong $(K \gg 1)$ perturbation. To start with this problem we come back to our original model (2.1.1) and write down its quantum version,

$$\hat{H} = -(\hbar^2/2I)\partial^2/\partial\theta^2 + \varepsilon_0 \cos \theta \, \delta_T(t) , \tag{2.2.1}$$

where $\hbar$ is Planck's constant and ε_0 is the perturbation strength. This model was first introduced in [CCFI79] and still it attracts many researchers. The motion of the quantum kicked rotator is governed by the time-dependent Schrödinger equation,

$$i\hbar \frac{\partial \psi}{\partial t} = -\frac{\hbar^2}{2I} \frac{\partial^2 \psi}{\partial \theta^2} + V(\theta)\delta_T(t)\psi , \quad V(\theta) = \varepsilon_0 \cos \theta , \tag{2.2.2}$$

which is much more difficult to analyse numerically than the classical standard mapping (2.1.4), (2.1.5). Nevertheless, the specific form of the perturbation given by periodic instantaneous kicks, as in the classical case, is used to simplify our investigation by reducing (2.2.2) to a mapping for the wave

function,

$$\psi(\theta, t + T) = \hat{U}\psi(\theta, t) ,$$

$$\hat{U} = \exp\left(i \frac{T\hbar}{4I} \frac{\partial^2}{\partial\theta^2}\right) \exp\left(-i \frac{\varepsilon_0}{\hbar} \cos\theta\right) \exp\left(i \frac{T\hbar}{4I} \frac{\partial^2}{\partial\theta^2}\right) . \qquad (2.2.3)$$

Here the value of the function ψ is determined just in the middle of the rotation, between two successive kicks. Actually, this expression corresponds to the formal solution of the Schrödinger equation (2.2.2) over one period of the perturbation. The evolution operator $\hat{U}$ of the system in one period, thanks to the instant action of the perturbation, can be written as the product of three noncommuting unitary operators, the first of which corresponds to the free rotation during half a period,

$$\hat{G}(\tau/2) = \exp\left(i \frac{\tau}{4} \frac{\partial^2}{\partial\theta^2}\right), \quad \tau \equiv \frac{\hbar T}{I} ; \qquad (2.2.4)$$

the second describes the kick,

$$\hat{B}(k) = \exp(-ik \cos\theta) , \quad k \equiv \varepsilon_0/\hbar , \qquad (2.2.5)$$

and the third one is the same as the first, eq. (2.2.4).

It is seen from (2.2.3) that, unlike the classical model, the behaviour of the quantum model essentially depends on two parameters: k and τ (in the following we put $I = 1$ as in section 2.1). This fact reflects the appearance of a pure quantum parameter, in addition to the classical one, $K = k\tau = \varepsilon_0 T$. As a new independent parameter we can choose, for example, the perturbation strength k, which gives the effective number of unperturbed states covered by one kick of the perturbation (see below). The transition to classical mechanics is described by the limit $k \to \infty$, $\tau \to 0$, $K = \text{const}$.

Since without perturbation ($k = 0$) the Hamiltonian (2.2.1) is time independent, the solution $\psi(\theta, t)$ of (2.2.2) is conveniently represented in the form of an expansion in eigenfunctions (EF) of the angular momentum,

$$\psi(\theta, t) = \frac{1}{\sqrt{2\pi}} \sum_{n=-\infty}^{\infty} A_n(t) e^{in\theta} , \qquad (2.2.6)$$

where the coefficients $A_n(t)$ are essentially the Fourier coefficients of the time-dependent wave function $\psi(\theta, t)$. It is easy to obtain that in the momentum representation the free rotation operator $\hat{G}$ has a diagonal form with matrix elements

$$G_{ll'}(\tau/2) = \exp[i(\tau/4)l^2]\delta_{ll'} . \qquad (2.2.7)$$

Correspondingly, for the matrix elements of the kick operator $\hat{B}$ we have

$$B_{n'm'}(k) = i^{n'-m'}J_{n'-m'}(k) , \qquad (2.2.8)$$

where $J_\nu(k)$ is a Bessel function. Therefore, the total operator $\hat{U}$ in one period T is given by

$$U_{nm} = G_{nn'}(\tau/2)B_{n'm'}(k)G_{m'm}(\tau/2) \, .$$ (2.2.9)

As a result, the mapping for the Fourier coefficients of ψ is

$$A_n(t + T) = \sum_{m=-\infty}^{\infty} U_{nm}A_m(t) = i^n \, e^{i(\tau/4)n^2} \sum_{m=-\infty}^{\infty} i^{-m}J_{n-m}(k) \, e^{i(\tau/4)m^2}A_m(t) \, .$$ (2.2.10)

Therefore, to follow the dynamics of the system (2.2.1) we have to numerically iterate the mapping for a given initial distribution $A_m(0)$. (As for the classical model, in what follows, time is measured in the number of kicks: $t = \tilde{t}T$ with $\tilde{t} = 1, 2, \ldots$ being the number of iterations.)

One of the peculiarities of any numerical experiment with (2.2.10) is the artificial truncation of the unperturbed basis at some finite size $|m| \le N$. One should therefore take into account the possible influence of such a truncation on the final result. For this purpose, we can use the normalization condition for the wave function

$$\sum_{m=-N}^{N} |A_m(t)|^2 \le 1 \, ,$$ (2.2.11)

where the summation is performed over a finite number $2N + 1$ of unperturbed states. It should be noted that there is the additional problem of the correct computation of Bessel functions with large indices $|n - m| \gg 1$ [see (2.2.10)]. On the other hand, the angular momentum basis, in which the matrix elements of the evolution operator are expressed by Bessel functions, has some advantage. Indeed, the values of the Bessel functions decrease very rapidly with increasing difference between indices and argument (for $|n - m| > k$). It means that the unitary matrix U_{nm} has the form of a band matrix with negligible matrix elements outside a band of size $\approx 2k$. Therefore, it is possible to put $U_{nm} = 0$ for off-band elements, say for $|n - m| > 2k$.

There is another numerical approach not connected with the computation of Bessel functions at all. It is even more efficient from the point of view of minimization of computational time. It is related to the specific form of the evolution operator [see (2.2.3)]. More precisely, from (2.2.4) and (2.2.7) it is seen that free rotation has the simplest form in the momentum representation and is represented as a shift of all phases of the Fourier components by the values $\tau l^2/4$. At the same time, the result of a kick is just a phase shift of the function ψ by an amount $k \cos \theta$; therefore, the kick operator (2.2.5) has the simplest (diagonal) form in the phase representation. For this reason it is very convenient to pass from one representation to another using in numerical experiments a subroutine of the Fast Fourier Transform. Such an approach allows a significant reduction of computational time but in this case the normalization of the function ψ turns out to be independent of the number of states and automatically is satisfied. Therefore, the only check of the effect of truncation is to repeat the run with increased size of the basis.

A typical numerical experiment consists of the iterative computation of the wave function components $A_m(t)$ according to (2.2.10) starting from a given initial state $\psi(\theta, 0)$. Then the time dependence of any averaged observable can be found and compared with its classical counterpart. For example, for the energy of our rotator we have

$$E(t) = \sum_{n=-N}^{N} w_n(t)\hbar^2 n^2/2 \, , \quad w_n(t) = |A_n(t)|^2 \, ,$$ (2.2.12)

where $w_n(t)$ is a probability distribution in momentum space after t kicks of the perturbation.

The first numerical data [CCFI79, CIS81] for the model (2.2.1) showed a quite strange behaviour of the rotator. It was expected that for $K \gg 1$ in the deep semiclassical region ($k \gg 1$) the energy growth should correspond to that in the classical model [see (2.1.11)]. For our convenience, in what follows we use a normalized energy, $\tilde{E} \equiv E/\hbar^2$; therefore, for $E(t)$ the expectation is

$$\tilde{E}(t) = \tilde{E}(0) + \tfrac{1}{2}D_n(t)t, \quad D_n \equiv \langle(\Delta n)^2\rangle/t = D_p/\hbar^2, \tag{2.2.13}$$

where D_n describes classical diffusion in unperturbed levels n: $D_n \approx k^2/2 \approx \varepsilon_0^2/2\hbar^2$ for $K \gg 1$. However, it turned out that such a correspondence took place only on some finite time scale t^* after which a considerable deviation was observed from (2.2.13) with an essential decrease of the diffusion rate. A typical example of such behaviour is represented in fig. 1, where for comparison the "theoretical" dependence (2.2.13) is also shown. As an initial condition the state $A_n(0) = \delta_{nn_0}$ with $n_0 = 0$ was taken, which corresponds to the set of classical trajectories with initial momentum $p_0 = \hbar n_0 = 0$ and equally distributed phases $0 \le \theta_0 \le 2\pi$. It was also found that with increasing perturbation k the characteristic time t^* of good correspondence with classical diffusion, eq. (2.2.13), increased for a fixed value of the classical parameter $K = 5$.

Such a remarkable behaviour of the quantum model in the region of strong classical chaos was called "the quantum suppression of classical chaos". This phenomenon for the model (2.2.1) turns out to be typical and does not, in fact, depend on the initial distribution and, therefore, on the shape of the initial wave function. For example, qualitatively the same picture appears when, instead of one unperturbed state, many low states ($|n_0| \lesssim 10$) with random amplitudes A_{n_0} are initially excited (with zero mean momentum $\langle n_0 \rangle = 0$). Also, the result remains qualitatively the same if the centre of the wave packet is shifted in momentum space to large values ($\langle n_0 \rangle = 500, 1000$) while the width of the packet is changed in the range $10 < \Delta n_0 < 200$ [CCFI79, S83]. In all these experiments the total number of levels is quite large, $M = 2N + 1 = 4001$.

On the other hand, it should be pointed out that there must exist special initial states for which diffusion will be strongly suppressed or even be absent just from the very beginning (for $t > 0$). Indeed, those states can be found from the dynamics of the model (2.2.1); namely, if we take as an initial state $\psi(\theta, 0)$, the wave packet $\psi(\theta, t)$ after diffusion has significantly decreased. However, it is clear that these states are exceptional because all components A_n of the function ψ should be strongly correlated to each other. It is hard to imagine how they can be constructed without using the mapping (2.2.10) itself.
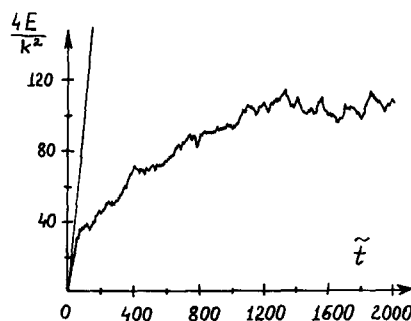

Fig. 1. Dependence of the normalized energy (2.2.13) on the discrete time $\tilde{t} = t/T$ for $k = 20$; $\tau = 0.25$; $K = k\tau = 5$; $\tilde{t}_{max} = 2000$. The straight line corresponds to classical diffusion, $E = \frac{1}{4}k^2\tilde{t}$ (after [CIS81]).

Moreover, since the paper [CCFI79] it has been known that there is a special type of motion in model (2.2.1) for which the energy is infinitely increasing. In this case the asymptotic (for $t \to \infty$) growth of energy is quadratic in time, unlike the linear growth for generic motion corresponding to the diffusive spread of the wave packet in momentum space. This phenomenon was called "quantum resonance" in [CCFI79], since it is caused by pure quantum interference effects and has no relation to the classical behaviour. The detailed analysis of quantum resonance behaviour is given in [IS79, IS80] (see also [CCFI79, CS86a, CS85, DGP84, CFGV86]) and will be discussed in section 2.5. Here we just note that quantum resonance corresponds to special resonant values of the dimensionless period τ,

$$\tau = (4\pi/q)r \,, \tag{2.2.14}$$

where r, q are integers which do not have a common integral factor. At a first glance, this relation can be important also in the general case because any irrational number can be well approximated by the rational ones. Moreover, in any computer all numbers are known to be rational for the reason of finite accuracy. However, as follows from the analysis in [IS79, IS80, CFGV86], for large values of the denominator $q \gg 1$ in (2.2.14) the motion of the model follows the nonresonant behaviour for a very long time, after which resonant behaviour reveals itself. This time of correspondence increases very rapidly with increasing q. Thus, resonant behaviour should be considered as a nongeneric type of behaviour which does not reflect the main properties of quantum systems in the region of classical chaos.

Suppression of the diffusion in energy means that in momentum space the spreading of the wave packet stops. In fig. 2 a typical distribution of w_n after sufficiently large time is shown in the normalized
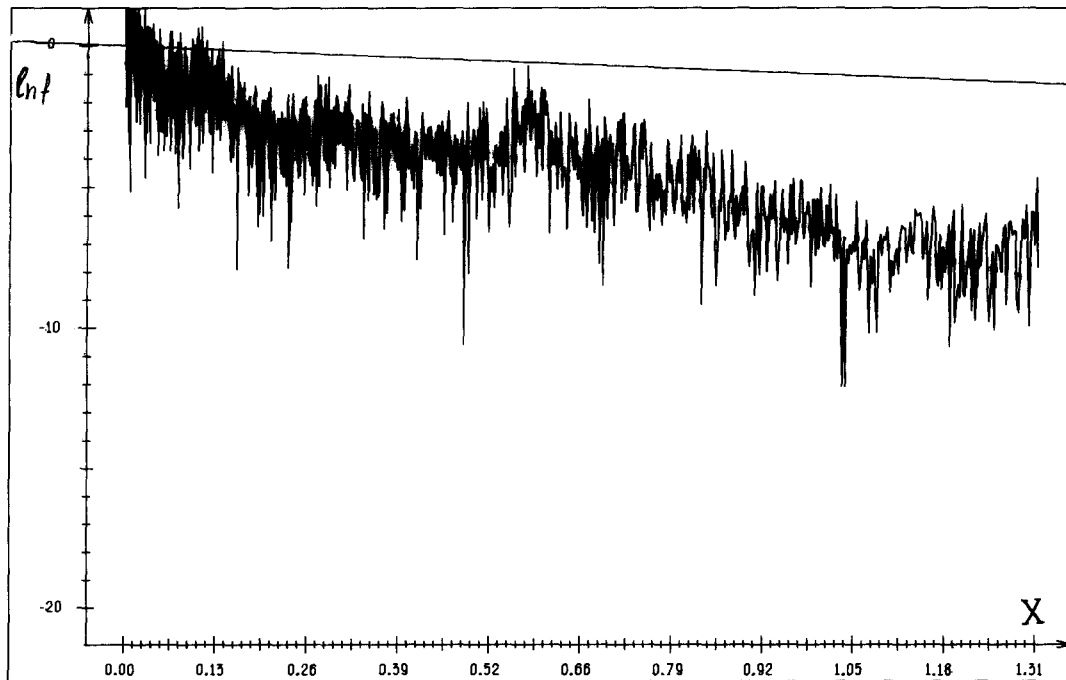

Fig. 2. Distribution of w_n over the unperturbed states in the normalized variables $f(n)$ and X [see (2.2.15)]. The straight line corresponds to the classical distribution $f = \exp(-X)$ (after [CIS81]).

variables

$$f(n) = w_n \sqrt{\pi t}\, k , \qquad X = n^2/k^2 t .$$ (2.2.15)

For comparison the dependence $f = \exp(-X)$, which represents distribution of w_n in the classical model, is also shown. A large difference with the classical results is clearly seen for large values of $|n|$, $|n| \gg 1$, reflecting the suppression of the diffusion in momentum space.

The characteristic time t^*, which gives the time of correspondence between classical and quantum diffusion, is of special interest because it can be used to connect classical and quantum characteristics of the model. It was found numerically [CIS81, S83] that the following approximate law holds for t^*:

$$t^* = Ck^\alpha ,$$ (2.2.16)

with the power $\alpha = 1.5$–2.0. It is quite difficult to establish a more detailed dependence of t^* on the parameters K and k. The main problem is that the definition of t^* itself is quite arbitrary, because the saturation of energy is not sharp. In addition, there are large fluctuations depending on the initial state $\psi(\theta, 0)$. Also, the size of the basis needed for correct numerical experiments grows very fast with the increase of the quantum parameter k. In (2.2.16), t^* was taken as the time t when the deviation of the quantum energy from the classical dependence (2.2.13) exceeds a given value (say, 25% of the classical value). As was shown in [CIS81, S81, S84], the quantum correction terms in the region of classical diffusion grow very fast and need to be taken into account for $t_D \sim k^2$. By assuming this time to be consistent with t^* we have good agreement with numerical data; therefore, one can assume that $\alpha = 2$.

Another interesting question is: how good is the correspondence between quantum and classical motion on the time scale $t < t^*$? As we already said above, detailed numerical experiments [CCFI79, CIS81, S83] have shown very good agreement for the time dependence of the energy as compared with classical diffusion when $K \gg 1$, $k \gg 1$. Moroever, it turns out that the quantum diffusion coefficient D_q has the same oscillations as a function of the classical parameter K as the classical expression (2.1.9). For this reason we will call the time scale

$$t_D \approx k^2 \sim 1/\hbar^2$$ (2.2.17)

the "diffusion scale".

As mentioned above, the smaller the quantum parameter k, the stronger is the suppression of diffusion. As a result, there is some critical value k_{cr} below which diffusion does not exist at all for any large value of the classical parameter $K \gg 1$. In other words, quantum effects can be so strong that they suppress any diffusion from the beginning, $t > 0$. This effect was discussed for the first time in [S76], where the influence of quantum effects in molecules was investigated provided the classical nonlinear resonances overlap and strong stochasticity occurs in the classical limit. It was found that in addition to the classical border of global stability ($K_{cr} \approx 1$), in the quantum model there appears another condition for suppression of the classical motion ("quantum stability border" or "Shuryak's border", see, e.g., [CS86]). To avoid confusion when determining the quantum border of stability, we discuss this problem in more detail taking our model (2.2.1) as a typical example (see also [CS86]).

The nature of the quantum stability border is directly related to the discreteness of the spectrum of the quantum system. Since our model (2.2.1) is time dependent, the perturbed ($k \neq 0$) eigenstates have no definite energy but a quasienergy, provided the perturbation is periodic in time (see below).

Nevertheless, it is possible to analyze the appearance of the quantum stability border in terms of unperturbed ($k = 0$) states. Indeed, if the perturbation parameter k is so small that the matrix elements describing the transition between neighbouring unperturbed states are negligible compared with the energy distance δE between the levels, then one might expect the stability of the motion independently of the value of the classical parameter K. In this case, expression (2.2.10) gives a critical value $k_{cr} \approx 1$, because off-diagonal elements of U_{nm} [see (2.2.10)] for $k \ll 1$ become very small. Nevertheless, the situation is more complicated since we should take into account that the motion of the classical model (2.2.1) depends, in an essential way, on whether the classical parameter K is below or above the critical value $K_{cr} \approx 1$.

The point is that there are two different quantum conditions: one is a condition for applicability of common perturbation theory ("perturbative border"), whereas the other one is a condition for the semiclassical approach to describe quasiperiodic or chaotic classical motion (Shuryak's border [S76]). From this point of view the critical value $k_{cr} \approx 1$ represents both the "perturbative border" and "Shuryak's border" for $K \gg 1$, when in the classical model stochastic diffusion occurs. In this case, for $k \ll 1$, all perturbed eigenstates are very close to unperturbed ones, resulting in a quasiperiodic stable motion of the quantum system. However, these two borders become different for $K \lesssim 1$, when in the classical model the motion is quasiperiodic inside a nonlinear resonance. Then, the number Δn of quantum states involved in the dynamics can be very large even for $k \lesssim 1$ and therefore the semiclassical approach is valid. The estimate for the size Δp (in momentum) of the main resonance is $\Delta p \approx \sqrt{\varepsilon_0 / T}$ for $K \lesssim 1$ (see [C79, LL83]), which gives for the number of unperturbed states

$$\Delta n = \Delta p / \hbar \approx \sqrt{\varepsilon_0 / T \hbar^2} \approx \sqrt{k/\tau} \approx k/\sqrt{K} .$$

It is now clear that $\Delta n \gg 1$ for $k \gg \sqrt{K}$ (or for $\tau \ll k < 1$). In this case the quantum motion will exhibit classical quasiperiodic oscillations even if the quantum parameter is small ($k \ll 1$). In the opposite case, for $k \lesssim \sqrt{K}$, quasiperiodic classical behaviour is completely suppressed by quantum effects because the size Δp of the nonlinear resonance is less than the distance between neighbouring unperturbed levels ($\Delta p = \hbar \Delta n < \hbar$). Therefore, Shuryak's border ($k_{cr} \approx \sqrt{K} \ll 1$) is different from the common perturbative border ($k_{cr} \approx 1$), if $K < 1$.

It should be noted that in the region $\sqrt{K} \lesssim k \lesssim 1$ the semiclassical approach is valid only for the motion inside the resonances. As for the motion in the vicinity of the separatrix, where narrow chaotic regions exist provided the resonances of high orders overlap, again the critical value $k_{cr} \approx 1$ appears as a stability border. The situation here is similar to that for strong classical chaos ($K \gg 1$). Inside the resonances, common perturbation theory fails because perturbed states contain many unperturbed states, despite the fact that the off-diagonal matrix elements U_{nm} are small. Nevertheless, it is possible to find new collective states which are to be close to exact eigenstates and perturbation theory will again be valid (for details see [BK87, BIKV86]). This situation has also been numerically investigated in [BIV87, TI87] for the model of two interacting resonances.

To conclude the discussion about the different types of motion in the quantum model (2.2.1) we summarize our results in fig. 3, where all regions are shown as a function of the classical and quantum parameters, K and k. Here, the border $k \approx 1$ is Shuryak's border for quantum stabilization (regions V, VI and IV in fig. 3) of the classical chaotic motion both for strong chaos ($K \gg 1$) in all of phase space and for weak chaos ($K \lesssim 1$) in small regions of phase space between nonlinear resonances. The two regions IV and VI, discussed above, are separated by the border $K \approx k^2$, which is Shuryak's border for suppression of quasiperiodic classical motion inside the main nonlinear resonance. The three regions IV,
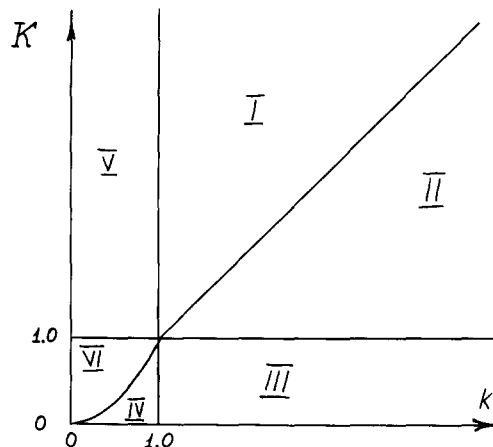
Fig. 3. Different regions of the behaviour of the quantum kicked rotator as a function of the values of the classical (K) and quantum (k) parameters. I: Pure quantum diffusion in the classically chaotic region; II: the region of full correspondence between quantum and classical diffusion (on the finite time scale $t \leq t_D$); III: semiclassical $(k \gg 1)$ region below the classical global stability border $(K < 1)$; IV: the region where the semiclassical approach is valid only inside the main nonlinear resonance; V: quantum stabilization $(k < 1)$ of classical chaotic motion above the global stability border $(K > K_{cr} \approx 1.0)$; VI: quantum stabilization both of the stable motion inside the main resonance and of the motion in the vicinity of the separatrix.

VI and III correspond to classical motion, bounded in momentum space. Above the classical border of global stability, for $K > 1$, there are three regions V and I, II. Unlike region V, where diffusion is absent because of quantum stabilization, for $K > 1$ and $k > 1$ (regions I and II) the motion of the quantum model has a diffusive character. These two regions are separated by the semiclassical border $K \approx k$ (or $\tau \approx 1$). Above this border $(K > k)$ the diffusion is of a pure quantum nature although it can be close to classical diffusion (for details see [S87]). We note that for the motion in the purely quantum region I to be of diffusive character, one only needs the condition $k \gg 1$; otherwise the behaviour has a clear quasiperiodic dependence (see example with $k \approx 2.87$, $\tau \approx 2.53$ in [HH82]). Our main interest is in the semiclassical region II, where diffusion in the quantum model follows all peculiarities of the classical diffusion (2.1.9). We should recall that now we are discussing the generic motion of the model (2.2.1) for irrational values $\tau/4\pi \neq r/q$ and not the specific quantum resonance behaviour, which will be investigated in section 2.5.

To end the discussion of fig. 3 it is worthwhile to add that region III is also of special interest when investigating the motion of the quantum system in the presence of many nonlinear resonances. It is known that in a classical nonlinear system below the global stochasticity border $(K \leq 1$ in our case) the phase space has a hierarchic structure of nondestroyed resonances of different orders (see, e.g., [C79, LL83]). The size of these resonance decreases very rapidly with the increase of the resonance order. Therefore, passing from large resonances to small ones, we again approach a quantum stability border, which is of the same nature as we discussed above for the main resonance (region IV). It means that even in a deep semiclassical region $(k \gg 1)$ quantum effects are essential for the resonances which are so small that they contain only a few unperturbed levels. This fact might be very important when applying classical results to quantum models. For example, some renormalization procedure can be used (see [LL83] and references therein) for models like our classical model (2.1.1), which allows one to pass from resonances of low order to those of the next order. It becomes clear that in this situation Shuryak's border breaks down this renormalization for any large value of the quantum (or

semiclassical) parameter $k \gg 1$. There are a number of papers where this problem is investigated (see, e.g., [BIV87, BK87, BIKV86]).

We now turn to the diffusion in region II (see fig. 3), where the quantum motion is remarkably close to the classical diffusion (2.1.9), albeit on a finite scale $t \lesssim t^* \approx k^2$. Such a time restriction turned out to be unexpected, reflecting the extraordinary character of quantum effects. At first glance, there is no contradiction with the known correspondence principle. Indeed, this time t^* goes to infinity when $k \to \infty$ ($\hbar \to 0$) providing the classical limit. However, the situation is much more complicated. Already in [K79] (see also the discussion in [CIS81]) it was pointed out that there is a major difficulty in attempts to describe chaotic motion in quantum systems. It is related to the fact that for autonomous quantum systems with bounded motion the energy spectrum has to be discrete independently of whether the corresponding classical system is integrable or all its integrals of the motion, apart from the total energy, are destroyed. This results in the quasiperiodicity of the wave function as well as of any average. At the same time, it is known that the spectrum of the motion in a classical system changes from discrete to continuous when the motion changes from quasiperiodic to chaotic. According to the modern theory of dynamical chaos, the possibility of chaotic motion is directly related to the continuity of phase space, which allows a classical trajectory to be extremely complicated without any restriction. This causes the so-called "local instability", which means that two initially close trajectories diverge exponentially fast in the phase space of the system. Actually, local instability is the mechanism for the appearance of chaos in a completely deterministic system. The average rate of this exponential instability, known as the "dynamical entropy" h (see, e.g., [CIS81, LL83]) (not to be confused with the thermodynamic entropy) is commonly used as a measure of chaos. Therefore, positiveness, $h > 0$, can be taken as a definition of chaos itself [A68, AJ81].

Coming back to our model (2.2.1) we should note that the system under consideration is not autonomous and therefore the notion of energy for the perturbed states fails. Nevertheless, because the perturbation is periodic in time, one can introduce quasienergies ε [Z66, R66], which are determined by the relation

$$\psi_\varepsilon(\theta, t) = e^{-i\varepsilon t/T}\varphi_\varepsilon(\theta, t), \quad \varphi_\varepsilon(\theta, t + T) = \varphi_\varepsilon(\theta, t),$$ (2.2.18)

where $\varphi_\varepsilon(\theta, t)$ are periodic functions with the same period T. Inserting (2.2.18) in eq. (2.2.3), one can see that $\varphi_\varepsilon(\theta, t)$ are eigenfunctions (EF) of the evolution operator $\hat{U}$ transforming $\psi(\theta, t)$ over one period T. It is also seen that the quasienergies ε are determined modulo 2π and related to the eigenvalues λ of the unitary matrix according to relation

$$\lambda\varphi_\varepsilon(\theta, t) = \hat{U}\varphi_\varepsilon(\theta, t), \quad \lambda = \exp(i\varepsilon).$$ (2.2.19)

Unlike the energy spectrum of autonomous systems, the quasienergy spectrum can be continuous. Therefore, in our case there is no restriction that prevents the motion from being chaotic, in the sense of classical chaos. This is why the model (2.2.1) was chosen in [CCFI79] to examine the possibility of chaos in quantum systems.

It is important to emphasize that the presence of a continuous spectrum does not automatically imply chaos because in our case (2.2.1) phase space is not bounded in momentum p. It was already mentioned above that unbounded growth of the energy in (2.2.1) appears when the quantum resonance condition (2.2.14) is satisfied and is not related to the classical behaviour at all. On the other hand, infinite increase of the energy means that the quasienergy spectrum has to be continuous. As a matter of fact,

in classical mechanics the origin of the continuous spectrum may not necessarily be related to chaos but to the unboundness of the motion. More precisely, for the spectrum to be continuous a distinctive property of the chaotic motion is needed: a border in phase space, which allows mixing of trajectories in some part of phase space. The discussion of the spectral properties of our model (2.2.1) will be continued in section 2.3; for now the only important conclusion is that in the model under consideration the quasienergy spectrum may be continuous, therefore, there is no contradiction in principle with the concept of classical chaos.

Nevertheless, a remarkable property of the model (2.2.1) has been discovered (see [CIS81, CIS88]) which poses a new problem. It was proved in [S81a] that local instability does not exist in the quantum model (2.2.1) either in the purely quantum region I or in the semiclassical region II for any $K \gg 1$, $k \gg 1$. Two questions then arise: (i) What is the mechanism which provides a diffusion similar to the one in the classical model? (ii) Does the correspondence principle hold in the case of classical chaos? To motivate the second question, we discuss the situation in more detail. Since the concept of an individual trajectory is not valid in quantum mechanics, we may expect that local instability, known in classical mechanics to be very important for chaos, has no sense in the quantum description. Therefore, to establish the correspondence between classical and quantum motion we have to deal with average physical quantities, like the energy of the rotator. In classical mechanics the local instability of motion is known to be also related to the behaviour of observables like time-dependent correlations. For example, typical correlations in classical chaotic systems decay in time very rapidly (exponentially, in the case of fully developed chaos) when local instability occurs. On the contrary, for quasiperiodic motion, correlations do not vanish for $t \to 0$. Therefore, we should also expect, in accordance with the classical result, that some other quantities exist which, unlike the energy, are more sensitive, on a time scale $0 < t \lesssim t^*$, to the rate of instability. Indeed, this is the case and numerous data [S81, BZ82, BI88] show nonvanishing residual correlations in quantum models compared with the fast decay of the corresponding classical correlations (see also section 2.4).

Thus, the absence of local instability in quantum models creates a very serious problem in the application of the correspondence principle in the case of classical chaos. The above questions were posed in [CIS81] and a possible explanation was given. The main point to solve this problem was to introduce two different time scales, one of which, the diffusive time t^*, was discussed above. Another scale appears when considering how the wave packet evolves in time depending on whether classical motion is quasiperiodic or chaotic. This shorter time scale was investigated for the first time in [BZ78, BZ78a] (see also [BK83, Z85]), where it was established that in the case of classical chaos wave packets spread in phase θ exponentially fast with time. It was also shown that the rate of this spreading is related to the dynamical entropy h of the classical system (2.1.1) (see also [CIS81]). As a result, the wave packet, modelling a set of classical trajectories with a small size both in momentum p and in phase θ, turns out to be completely spread over all phases $0 \le \theta \le 2\pi$ in a time estimated as

$$t_E \approx \frac{\ln(k/K)}{2 \ln K} \sim \ln(1/\hbar) \,. \tag{2.2.20}$$

It is now clear that for times larger than "the spreading time" t_E the concept of wave packets cannot be used to describe the motion of individual classical particles, since the meaning of the centre of the packet is not clear. Therefore, the fundamental Ehrenfest theorem, which claims that the centre of the wave packet should follow the classical trajectory, is not valid for $t \gtrsim t_E$. Note, this time t_E turns out to be extremely short. For example, for the typical parameters used in numerical experiments with the

model (2.2.1), it corresponds to a few kicks of the perturbation. This estimate can be easily obtained [C79, LL83] with the help of the expression for the dynamical entropy, $h = \ln(K/2)$; thus for $k = 40$, $K \approx 5$ we have $t_E \sim 1$.

As a result, we can see that two different time scales, t_E and t_D, are of importance to describe quantum evolution in a semiclassical region corresponding to classical chaos. Another point of the approach [CIS81] is the statement that the correspondence principle is valid only on the logarithmic time scale (2.2.20), with all the properties of classical chaos appearing in the quantum behaviour. For intermediate times, $t_E \lesssim t \lesssim t^*$, only rough statistical properties like diffusion remain, while quantum interference effects become stronger leading to the suppression of chaos.

This conclusion has also been supported by analytical investigations of the role of quantum corrections to semiclassical variables as a function of time. In particular, quantum corrections in the slightly different model of a periodically kicked nonlinear oscillator [BK83, KS80] were found to increase exponentially fast, resulting in the divergence of the semiclassical series for the average action. At the same time it was shown in [KS80] that exponentially increasing terms in the semiclassical expansion might be effectively summed by a special procedure. Earlier, the idea that the semiclassical description, in spite of exponential growth of terms, can be valid for times larger than the logarithmic time t_E, was used in a different approach [S81], where the expansion is constructed for a semiclassical function ψ. In such an approach another time scale t_D appears when quantum corrections become significant. A more rigorous result is presented in [S84] (see also on this subject [Z81, S81, BZ78, Z85]), where the approach of [KS80] was developed to sum all semiclassical terms for the time dependence of the quantity $\langle p^m \rangle$ in the model of a kicked nonlinear oscillator (here p is action and $m \geq 1$ is an integer).

The final conclusion is that exponentially increasing terms are, indeed, effectively summed after t_E, resulting in the diffusive behaviour of the average momentum on the scale $t_E \lesssim t \lesssim t_D$, while the correlation functions correspond to the classical result only on the small time scale $t \lesssim t_E$. For a more detailed discussion of the relation between diffusion and correlation, see section 2.6.

Thus, complete correspondence in the behaviour of the quantum (2.2.1) and classical (2.1.1) models should be expected only on the shortest time scale $t \lesssim t_E$. Unfortunately, detailed numerical experiments on this time scale are very difficult because of the very fast spreading of wave packets. Recently, however, new data appeared [TI87a] where this time t_E for similar models was increased up to 5–7 kicks using a special choice of the initial state $\psi(\theta, 0)$. The data showed quite good correspondence with the classical result for the exponential time dependence of the distance between the centres of two wave packets before they spread in phase θ.

Now we turn to the question of the diffusion mechanism on the second time scale $t_E \lesssim t \lesssim t_D$, where the quantum diffusion exhibits classical properties, local instability is absent and quantum correlations do not vanish. The answer turns out to be quite unexpected: we are dealing with a very good imitation of chaotic diffusion whereas the motion itself is quasiperiodic. The situation is similar to that occurring in statistical mechanics, which is not related to nonlinearity and local instability (see [B81a] and the discussion in [C86]). The only condition to obtain statistical properties is the existence of the thermodynamic limit when the number of degrees of freedom goes to infinity.

A simple example of such a classical model with a complete set of integrals of the motion was proposed by Bogolyubov in [B70] (see also [C86]) to construct a dynamical system which is described by classical statistical mechanics. This model is represented by N linear oscillators with randomly distributed frequencies and linear couplings. It was rigorously proved in [B70] that in the limit $N \rightarrow \infty$ this model reveals all the properties needed for statistical mechanics. In particular, a continuous

spectrum and relaxation of the distribution function appear. As is seen, the large number of uncorrelated frequencies in the motion is the basis of this classical "pseudochaos". For comparison, in the modern theory of dynamical chaos a large number of frequencies does not result from an increase of the number of degrees of freedom but appears as a result of a complication of the motion itself. As was pointed out, the mechanism of such a complication is just the local instability of the motion. This is why, in contrast to the traditional approach in statistical mechanics, dynamical chaos is also possible in systems with a few degrees of freedom.

Convincing evidence that chaos in the quantum model (2.2.1) is not "true", is given by the remarkable numerical experiment on the reversibility of the motion after a long time of diffusive evolution [S83] (see also [CIS88, CCSG87]). It is well known that in any classical model with chaotic behaviour round-off errors make it impossible to retrace the same trajectory when the motion is reversed. The reason is the local instability which for the classical model (2.1.1) allows one to follow the same trajectory only during a short time (≈ 10 kicks for a round-off level $\sim 10^{-12}$ and a typical value $K = 5$, see [S83, CIS88]). In contrast, in the quantum model (2.2.1) the motion proved to recur to the initial state with an accuracy comparable to the round-off errors in spite of hundreds of unperturbed states excited at the moment t_R when the motion is reversed. This fact implies that when quantum diffusion occurs all phases of the Fourier components are strongly correlated to each other. It is interesting to note that even a quite large random distortion of the phases at time t_R cannot destroy "antidiffusion".

2.3. The principle of quantum localization of classical chaos

As was shown in section 2.2, the correspondence principle does not fail in the case of fully developed classical chaos, but the time t_E of complete correspondence between the classical and quantum dynamics is restricted by the exponential spreading of wave packets and turns out to be extremely small [see (2.2.20)]. Nevertheless, on the second time scale ($t_E \lesssim t \lesssim t_D$) numerous experiments with model (2.2.1) have revealed remarkable agreement with classical predictions for the diffusive energy growth (for $K \gg 1$ and $k \gg 1$, see region II in fig. 3). Here we discuss in more detail the mechanism which provides both the diffusion itself for $t_E \lesssim t \lesssim t_D$ and the appearance of the critical time t_D which restricts this diffusion (see [CIS81, CIS88]).

We proceed here from the experimental fact that diffusion in the quantum model (2.2.1) is completely suppressed as $t \to \infty$. Of course, this fact does not rigorously stem from numerical experiments, which always deal with finite t, but all the data indicate that it seems to be true. Note, that we are not concerned here with the specific case of quantum resonance (2.2.14), which will be discussed separately in section 2.6.

Our approach [CIS81, CIS88] is mainly based on the conclusion that the quasienergy spectrum has to be discrete, resulting from the complete suppression of energy growth. At first glance, there is no real difference in the dynamics of our model whether the spectrum of quasienergies is discrete or continuous. In fact, all quasienergies ε [see (2.2.18) and (2.2.19)] are determined modulo 2π and the spectral density (number of levels per unit interval) happens to be infinite provided that the total number of quasienergies is infinite. Nevertheless, we are interested in the time evolution of some initial state $\psi_0(\theta) \equiv \psi(\theta, 0)$. Therefore, only those quasienergies that are initially excited by this state should be taken into account. It is useful to represent $\psi_0(\theta)$ in terms of perturbed quasienergy eigenfunctions $\varphi_\varepsilon(\theta, t)$ taken at $t = 0$. The main point of the approach [CIS81, CIS88] is that all these EFs are to be localized in the unperturbed ($k = 0$) basis of the momentum representation. In other words, the

coefficients $\varphi_n(\varepsilon, t)$ in the expression

$$\varphi_\varepsilon(\theta, t) = \frac{1}{\sqrt{2\pi}} \sum_n \varphi_n(\varepsilon, t) \, e^{in\theta} \qquad (2.3.1)$$

vanish very rapidly for $|n| \to \infty$. Therefore, each perturbed EF effectively contains a finite number of unperturbed states and, vice versa, each unperturbed state $\exp(in_0\theta)$ can be effectively represented as a superposition of a finite number of perturbed states $\varphi_\varepsilon(\theta, 0)$.

To establish a relation between $A_m(t)$ [see (2.2.6)] and $\varphi_n(\varepsilon, t)$ we write $A_m(t)$ in the form

$$A_m(t) = \sum_\varepsilon A_m(\varepsilon, t) . \qquad (2.3.2)$$

Then, from (2.2.10) one can obtain

$$e^{i\varepsilon}\varphi_n(\varepsilon, t) = \sum_m U_{nm}\varphi_m(\varepsilon, t) , \qquad (2.3.3)$$

$$\varphi_n(\varepsilon, t) = e^{i\varepsilon t/T}A_n(\varepsilon, t) . \qquad (2.3.4)$$

As far as only the values of time $t = \tilde{t}T$ with $\tilde{t} = 0, 1, 2, \ldots$ are of interest to us, we use for simplicity in what follows the notations $\varphi_n(\varepsilon) \equiv \varphi_n(\varepsilon, t)$ and $A_n(\varepsilon) \equiv A_n(\varepsilon, t)$, or φ_n and A_n if it does not lead to confusion.

As a result, we can see that any initial state $\psi_0(\theta)$ containing a finite number of unperturbed states effectively excites some finite number N_ψ of perturbed states φ_ε with different quasienergies ε, if all $\varphi_n(\varepsilon)$ are strongly localized in n. For this reason, the spectrum of quasienergies can be characterized by the average spacing Δ_ψ between a number N_ψ of perturbed states φ_ε, or by the finite density $\rho_0 \approx N_\psi/2\pi$ of these states. This important fact gives a further interesting conclusion: on the time scale $t \lesssim \rho_0$ our model (2.2.1) does not "feel" that the spectrum is discrete. Indeed, the smallest frequency ω_{ij} present in the motion corresponds to the spacing between two close quasienergies $\omega_{ij} \approx \varepsilon_i - \varepsilon_j$; therefore, to resolve this frequency, one needs a time larger than $t \approx 1/\omega_{ij} \sim \rho_0$ kicks. For this reason one can assume that on the time scale

$$t_D \approx \rho_0 \sim N_\psi \qquad (2.3.5)$$

the motion of the quantum model is similar to classical diffusion with the same rate. This allows one to estimate t_D in the following way. According to classical predictions, for $t \lesssim t_D$ the effective number Δn of unperturbed states involved in the dynamics increases with time as

$$\Delta n \approx \sqrt{D_n t} , \qquad (2.3.6)$$

and reaches its maximal value $(\Delta n)_{\text{max}}$ at $t \approx t_D$. On the other hand, this value $(\Delta n)_{\text{max}}$ is approximately of the same order as the total number N_ψ of perturbed states $[(\Delta n)_{\text{max}} \approx N_\psi]$ and is proportional to t_D. Therefore, from (2.3.5) and (2.3.6) we have

$$t_D \sim D_n \sim k^2 , \qquad (2.3.7)$$

which is consistent with numerical data [see (2.2.17) and the discussion in section 2.2].

Another remarkable relation appears when taking into account that N_ψ [or $(\Delta p)_{max}$] determines the effective size l of perturbed EFs in momentum n,

$$l \sim D_n \sim k^2 .$$
(2.3.8)

As a result, such a quantum characteristic as the average localization length l turns out to be directly related to the classical diffusion rate D_n. This conclusion plays an essential role in the understanding of the peculiarities of the quantum motion in the classically chaotic regime.

Typical shapes of quasienergy states $\varphi_n(\varepsilon)$ for a few different quasienergies (QE) ε are shown in figs. 4a, b, where $|\varphi_n(\varepsilon)|^2$ is plotted versus the number n of unperturbed states. Due to parity conservation, $H(\theta) = H(-\theta)$, for the given Hamiltonian (2.2.1), all EFs are even or odd in the phase θ, $\varphi_\varepsilon(\theta) = \pm \varphi_\varepsilon(-\theta)$. Correspondingly, in the momentum representation we have $\varphi_n(\varepsilon) = \pm \varphi_{-n}(\varepsilon)$. This property is clearly seen in fig. 4a. Like 4b, for simplicity, only half of EFs are shown with $n \geq 0$. All these EFs have been numerically found by diagonalization of some finite matrix $\tilde{U}_{nm}$ of size $N = 600$ describing only odd-parity states (see details in section 3.1). It is clear that any rough truncation of the infinite matrix U_{nm} [see (2.2.10)] breaks unitarity and somehow changes all QEs and EFs. In spite of the fact that the matrix $\tilde{U}_{nm}$ has been constructed in a special way, without breaking of unitarity, its EFs are different from those of the infinite matrix U_{nm}. Nevertheless, those EFs of the matrix $\tilde{U}_{nm}$ that are localized far from the edge $|n| = N$ seem to be very close to the exact ones (see FFGP85, FF87]). For this reason, the EFs shown in fig. 4 are expected to represent the exact EFs of our matrix U_{nm}. In this figure the strong (exponential) localization of the EFs as $|n| \to N$ is clearly seen.

There are different ways to determine the localization length l. One way is direct computation from the matrix $\tilde{U}_{nm}$ by its diagonalization, as was shown above. But this method is rather expensive in numerical simulations. In addition, there is a serious restriction in the operations with matrices with very large N. We should remember that the size of these matrices must be much larger than $l \sim k^2$ to have clear exponential tails in the EFs. For this reason in [S86, BFGS86] another approach has been used, which is based on the well-known transfer matrix method of solid states (see, e.g., [LGP82, PS81, MK81, MK83]). As was noted in the previous section, the matrix elements U_{nm} rapidly vanish outside a diagonal band of effective size $\approx 2k$ (for $|n - m| > k$). It means that in (2.3.3), which determines the eigenfunctions $\varphi_n(\varepsilon)$, one can perform the summation over a finite number $\tilde{N} > 2k + 1$ of elements. Then, eq. (2.3.3) can be considered as some new dynamical system ($\tilde{N}$-dimensional mapping) where n plays the role of time. This system can be shown to be of Hamiltonian form and therefore, its dynamics is completely determined by the Lyapunov exponents,

$$\Lambda_j = \lim_{n \to \infty} (\ln |\psi_\varepsilon(n)| / n) .$$

On the other hand, the minimal exponent $\Lambda_{min} > 0$ can be associated with the localization length $l_\infty = \Lambda_{min}^{-1}$ as the inverse rate of exponential decrease of the EFs, $\varphi_n(\varepsilon) \sim \exp(-|n - n_0| / l_\infty)$. Detailed numerical experiments [S86] have shown that the relation

$$l_\infty \approx D_n / 2 \approx D_{cl} / 2\hbar^2 T^2$$
(2.3.9)

is satisfied with an accuracy better than 10%. This expression (2.3.9) was found to be valid in a wide range of the parameters of the model (2.2.1): $5 \leq k \leq 75$, $1.5 \leq K \leq 29$, $T \leq 1$. Hence, this may also be
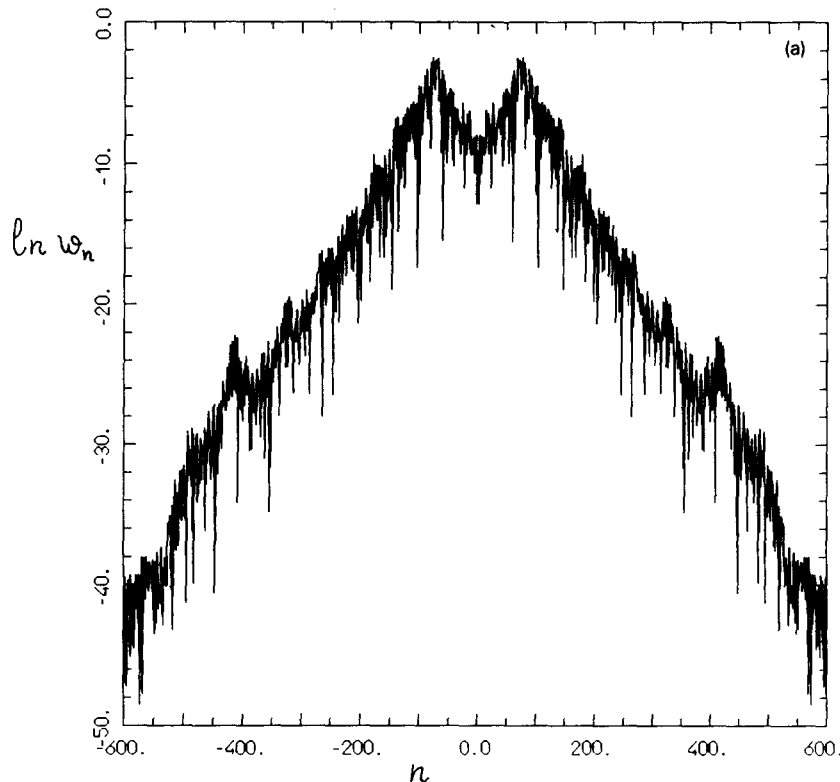
Fig. 4. A few quasienergy states $w_n = |\varphi_n(\varepsilon)|^2$ are shown in the unperturbed $(k = 0)$ basis for $k \approx 9.2$, $K \approx 5.0$, $\tau = 4\pi r/(2N + 1) \approx 0.54$, $N = 600$, $r = 52$. (a) The symmetry $|\varphi_n|^2 = |\varphi_{-n}|^2$ is shown for some EFs; (b) only w_n with $n > 0$ are presented for three EFs (after [CGIS90]).

treated as numerical evidence for the exponential localization of EFs (in the case of irrational values of $\tau/4\pi$). But the most impressive result is that the localization length l_∞ turns out to follow all oscillations in the classical diffusion coefficient D_{cl}, in accordance with (2.1.9) (see details in [S86, CIS81, CIS88]). Moreover, such a good correspondence exists not only in the region of well-developed chaos ($K \gtrsim 5$), when the total area of the islands with quasiperiodic classical motion is negligibly small, but also slightly above the border of global stability ($\Delta K = K - K_{cr} \ll 1$), when the stable component is quite large ($\approx 50\%$, see [C79]). In this region of K the rate of classical diffusion drops by a few orders of magnitude, nevertheless, relation (2.3.9) remains valid.

It should be noted that such a correspondence (2.3.9) between the localization length and the classical diffusion coefficient occurs when l_∞ is much larger than the number of neighbouring unperturbed states covered by one kick ($l \gg \tilde{N} > 2k$). The latter condition is true for $K \gg 1$ but fails in the case of not fully developed classical chaos ($K \gtrsim 1$), if the quantum parameter k is not large enough (see details in [CS86, CIS88]). It is related to the fact that for $K \gtrsim 1$ considerable regions with quasiperiodic motion remain in phase space and the chaotic component has a very complicated structure. Therefore, quantum effects in first instance appear in those regions of momentum p where stochastic layers are narrow and classical diffusion is decreased very much (see discussion in section 2.2 about the influence of Shuryak's border). In contrast, for $K \gg 1$ classical diffusion does not depend on p and turns out to be homogeneous in all infinite momentum space. Detailed analyses [CS86] have shown that the condition for the validity of relation (2.3.9) has the form
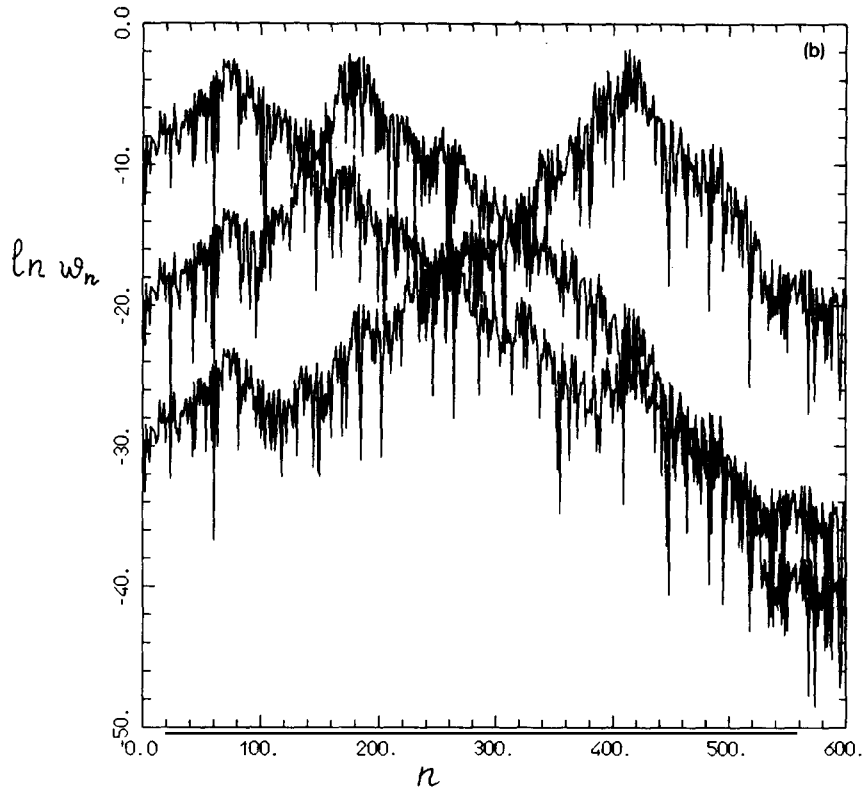
Fig. 4b.

$$k > k_{cr} \approx K^2/D_{cl} \gg 1, \qquad K \gtrsim K_{cl} \approx 1. \tag{2.3.10}$$

The quantum localization of classical chaos, which we are now discussing, concerns the case of the deep semiclassical region $k \gg 1$ for which quantum effects start to suppress classical diffusion after a long time $t \gtrsim t_D \gg t_E$. For this reason, we term this suppression "dynamical localization". Of course, suppression of the diffusion also takes place when $k \lesssim 1$, and sometimes in the literature this is also called localization. Such a case of complete suppression of any classical motion is described by quantum perturbation theory (see discussion in section 2.2) and we will term it "perturbative localization" to distinguish it from dynamical localization.

As we already pointed out, all these results concerning localization of EFs for the model (2.2.1) are not rigorous in the sense that they are based on numerical data. Rigorous mathematical analysis appears to be extremely difficult not only for $k \gg 1$ but even for $k \lesssim 1$. The only analytically proved result [S87a] is the exponential localization of EFs in the perturbative case, when $k \ll 1$.

In the case of inhomogeneous diffusion ($k \lesssim K^2/D_{cl} \ll 1$) numerical data [CS86] indicate a linear dependence on k for the localization length, $l_\infty \sim k$. A similar dependence also appears in another situation, where classical motion is stable ($K < 1$) inside the regions of nonlinear resonances. In both cases the localization length is of the same order ($\sim k$) as the effective number of unperturbed levels covered by one kick of the perturbation. Therefore, it is clear why diffusion has to be strongly suppressed in these cases, unlike the regime where the localization length l_∞ (or the length l_s of localization of the final stationary distribution) is much larger than one excitation step.

Another approach to determine the localization length in numerical experiments has been used in [CS86]. The main idea consists in the detailed investigation of the so-called stationary distribution for the probabilities $w_n(t) = |A_n(t)|^2$ of the components of the wave function [see (2.2.6)] in the unperturbed basis. Here the time t is large enough to ensure that diffusion has stopped and only stationary oscillations of $w_n(t)$ occur, which can be effectively averaged. Then, for some initial state $\psi_0(\theta)$, say, for $\psi_0 = $ const. (when only one unperturbed state with $n_0 = 0$ is excited) we have

$$\overline{w_n(t_s)} = \overline{|A_n(t_s)|^2} = \sum_{\varepsilon_m} \overline{|\varphi_{\varepsilon_m}(0)\varphi_{\varepsilon_m}(n)|^2} , \qquad (2.3.11)$$

where ε_m are quasienergies and averaging is performed over a large time interval $\Delta t \gg 1$ starting from $t = t_s \gg t_D$. In accordance with the expectation that all EFs are exponentially localized, the φ_{ε_m} were assumed in [CS86] to be of the form

$$\varphi_{\varepsilon_m}(n) = \frac{a_{m,n}^{\pm}}{\sqrt{2l}} \, e^{-|n-m|/l} \pm \frac{a_{m,-n}^{\pm}}{\sqrt{2l}} \, e^{-|n+m|/l} , \qquad (2.3.12)$$

where $m \geq 0$ corresponds to the centre of the EF in the momentum representation n and the symmetry $\varphi_{\varepsilon_m}(-n) = \pm\varphi_{\varepsilon_m}(n)$ is taken into account. Expression (2.3.12) corresponds to an exponential decrease as $|n| \to \infty$ but cannot describe the shape of the EF for any n since the amplitudes $a_{m,n}^{\pm}$ and $a_{m,-n}^{\pm}$ are unknown. Then, a very serious question arises about the typical shape of the EFs at the place where they are localized. Since we are mainly interested in large values of $k \gg 1$, the effective size of each EF in n is quite large $(\sim k^2)$. It means that on the scale $|n - m| \lesssim k^2$ large fluctuations of $\varphi_{\varepsilon_m}(n)$ are expected. Numerical data show that this is true and moreover, the size of the EFs turns out to exhibit extremely large fluctuations (see [188, 189]). By the effective size of EFs here we mean some effective number of unperturbed states which contain the main part (say, 95%) of the total probability of an individual EF (see section 4.2). One of the interesting problems is whether the shape of the EFs, obtained by averaging over all fluctuations, can be described by the same exponential form as in the tails, or if there is some "hat" around the centre of the EF which needs a special description (see discussion in section 4.2).

In [CS86] it was suggested that $a_{m,n}^{\pm}$, $a_{m,-n}^{\pm}$ are statistically independent and fluctuate in such a way that $a_{mn} \sim \exp(\xi_{mn})$ with $\langle \xi_{mn} \rangle = 0$. In this case it is possible to obtain an analytical expression for $\bar{w}_n$ [CS86, CIS81, CIS88],

$$\bar{w}_n = \frac{1}{2l_s} \, e^{-2|n|/l_s}(1 + 2|n|/l_s) , \quad \langle n^2 \rangle \equiv l_s^2 , \qquad (2.3.13)$$

where a new localization length l_s is introduced (s emphasizes that it may be different from l_∞). Indeed, detailed numerical experiments [CS86] have led to the relation

$$l_s \approx 2l_\infty \approx D_n , \qquad (2.3.14)$$

which is satisfied to a good accuracy in a wide range of parameters ($k = 5$–120, $\tau \leq 1$, $l_s = 9$–180). The origin of the relatively large difference between l_∞ and l_s was explained in [CS86] by the influence of fluctuations in ξ_{mn}. Nevertheless, the statistical properties of ξ_{mn} are not well understood. In particular, it is important to understand the role of the other Lyapunov exponents rather that only the smallest one related with l_∞. It seems reasonable to expect that all exponents take part in the construction of the core

of the EF, while only one is responsible for the limiting ($|n| \to \infty$) behaviour. It is interesting to note that numerical data [CS86] for $\bar{w}_n$ are in good agreement with the analytical dependence (2.3.13), even though a large range of n was analyzed where $\bar{w}_n$ changes over four orders of magnitudes. Also, a sensitivity of the distribution of the $\bar{w}_n$ to the ratio K^2/D_{cl} [see (2.3.10)] has been found, which confirms the concept of homogeneous diffusion in the quantum model.

It turned out that for $k \ll K^2/D_{cl}$ in the region of incomplete classical chaos ($K \lesssim 1$), the distribution of the $\bar{w}_n$ exhibits a numerical plateau in n instead of a clear exponential dependence. This remarkably reflects inhomogeneous classical diffusion which occurs between remnants of nonlinear resonances of different harmonics. In particular, the most noticeable plateaus in $\bar{w}_n$ are well associated with the regions of classical resonances of low harmonics.

It should be noted that in the approach where the localization length l_s is extracted from the distribution of the $\bar{w}_n$, the initial state $\psi_0(\theta)$ has to be well localized in momentum space. Indeed, if the size of the initial packet in n is comparable with the localization length l_s, then the stationary distribution will essentially depend on this initial state. Unlike this, in the approach where l_∞ is determined from the smallest Lyapunov exponent, the shape of the initial state $\psi_0(\theta)$ is not important since l_∞ is determined as $|n| \to \infty$; therefore, it entirely depends on the parameters K and k only.

A special question is whether in numerical simulations the distribution of the $\bar{w}_n$ can be really taken as stationary because of the finite times t_s. Strictly speaking, diffusion is not completely suppressed at the time t_s, but, as was mentioned above, it has decreased substantially. For example, in [CS86] measurements of the rate of diffusion give $2|\dot{\tilde{E}}|/D_n \lesssim 2 \times 10^{-6}$ at times $t \gtrsim t_s$ (here $\tilde{E} = \langle n^2 \rangle /2$ and $\tilde{E} = E/\hbar^2$). Nevertheless, a rigorous analysis is very desirable.

In the above approach where the distribution (2.3.13) is obtained and numerically examined, some conclusion can be drawn concerning the final energy of the system (as $t \to \infty$) resulting from diffusive excitation [see (2.2.12)],

$$E_\infty \approx \hbar^2 l_s^2/2 \approx D_{cl}^2/2T^4\hbar^4 \approx K^4/8T^4\hbar^2 \approx \varepsilon_0^4/8\hbar^2 . \tag{2.3.15}$$

This result for E_∞ can also be used as an independent check of the validity of the exponential form of localization, eq. (2.3.13) (see details in [CS86]). Note that the expressions obtained for l_s and E_∞ are consistent with the correspondence principle. Indeed, both the localization length l_p in momentum space, $l_p \approx \hbar l_s \approx \hbar D_n \sim \varepsilon_0^2/\hbar$, and $E_\infty \sim \varepsilon^4/\hbar^2$ go to infinity providing the classical limit with un-suppressed diffusion.

Another interesting problem is the diffusion in region I (see fig. 3), where one semiclassical condition is fulfilled ($k \gg 1$) but the other one ($\tau \ll 1$) is violated. In the previous section this region ($T \gtrsim 1$) was treated as purely quantum; however, numerical data show that even in this case there is some similarity to the classical motion. First, for large values of the semiclassical parameter $k \gg 1$ it is natural to expect some sort of diffusion of the energy of the system. According to numerical data, this is true but, unexpectedly, it turned out that the classical expression (2.1.9) for the diffusion coefficient is also valid for pure quantum diffusion when the classical parameter K is rescaled. Namely, the quantum motion can be described by introducing the quantum diffusion coefficient D_q instead of D_{cl} for the energy growth, $E(t) \sim D_q t + E_0$, which is obtained from (2.1.9) by the change $K \to K_q = 2k \sin(\tau/2)$.

This result [CS86, CIS88] was obtained when investigating the role of classical correlations which provide the oscillations in (2.1.9) as a function of K. It was found that the same approach can be applied to relate the diffusion coefficient D_q with quantum correlations. Analytical expressions for the most important correlations $C(t_n) = \langle \sin \theta(t_n) \sin \theta(0) \rangle$ with time shift $t_n = 1, 2, 3, 4$ (in number of

kicks) have been found to be close to those in the classical model with the only difference $K \to K_q$. This allows one to assume that the general expression (2.1.9) could be valid also for the quantum case with K_q replacing K. Numerical simulations [BFGS86] are, in general, consistent with this prediction; however, a more detailed analysis is needed.

Thus, all numerical data give strong evidence that in our model (2.2.1) quantum localization of classical chaos always occurs for any finite $k \gg 1$ and $K > 1$ (apart from the case of quantum resonance, which is exceptional for real physical systems). Then immediately the serious question arises whether this phenomenon is generic for quantum systems of the type (2.1.3) or localization is closely related to some peculiarities of the given model. Indeed, the most essential property of the model (2.2.1) is homogeneity of the phase space in momentum p. It is clear that for real physical systems, like atoms and molecules, the density of states increases with increasing quantum numbers. This means that the classical diffusion coefficient D_{cl} generically depends on the number of excited states n (or, equivalently, on the momentum p). Indeed, unbounded diffusion in classical models occurs when nonlinear resonances overlap and the border of global stability breaks. However, the threshold for overlapping of resonances typically decreases with increasing p, therefore, diffusion increases with n for a fixed perturbation strength.

On the other hand, the main point of our approach is that localization arises when the number of unperturbed states $\Delta p(t) \sim k\sqrt{t}$ [see (2.3.6)] increases more slowly than the diffusion scale, $t_D \sim t$. For this reason, if diffusion also increases in p (therefore, in time) we would expect that $\Delta p(t)$ can grow faster than t, resulting in delocalization. This idea has been discussed for the first time in [CIS81], where some modification of the model (2.2.1) was proposed to investigate the possibility of delocalization. For this, the perturbation strength in (2.2.1) was taken in a form directly dependent on time,

$$k(t) = k_0 t^\alpha ,$$ (2.3.16)

with some parameter α. Then, a rough estimate for $\Delta p(t)$ can be obtained,

$$\Delta p(t) \sim k_0 t^{\alpha + 1/2} ,$$ (2.3.17)

with the conclusion that for $\alpha \geq 1/2$ one would expect unbounded diffusion (delocalization). Of course, in this case we cannot use the concept of quasienergies and eigenfunctions because the perturbation is no longer periodic, hence, the meaning of localization length l_∞ fails. However, the dynamics of the model (energy growth and stationary distribution) is expected to be sensitive to the value of α. The numerical simulation performed in [CIS81] with the model (2.3.16) did not give a clear answer about the critical value of α, because the number of states $2N + 1$ that is needed for a good numerical accuracy increases very rapidly when α increases. Nevertheless, the diffusive time scale t_D was found to increase sharply for $\alpha > 0$ and these numerical data may be treated as qualitative evidence of the possibility of delocalization (the largest value of α attained in [CIS81] was $\alpha \approx 0.35$; below this value clear localization was observed).

In a similar way one can obtain some predictions on the delocalization border for inhomogeneous diffusion [CS86] assuming that

$$D_{cl}(n) = D_1 n^\beta .$$ (2.3.18)

Then, for large enough β, the number of unperturbed levels $\Delta n(t)$ involved in the dynamics by diffusion

can grow faster than t. Estimates have shown [CS86] that this happens for

$$\beta \geq 1, \qquad D_1 > n_0^{1-\beta}, \tag{2.3.19}$$

where n_0 is an initial state. In the case of (2.3.19), delocalization arises with a rate of diffusion that equals, as $t \to \infty$, the classical one. Below this border, when condition (2.3.19) does not hold, the character of the localization is not clear. According to the conjecture presented in [C86], for $\beta < 1$ localization is complete in the sense that $D_n \to 0$ as $t \to \infty$, corresponding to a discrete QE spectrum. In the other case, for $\beta > 1$ and $D_1 < n_0^{1-\beta}$, localization does not occur but the rate of quantum diffusion substantially drops in comparison with classical diffusion.

The ideas discussed in this section were recently applied to the problem of diffusive ionization of hydrogen atoms under a strong periodic microwave perturbation (see the reviews [CCSG87, CGS88] and references therein). It turned out that for the parameters used in the first experiments [BGK77, BK74], the delocalization border was, accidentally, of the same order as the classical chaotic threshold. For this reason earlier numerical simulations [LP78, JLP80] with the corresponding classical model gave good agreement both with analytical classical predictions and experimental data [BGK77, BK74]. It led to the conclusion that in the deep semiclassical region, for highly excited states, the behaviour of the quantum system always follows classical diffusive motion. Therefore, some contradiction appeared in view of the predictions of quantum localization theory.

This problem was solved by a detailed analysis of the conditions under which the quantum suppression of classical diffusion occurs in such a physical model (see, e.g., [CCSG87]). In particular, an analytical expression for the delocalization border was found, with an indication of the range of parameters where classical and quantum predictions give different results. To check these predictions, numerical simulations for the quantum model of hydrogen ionization have been carried out with a clear confirmation of quantum localization (see details in [CCSG87, CGS88]). Using these results, special experiments with highly excited hydrogen atoms in a strong microwave field have recently been performed [BS88, GSMKR88, KMSGLR89, BCGS89]. The data showed the expected suppression of ionization compared with numerical data for the classical model. This is the first experimental evidence of dynamical localization of classical chaos.

Coming back to our model, the kicked rotator, we note that localization of EFs in momentum space is similar to the well-known Anderson localization in solid state physics [A58]. For the first time this analogy was discovered in [FGP82, PGF84], where a transformation was found from (2.2.1) to a so-called tight-binding model (see also [S86]),

$$\phi_n u_n + \sum_r W_r u_{n+r} = E_\varepsilon u_n . \tag{2.3.20}$$

Here the u_n are directly related to the values of the eigenfunctions $\varphi_n(\varepsilon)$ before and after one perturbation kick; W_r is a new perturbation (coupling) between the elements of a one-dimensional discrete chain ($E_\varepsilon \equiv -W_0$) and ϕ_n plays the role of a diagonal potential which depends on some free parameter ξ (for more details see the original papers [FGP82, PGF84] or the reviews [S84a, E88]),

$$\phi_n = \tan \tfrac{1}{2}(\xi - \tfrac{1}{2}n^2\tau) . \tag{2.3.21}$$

Equations of the type (2.3.20) arise in the description of the behaviour of quantum excitation in the solid state (see, e.g., [LGP82]). Mainly, models with interaction of only neighbouring "quasiparticles"

$u_n(r = \pm 1)$ are investigated with the assumption that ϕ_n is a random potential. In this case Anderson localization occurs, which means that all EFs corresponding to the energies E_ε in (2.3.20) are exponentially localized in n. It results in the localization of any initial (localized) state after some time t^* of spreading. For this reason, the diffusion of electrons in such a model will be suppressed by quantum effects.

The sequence ϕ_n seems to have some statistical properties and may be used in the model (2.3.20) instead of a random potential (for irrational values of $\tau/4\pi$). As for the nondiagonal terms, W_r, it is seen that only for $k \sim 1$ this model is close to the Anderson model, since the W_r decrease very rapidly for $|r| \geq k$. Indeed, numerical data [FGP82, PGF84] for not very large $k \gtrsim 1$ have shown the exponential localization of EFs. It also corresponds to the localization of EFs in our model (2.2.1) in momentum space. As far as all these results are based on numerical data, any rigorous statement is very important. In particular, the conclusion [FGP82, PGF84] that the sequence ϕ_n in (2.2.1) is random, appears not to be rigorously true (see next section). From this point of view it is of interest to understand what statistical properties are needed for all EFs to be exponentially localized. In any case, there is a major difference between Anderson localization in the solid state and dynamical localization. Namely, in the latter case there are no random parameters in the model, while for Anderson localization randomness has to be assumed from the beginning. To stress this difference, one should note that the nature of the "pseudorandomness" in dynamical models, as was shown above, is closely related to chaos in the corresponding classical models.

2.4. Relevance of dynamical chaos to the spectral properties of quasienergies

In the previous section the quantum suppression of classical diffusion was explained by the relation between the dynamics and properties of the EFs and the spectrum. It is clear that complete knowledge of the EFs and quasienergies (QE) makes it possible, in principle, to predict all dynamical properties of the model. In particular, we have seen how localization of the diffusion in time is associated with localization of the EFs in momentum space. Moreover, an expression was found connecting two quantities: the localization length l_s of the stationary distribution for the final state $\psi(\theta, t_s)$ when $t_s \gg t_D$, and the localization length l_∞ of EFs in the tails, as $|n| \to \infty$. The approach of establishing any relations between the dynamics and the structure of the EFs and the QE spectrum is very useful for understanding both the quantum dynamics and the statistical properties of spectra and EF structure. Unlike the previous section, where main attention was given to the EFs, here we discuss the properties of the QE spectrum of model (2.2.1), restricting ourselves to the nonresonant case (for irrational values of $\tau/4\pi$).

We have already mentioned that the most important result in the investigation of spectral properties, is the numerically established fact that the QE spectrum of the model under consideration, eq. (2.2.1), should be discrete for any finite $k \gg 1$. This fact rigorously stems from the complete localization of the diffusion, $D_n \to 0$, as $t \to \infty$, and implies the relaxation of any initial distribution $A_n(0)$ to some stationary oscillatory state involving a finite number of unperturbed states. Strictly speaking, in this case the quantum motion is quasiperiodic, being recurrent both for the function ψ and the energy of the system. However, the typical time T_r for such a recurrence is enormously large (see on this subject [P82]). A rough estimate seems to be given by $T_r \sim \exp(N_\psi)$, where $N_\psi \sim l_s \sim k^2$. For this reason, quasiperiodicity of the motion for $k \gg 1$ does, practically, not exist. Nevertheless, for small $k \gtrsim 1$, the quasiperiodic behaviour of the energy is well detected in numerical simulations (see, e.g., [HH82]). The latter case of perturbative localization is not of interest to us in what follows.

The discreteness of the QE spectrum in the case of well-developed classical chaos $(K \gg 1)$ and $(k \gg 1)$ is far from being a trivial fact. Indeed, unlike bounded autonomous systems, where the energy spectrum is rigorously discrete for any values of the dynamical parameters, in our model it can be continuous since momentum space is unbounded. To stress this point, we emphasize that for quantum resonance this is just the case (see section 2.5). Nevertheless, for generic (nonresonant) values of τ, the spectrum is always discrete, which can be treated as an indication of the appearance of dynamical integrals of the motion which restrict diffusion in momentum space. Starting from this relevant fact of discreteness, other important statistical properties of the QE spectrum can be brought to light.

The problem of the statistical properties of spectra has a long history (see the reviews and books [P65, M67, BFFMPW81, BG84]). Up to now, much attention has been paid to autonomous systems such as nuclei, atoms and molecules with a complex energy spectrum. As for QE spectra, investigations have started only recently, through the theoretical and numerical analysis of some models and new experimental data on the behaviour of atoms and molecules in strong periodic electromagnetic fields. The traditional approach to the description of quantum systems with very complex behaviour consists in the use of some statistical assumptions concerning the interaction between numerous states in a given basis. Such an approach is the core of the Wigner–Dyson theory (see, e.g., [P65]), in which all matrix elements of the Hamiltonian are taken as random and statistically independent. Then, classifying systems according to different invariant properties, three classes of ensembles of random matrices have been established: GOE (Gaussian Orthogonal Ensemble) for systems which are time reversal invariant, GUE (Gaussian Unitary Ensemble) for systems with broken time reversal symmetry and GSE (Gaussian Symplectic Ensemble) for systems with an odd number of particles with half-integer spin. Correspondingly, these ensembles are represented by matrices with dfferent symmetries of the matrix elements: GOEs are described by real symmetric random matrices, GUEs by Hermitian random matrices and GSEs by so-called symplectic random matrices (see [P65, M67, BFFMPW81]).

Another version of random matrix theory (RMT) has been extensively developed by Dyson [D62] (see [P65]). Here, instead of real matrices which are assumed to represent statistical properties of real Hamiltonians, random unitary matrices are investigated with different symmetries (in the literature, to distinguish them from real matrices, the notations COE, CUE and CSE are used with the C standing for "circular" ensembles). In Dyson's approach these unitary matrices were not directly related with real systems since even the correspondence with Hamiltonians was not clear.

The basic idea of RMT both for Gaussian and circular ensembles is that RMT can be applied to describe fluctuations in the spectra, which are assumed to be universal, rather than predict specific properties of real physical systems such as the density of states. In other words, in spite of the big difference in spectra, say, of different atoms, the statistical properties do not depend on the local density in the limit of sufficiently strong interaction. The question of the conditions under which RMT can be applied to real physical systems is a different problem, which is outside the scope of RMT. However, even without any approach to decide when RMT can be used in real situations, it is of great interest to determine these universal statistical properties in the framework of RMT and to compare them with experimental data.

There are many predictions of RMT which may be used for comparison with the data (see [P65, M67, BFFMPW81]). Here we shall discuss only a few of them, the best known in the literature. One commonly used quantity is the so-called "level spacing distribution" $P(s)$ for the spacings s between neighbouring levels. Since the density of levels depends, as a rule, on the energy, s is defined as the mean local spacing. Therefore, s is the normalized spacing hereafter. There are two ways to obtain $P(s)$ from an experimental sequence of energies. In the first one just computes the local density $\rho(E)$ of

states by averaging over some part of the spectrum. Then, the total $P(s)$ can be obtained by normalizing s with further summation of $P(s)$ for all segments of the spectrum. In spite of the nonrigorous procedure for finding the local density, this procedure works quite well and is often used.

Another approach is related to the so-called "unfolding" of the whole spectrum under consideration (see, e.g., details in [BG84]). As a result of such unfolding, a new spectrum with a constant local density is constructed which contains the same fluctuations as the given spectrum. In our case of QE spectrum, all quasienergies are located on the unit circle; therefore, the problem of unfolding does not exist since the density of levels has to be constant. This simplifies the numerical investigation of the QE spectrum.

One of the most important results of RMT is the prediction of the form of $P(s)$. The analytical derivation of $P(s)$ turned out to be extremely difficult (see [P65, M67]) and rigorous analytical expressions are known only for the limiting cases of small, $s \ll 1$, and large, $s \gg 1$, spacings. Nevertheless, it was shown that the approximate formula suggested earlier (the so-called "Wigner surmise", see [P65]),

$$P(s) = As^{\beta} e^{-Bs^2} , \qquad (2.4.1)$$

is very close to the exact one obtained numerically in the framework of RMT with use of a special method by Mehta (see [P65, M67] and discussion in section 4.1). In (2.4.1) the coefficients A and B are normalization parameters determined by the conditions

$$\int_0^\infty P(s)\, ds = 1 , \qquad \int_0^\infty sP(s)\, ds = 1 , \qquad (2.4.2)$$

and β is a parameter connected with the symmetry of the random matrices: $\beta = 1$, 2 and 4 for GOE, GUE and GSE, respectively (or, for COE, CUE and CSE, in case of unitary matrices). The parameter β, which is known as the "repulsion parameter", characterizes the degree of repulsion of nearby levels and is of great importance in describing the properties of spectra. The appearance of repulsion of energy levels for complex quantum systems has been discussed earlier than RMT (see, e.g., [LS55]). The physical explanation of the repulsion is based on the fact that coincidence of two levels (degeneracy) is highly unlikely for levels with the same symmetry. For this reason, in the case of very complex systems, it is natural to expect that all quantum numbers corresponding to the symmetries are destroyed, resulting in a nondegeneracy of the levels. To our knowledge, the first experimental data where the repulsion of levels has been clearly seen, were reported in [G39] (see also [GP57]) for nuclear spectra.

A more detailed comparison of experimental data for $P(s)$ with (2.4.1) has been made in [RP60, CG83] for complex atoms and in [HPB82] for heavy nuclei (see also references in [BG84]). In general, the dependence (2.4.1) is better confirmed by the data for nuclei than for atoms where statistical properties seem not to be so strong (see, e.g., [C85]). It is interesting to note that in investigations of experimental data, many sequences of energy levels for different nuclei (or atoms) have been summed independently in the spirit of Wigner–Dyson's conjecture about the universality of fluctuations. Also, when some quantum numbers are not destroyed, the sequences with fixed numbers can be treated as independent. Recently, some experimental data have appeared for molecules (see, e.g., [HKC83, AFIIK84] and references in [BG84]) and for hydrogen in a strong magnetic field [DG86, WF86, WF87]

where qualitative agreement with (2.4.1) has been observed. However, although they give strong evidence for level repulsion, all these experimental data cannot be used for a detailed comparison with the analytical prediction (2.4.1), because of insufficient statistical significance of the data.

Independently of the development of RMT, the problem of finding distinctive properties of quantum spectra for classically chaotic systems has been under consideration since the late 1970s (see, e.g., references in [E88a]). A very stimulating idea for distinguishing classically chaotic systems from integrable ones in terms of the properties of the energy spectrum, was Percival's conjecture about the sensitivity of levels to a small perturbation, depending on the character of the classical motion. As a quantity for testing the level sensitivity the second derivative of the energy with respect to the perturbation strength has been suggested in [P73]. Leaving this very interesting problem out of the discussion (see, e.g., the review [E88a]), we would like to note that the statement about strong repulsion of the levels for classically chaotic motion is inherent to this approach.

At a late stage came the understanding of the similarity of the level spacing distribution $P(s)$ for quantum dynamical systems exhibiting strong chaotic properties in the classical limit, to that known in RMT, eq. (2.4.1) [MK79, CVG80, B81] (see also [ZF73, Z77, Z81], where $P(s)$ for quantum chaotic systems as a function of the classical entropy has been investigated). This understanding has led to extensive numerical simulations with two famous quantum models which are known to be chaotic in classical mechanics. The first model is the so-called "stadium" (see [MK79, CVG80, BGS84a]) for which classical chaotic properties have been analytically proved [B74, B79]. The second model is known as the "Sinai billiard" [S70] which also has strong chaotic properties. The best correspondence with the RMT prediction (2.4.1) has been found with the Sinai billiard [BGS84], for which about 740 energy levels were analysed (see also earlier results [B81]). Up to now, this result seems to provide the best quantitative agreement for autonomous dynamical systems with (2.4.1) according to the χ^2 approach (for other examples see references in the reviews [BG84, E88, E88a]). The use of the χ^2 test is quite important for our purpose since it gives a statistical significance to the final statement concerning the correspondence of numerical data with theoretical predictions.

To summarize the above discussion, one may conclude that quantum chaos has a close relation to RMT, and it is our purpose to analyse this correspondence in more detail (see further). We now turn to our model and ask the question: what is $P(s)$ for the QE spectrum in the case of classical chaos ($K \gg 1$) and the semiclassical condition $k \gg 1$? From the point of view of previous numerical experiments with autonomous systems (stadium, Sinai billiard etc.) we may expect that the spacing distribution $P(s)$ should be close to the form (2.4.1) or, at least, exhibit some sort of repulsion. On the other hand, if one proceeds from the analogy with the solid state model (2.3.20), one can foresee a completely different result. Indeed, for the one-dimensional Anderson model the dependence $P(s)$ is known to be of Poissonian form,

$$P(s) \sim e^{-s}. \tag{2.4.3}$$

This rigorous result [M81] is closely related to the exponential localization of EFs, which occurs for any weak diagonal disorder. Of course, our model (2.2.1) is not completely analogous to an Anderson model. Moreover, for large k, $k \gg 1$ we have a strong difference, since the parameter k determines the effective number of neighbours [nondiagonal elements in (2.3.20)], whereas in the Anderson model the corresponding matrix is three-diagonal.

However, one can give a qualitative argument [I84] which explains the Poisson dependence for $P(s)$ (see also [MT61]). Indeed, assuming that all EFs of the model (2.2.1) are exponentially localized in

momentum space, one can see that each quasienergy level effectively "feels" only those levels whose EFs strongly overlap. On the contrary, if two EFs are located very far from each other in momentum space, then the corresponding overlap integral is exponentially small due to the exponential decrease of the EFs far from their centres. Therefore, these two states cannot feel each other in the sense that, if one state is slightly perturbed, the other one does not change at all. In other words, these levels are independent and can be very close to each other resulting in the absence of repulsion. Only those states whose EFs substantially overlap, give a nonvanishing overlap integral and therefore, the corresponding levels are sensitive to each other. However, the number of effectively overlapping states vanishes when the localization length remains finite for any finite k (in infinite momentum space). Thus, the statistics of level spacings $P(s)$, for all quasienergies of model (2.2.1), is expected to be of Poissonian form (2.4.3) (so-called uncorrelated statistics).

Of course, all these arguments are qualitative, but they seem to be true from a physical point of view. Then another question immediately arises, related to the role of the Poisson distribution for the spacings s in automonous systems. One may recall that such a dependence, eq. (2.4.3), is known to be a distinctive property of the spectra of systems which are integrable in the classical limit. This prediction has been claimed in [BT77] when analysing generic nonlinear systems which are classically integrable. It was pointed out that the one-dimensional case is an exceptional one, with a strong repulsion which is due to the nondegeneracy of one-dimensional spectra. For more than one dimension, numerical simulations [BT77] with some simple nonlinear models have shown good qualitative agreement with (2.4.3). Nevertheless, some suspicion remained whether $P(s)$ for integrable systems exactly follows the Poisson distribution. For this reason, in [CCG85] a detailed numerical analysis has been carried out for the model of a two-dimensional nonlinear oscillator with energies given by the expression

$$E_{nm} = an^2 + m^2 , \qquad (2.4.4)$$

with some irrational parameter a. It was found that in spite of the rough correspondence of $P(s)$ with (2.4.1), there is serious deviation from (2.4.1) for small spacing $s \ll 1$. Moreover, the fluctuations around the Poisson distribution on all scales of s turn out to be strongly correlated. Such "correlated statistics", which on the other hand appears to be quite close to the Poisson law, reflects the nonstatistical character of $P(s)$. To summarize these results, we may conclude that the Poisson-like distribution (2.4.1) for the spacings between neighbouring energy levels for autonomous systems is not directly related with classical integrability, although it may be an indication of the complete suppression of quantum chaos.

To clarify the role of the Poisson dependence (2.4.1) for quasienergy levels we first discuss the simplest case ($k = 0$), which appears in our model (2.2.1) when the perturbation vanishes. As was noted, this question is also of special interest, since it relates to the other question, namely, whether the statistical properties of ϕ_n in the tight-binding model (2.3.20) are really good (see [CGI87]). For this, we consider the generalized sequence

$$\lambda_n = \{ \lambda_0 + n\theta_0 + \tfrac{1}{2}\tau n(n - 1) \} = \{ \lambda_0 + \tfrac{1}{2}\tau n^2 + (\theta_0 - \tfrac{1}{2}\tau)n \} , \qquad (2.4.5)$$

which also describes the unperturbed QE spectrum of our model for the particular choice of free parameters $\lambda_0 = 0$ and $\theta_0 = \tau/2$,

$$\lambda_n = \{ \tfrac{1}{2}\tau n^2 \} . \qquad (2.4.6)$$

Here { } denotes that λ_n is taken modulo 1, or, in other words, the fractional part of λ_n. By comparing (2.4.5) with (2.4.6) it appears that for the quasienergies λ_n in (2.4.5) an additional "mixing" has occurred; also, all QE levels are located in a finite interval, unlike the energy levels for autonomous systems. For this reason, the statistical properties of QE spectra are expected to be stronger.

It is interesting to note that the model (2.4.5) for $\tau > 0$ can be represented in the form of a two-dimensional mapping defined on the torus,

$$\lambda_{n+1} = \{\lambda_n + \theta_n\} , \qquad \theta_{n+1} = \{\theta_n + \tau_0\} . \tag{2.4.7}$$

This mapping is obviously not mixing in the common mathematical sense, namely, a small separation $(\delta\lambda)_n$ does not increase exponentially with n and therefore the dynamical entropy $h = 0$. A numerical analysis with irrational values of τ_0 and θ_0 (the value of λ_0 is not important since it gives a constant shift) has shown a large difference between the statistical properties of (2.4.5) and (2.4.6). It turned out that level spacing distribution $P(s)$ obtained for (2.4.6) with the total number of QE levels $N = 10^5$ seems to have the same features as in the case of the autonomous system investigated in [CCG85] (see fig. 5). First, for small spacings $s < 0.01$ there is an extremely large deviation from the Poisson dependence. A statistical χ^2 probe $(\chi^2_{10} \approx 125$ with 10 subintervals in $0 < s < 0.01$) gives the probability of such a deviation (confidence level) to be $\sim 10^{-4}$. Secondly, even for all other intervals the χ^2 value appears to be quite bad indicating that deviations from the Poisson law are not of a statistical nature.

Then, a more sensitive test has been used to check whether these deviations from (2.4.1) are really correlated. For this, a histogram for normalized deviations of the observed number of spacings in 1000 intervals was constructed in such a way that the expected number of levels in each interval according to the Poisson law is equal 100. The result presented in fig. 6a gives an extremely bad correspondence with the expected Gaussian distribution of fluctuations around the Poisson law. These data can be treated as strong evidence of correlated fluctuations, while fig. 5 may be regarded as a good correspondence to the Poisson law for all s (except $s \lesssim 0.01$).
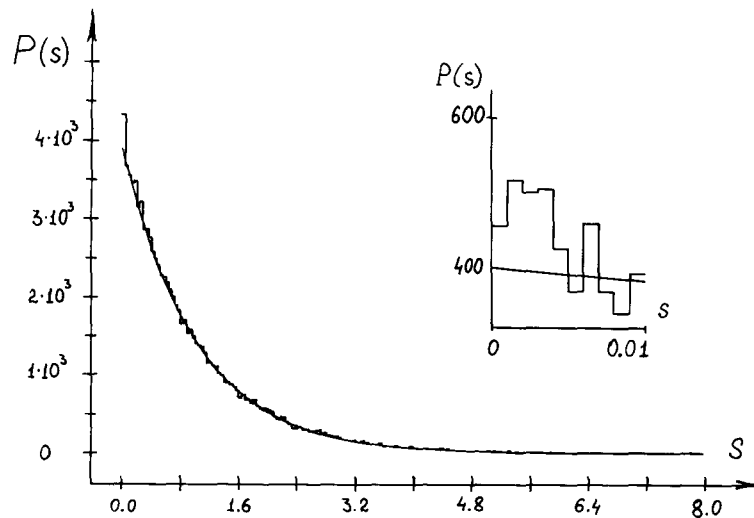

Fig. 5. Distribution $P(s)$ of the nearest level spacings computed for $N = 10^5$ values of λ_n [see (2.4.6)] for $\tau_0 = 1/\sqrt{3}$. The smooth curve is the Poisson distribution. The inset shows the distribution in the first interval $(0, 0.01)$ with the straight line as the Poisson distribution. (Here s is the normalized spacing, $s = 1$ corresponds to the mean spacing, 10^{-5}.) (After [CGI87].)
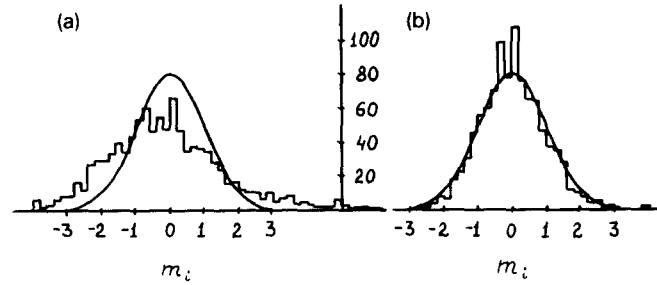
Fig. 6. Histogram of the distribution of deviations $m_i = (n_i^0 - n_{ex})/n_{ex}^{1/2}$ of the observed number of spacings n_i^0 from the expected n_{ex} in the ith interval. Full line corresponds to the Gaussian distribution with $\sigma = 1$. (a) The sequence (2.4.6) with $\tau_0 = 1/\sqrt{3}$; χ^2_{1000} for the deviation from the Poisson distribution is 3184; (b) the sequence (2.4.5) with $\tau_0 = 1/\sqrt{3}$ and $\theta_0 = \tau_0/2 - \sqrt{\tau_0}$. Here $\chi^2_{1000} \approx 934$ with a good confidence level. (After [CGI87].)

A clearly different result has been observed for the model (2.4.5), which has, in comparison with (2.4.6), an additional linear shift in n. This shift was discovered to give rise to very good statistical properties. In particular, $P(s)$ was found to be in good agreement with (2.4.1) according to a χ^2 test (see [CGI87]). Also, quite good agreement has been obtained for the distribution of the fluctuations around (2.4.1) with the Gaussian distribution ($\chi^2_{24} \approx 30$, see fig. 6b). As an additional trial, the well-known sequence

$$\lambda_{n+1} = \{\xi\lambda_n\}, \quad \xi \gg 1,$$ (2.4.8)

which is often used as a random number generator, has been taken [CGI87]. This one-dimensional mapping (2.4.8) was thoroughly investigated both analytically and numerically. The model (2.4.8) exhibits all strong statistical properties such as mixing and local instability. Numerically, the sequence (2.4.8) has been investigated extensively in [CI68] by many special tests; however, no deviations from statistical predictions have been found. In [CGI87] the statistical properties of (2.4.8) have been compared with those of (2.4.5) by making use of the same test when investigating the Gaussian character of the fluctuations around the Poisson law. The result is that no clear difference has been detected in comparison with (2.4.5). It is of special interest to find good tests that can distinguish between a nonmixing mapping (2.4.5) and a mixing mapping (2.4.8).

Rigorous analysis of the model (2.4.5) turned out to be quite difficult. It has been proved in [P88] that the first four moments of the distribution of the values λ_n in the limit $N \to \infty$ correspond to the Poisson distribution.

From the point of view of the statistical properties of the unperturbed QE spectrum, two results seem to be important. First, the sequence (2.4.6) appears to have relatively pure statistical properties. Therefore, one may expect that for the localization of EFs in the model (2.3.20) weak statistical properties of ϕ_n are sufficient. We would also like to note than an additional linear term in (2.4.5) corresponds in our model (2.2.1) to the first derivative $\partial/\partial\theta$ in the unperturbed Hamiltonian. Such an additional term can be treated as a magnetic field which breaks time reversal invariance of the given model (for more details see section 3.2).

Another quantity which is expected to be sensitive to the spectral fluctuations is the so-called Δ_3

statistics (see, e.g., [P65, M67, BFFMPW81, BG84]. This quantity can be used as some measure of the rigidity of the spectrum, depending on the correlations between all levels in the spectrum. Some analytical expressions for Δ_3 are predicted for the three different classes of ensembles in RMT, which are usually compared with the data. However, for details on the discussion of the Δ_3 statistics of the models (2.4.6) and (2.4.4) we refer the reader to the above references [CCG85, CGI87]. The reason we are not discussing these results here is mainly related with the fact that for the model (2.4.5) this quantity turned out to be much less informative than the $P(s)$ (see [CGI87]).

There is serious difficulty in observing the Poisson statistics (2.4.1) in numerical experiments with the model (2.2.1) for nonzero perturbation $(k \neq 0)$. Indeed, for any finite k, especially for $k \gg 1$, the localization length l_∞ has to be compared with the size of the matrix. The latter is always finite in numerical experiments according to any type of truncation. Previously, we discussed the problem of a truncation of our unitary matrix (2.2.9), which should be performed in such a way that unitarity is not destroyed. However, for any truncation we are restricted to some finite basis in which localization is considered. For this reason, some new quantity appears, which is the ratio of the average localization length l_∞ to the size of the chosen basis, $\Lambda = l_\infty/N$. Then it is natural to assume that this parameter essentially affects the level spacing distribution $P(s)$ for $K \gg 1$ [I84]. From this point of view, to obtain numerically $P(s)$ in the case of strong classical chaos $K \gg 1$ (for $k \gg 1$) one needs huge matrices of size $N \gg l_\infty \sim k^2$. As a result, in numerical experiments [I84] some deviations from the Poisson dependence (2.4.1) with visible repulsion have been observed even for a quite small ratio $k^2/N \lesssim 0.1$ with $N = 350$. The problem of how $P(s)$ and the repulsion depend on Λ will be discussed in more detail in section 4.3. Here we only emphasize that the deviation from (2.4.1) in our model (2.2.1) with an infinite number of states is entirely related to the truncation of the basis, and therefore should be treated as an artifact. Some evidence for this statement is given in [I84], where $P(s)$ slightly approaches (2.4.1) when N increases for fixed K and k (see also [FM86, FM88]).

Important results on this subject have been presented in [FFGP85, FF87], where the distribution $P(s)$ in the model (2.2.1) was examined as a function of the separation of the centres of the EFs in the unperturbed basis. In particular, the clear tendency has been obtained that $P(s)$ approaches the Poisson distribution (2.4.3) when the separation increases. These data can be regarded as a confirmation of the statement that the level spacing distribution $P(s)$ is expected to be of Poissonian form like in the case of the one-dimensional Anderson model (see also the discussion in [FFGP88, FM88a]).

Another interesting problem arises when we are interested in $P(s)$ not for all eigenstates, but only for those that are excited by some initial wave packet, $\psi_0(\theta)$. This problem also appears in other physical models, for example, in plasma physics (see [BJ88]). We already discussed the point that only perturbed states take part in the dynamics of the model providing bounded diffusion on some finite time scale $t \lesssim t_D$. One can say that the QE statistics of these states has even more meaning than the statistics of the total number of eigenstates of the matrix U_{nm}. Indeed, the statistical properties of the perturbed part of the spectrum are responsible for the details of the dynamics of the wave packet $\psi(\theta, t)$. From this point of view, it is of great interest to establish the form of $P(s)$ which corresponds to the initially excited spectrum. For simplicity, one may start with the case $l_\infty \gg 1$ and with typical initial packets $\psi_0(\theta)$ which should be well localized in momentum space, $\Delta n \ll l$. Then some universality may be expected for $P(s)$ because with increasing $k \gg 1$ (for fixed $K \gg 1$) the effective number of perturbed states increases and the same character of overlap of EFs could persist provided that the absolute number of perturbed states does not affect the shape of $P(s)$. The connection of such a $P(s)$ distribution with the diffusive dynamics of our model (2.2.1) is the subject of section 2.6.

2.5. Special case: quantum resonance

In this section we discuss some exceptional properties of the kicked rotator model (2.2.1) in the case of special values of the rescaled period $\tau = 4\pi r/q$ [see (2.2.14)]. In [CCFI79] this case has been termed "quantum resonance", to stress the quantum origin of the phenomenon. The specific motion of the system in quantum resonance is clearly seen in the simplest case of $\tau = 4\pi$, discovered in [CCFI79]. For convenience, we use here a form of the unitary evolution operator $\hat{U}$ which is slightly different from the symmetric one given by (2.2.3). It is clear that any shift in time does not change the QE spectrum of $\hat{U}$. As for the eigenvectors, they only change in phase, if the time shift does not include a kick (see further). Instead of (2.2.3) we write down the transformation for the function ψ in one period with $\tilde{\psi}(\theta, t)$ taken just after each kick,

$$\tilde{\psi}(\theta, t + T) = \hat{\tilde{U}}\psi(\theta, t) = e^{-ik\cos\theta}\, e^{i(\tau/2)\partial^2/\partial\theta^2}\tilde{\psi}(\theta, t) \, . \tag{2.5.1}$$

The free rotation from one kick to another only shifts all phases of the Fourier components of the function ψ by $\chi_n = \tau n^2/2$. Therefore, χ_n appears to be the same after one rotation if $\tau = 4\pi$. As a result, only kicks affect the dynamics through the exact expression for the solution of the Schrödinger equation,

$$\tilde{\psi}(\theta, t) = e^{-ikt\cos\theta}\tilde{\psi}(\theta, 0) \, , \tag{2.5.2}$$

where t is measured in the number of kicks, $t = \tilde{t}T$, and $\tilde{\psi}(\theta, t)$ is any initial state. Using the usual definition, the energy of our system is given by

$$E(t) = -\frac{\hbar^2}{2} \int\limits_0^{2\pi} \tilde{\psi}^*(\theta, t) \frac{\partial^2}{\partial\theta^2} \tilde{\psi}(\theta, t) \, d\theta \, , \tag{2.5.3}$$

from which the quadratic term $\sim t^2$ for the time dependence of the energy can be easily obtained. For example, in case of $\tilde{\psi}(\theta, 0) = \exp(in_0\theta)$ (only one unperturbed state is initially excited), the exact expression is

$$E(t) = \tfrac{1}{2}k^2\hbar^2 t^2 + E(0) \, . \tag{2.5.4}$$

For other choices of $\tilde{\psi}(\theta, t)$, additional linear terms $\sim t$ may appear. In any case, for $t \to \infty$, the energy $E(t)$ turns out to increase quadratically in time, independently of the values both of the classical (K) and the quantum (k) parameters. The resonance character of this pure quantum effect can be clarified by comparing the driving frequency $\Omega = 2\pi/T = \hbar/2$ with the frequencies for the transition between neighbouring unperturbed states, $\omega_n \equiv (E_{n+1} - E_n)/\hbar \simeq 2n\Omega$. A quadratic energy growth is also known to be the case for classical models like our kicked rotator. It is the so-called "microtron acceleration" (see, for details, [C79, HOA84]). However, in classical models this type of motion is directly related to the existence of stable regions equally spaced in momentum space and occurs only for special values of the perturbation strength K_0 (for example, for $K_0 \sin\theta_0 = 2\pi m$ in (2.1.5), where θ_0 is a fixed point of period 1). In contrast, quantum resonance behaviour does not depend on K and therefore arises also for $K \ll 1$, when the classical motion is bounded in momentum.

The detailed analysis of the quantum resonance behaviour in the general case of (2.2.14) has been performed in [IS79, IS80]. It was rigorously shown that for $\tau = 4\pi r/q$, with integers r and q, the transformation (2.5.1) for the function ψ in the θ representation can be reduced to the form

$$\tilde{\psi}(\theta + 2\pi n/q, t + T) = \sum_{m=0}^{q-1} S_{nm}(\theta)\tilde{\psi}(\theta + 2\pi m/q, t) \ . \tag{2.5.5}$$

Here a finite matrix $S_{nm}(\theta)$ has appeared, instead of the infinite matrix in (2.2.10),

$$S = \begin{pmatrix} \beta_0 & & & \\ & \beta_1 & & 0 \\ & & \ddots & \\ 0 & & & \beta_{q-1} \end{pmatrix} \begin{pmatrix} \gamma_0 & \gamma_1 & \cdots & \gamma_{q-1} \\ \gamma_{q-1} & \gamma_0 & \cdots & \gamma_{q-2} \\ \vdots & \vdots & & \vdots \\ \gamma_1 & \gamma_2 & \cdots & \gamma_0 \end{pmatrix}, \tag{2.5.6}$$

$$\beta_j = \exp[-\mathrm{i}k\cos(\theta + 2\pi j/q)] \ , \tag{2.5.7a}$$

$$\gamma_n = \frac{1}{q} \sum_{m=0}^{q-1} \exp\left(-\mathrm{i}\frac{2\pi r}{q}m^2 - \mathrm{i}\frac{2\pi mn}{q}\right) \ . \tag{2.5.7b}$$

Therefore,

$$S_{nm} = \beta_n \gamma_{m-n} \ . \tag{2.5.8}$$

It is interesting to note that all matrix elements S_{nm} are constructed from $2q$ values of β_j and γ_n, as follows from (2.5.6).

A very important conclusion resulting from (2.5.5) is that only q discrete points in θ space are involved and map onto each other (for odd q; otherwise, for even q, only $q/2$ are mapped; for simplicity we assume q odd). These points are equally spaced in the interval $(0, 2\pi)$ with θ_0 being the initial point of each set of these points. Therefore, all points in θ space are conveniently represented by a set of q-vectors which depend on some continuous parameter θ_0 from the range $[0, 2\pi/q)$. Correspondingly, the quasienergy EFs in the θ representation are eigenvectors of the finite unitary matrix S_{nm} of size $q \times q$ depending on θ_0. As a result, operations with such EFs are the same as with q-dimensional EFs, with integration over θ_0 from 0 to $2\pi/q$.

All these properties of EFs in θ space can be easily converted to momentum space with the remarkable result that in the momentum representation all the EFs of our model (2.2.1) are Bloch states with period q. More precisely, all EFs in p space are represented by the set of q-vectors which depend on the same continuous parameter θ_0. Under the transformation $n \to n + q$ each EF is multiplied by the factor $\exp(\mathrm{i}\theta_0 q)$,

$$\varphi_{n+q}(\varepsilon(\theta_0)) = \mathrm{e}^{\mathrm{i}\theta_0 q}\varphi_n(\varepsilon(\theta_0)) \ . \tag{2.5.9}$$

This situation is very similar to that known in solid state physics, namely, our model in the momentum representation in the case of quantum resonance can be associated with a one-dimensional model of a periodic crystal, with a periodicity of q atoms. This analogy seems to be very important to establish properties of the model under consideration (see also the discussion in section 5).

In the momentum representation, the transformation for the $\tilde{A}_n(t)$ resulting from (2.5.5) [see (2.2.6) with the change $A_n \to \tilde{A}_n$ and $\psi \to \tilde{\psi}$, to stress the fact that the $\tilde{A}_n$ are determined after the kicks, and not in the middle of the free rotation], is

$$\tilde{A}_n(t + T, \theta_0) = \sum_{m=0}^{q-1} \tilde{U}_{nm}(\theta_0) \tilde{A}_m(t, \theta_0) ,$$ (2.5.10)

where $n, m = 0, 1, \ldots, q - 1$. Therefore, for fixed θ_0 the coefficients $\tilde{A}_n$ are determined in $q \times q$ space. To come back to the previous representation of A_n in infinite momentum space, one can use the relation (see also [CS86a])

$$\tilde{A}_{n+qL} = \frac{1}{\sqrt{2\pi}} \int_0^{2\pi/q} d\theta_0 \, e^{-i\theta_0 Lq} \tilde{A}_n(\theta_0) ,$$

with integer L from the range $(-\infty, \infty)$. The evolution of the q-dimensional vector $\tilde{A}_n(\theta_0)$ is described by a unitary matrix $\tilde{U}_{nm}$ taking the form, for (2.5.1),

$$\tilde{U}_{nm}(\theta_0) = B_{nm'}(k, \theta_0) G_{m'm}(\tau) ,$$ (2.5.11)

where the matrix $B_{nm'}(k, \theta_0)$ corresponds to a kick perturbation,

$$B_{nm'}(k, \theta_0) = \frac{1}{q} \sum_{l=0}^{q-1} \exp[-ik \cos(2\pi l/q + \theta_0)] \exp[-i(2\pi/q)l(n - m')] \exp[-i(n - m')\theta_0] ,$$ (2.5.12)

and the diagonal matrix $G_{m'm}(\tau)$ describes free rotation in one period τ,

$$G_{m'm}(\tau) = e^{i(\tau/2)m'^2} \delta_{m'm} .$$ (2.5.13)

Comparing (2.5.11) with (2.2.9) one can write down the finite matrix $U_{nm}(\theta_0)$ for the transformation of $A_n(t, \theta_0)$, where t is taken in the middle of free rotation,

$$U_{nm}(\theta_0) = G_{nn'}(\tau/2) B_{n'm'}(k, \theta_0) G_{m'm}(\tau/2) .$$ (2.5.14)

Both these expressions (2.5.11) and (2.5.14) are used in the literature (see, e.g., [CS85, CS86, I88]); however, the latter is written in a symmetric form and more convenient for the analysis of the symmetry properties depending on θ_0 (see section 3.1). It is clear that both $\tilde{U}_{nm}(\theta_0)$ and $U_{nm}(\theta_0)$ have the same quasienergies, $\varepsilon_j(\theta_0)$. As for the EFs of $\tilde{U}_{nm}(\theta_0)$ and $U_{nm}(\theta_0)$, they differ from each other only by the phases $\tau n^2/4$ in the components $\tilde{\varphi}_n(\varepsilon_j(\theta_0))$ and $\varphi_n(\varepsilon_j(\theta_0))$; hence the probabilities are the same, $|\tilde{\varphi}_n|^2 = |\varphi_n|^2$.

From above discussion it is clear that the spectrum of QEs in quantum resonance consists of q bands with a dependence on the continuous parameter $0 \le \theta_0 < 2\pi/q$ inside each band. This is the continuity of the spectrum which provides the unbounded increase of the energy. Exact expressions for $\varepsilon_j(\theta_0)$ have been obtained [IS79, IS80] only for the simplest cases, $\tau = 4\pi$ (main quantum resonance, previously

discussed in section 2.2) and for $\tau = \pi$ (correspondingly, $r = 1$, $q = 4$). Also, the case $\tau = 2\pi$ has been investigated in [IS79, IS80]; however, unexpectedly, the latter case appeared to be extremely exceptional, since only in this case did the function ψ prove to be completely periodic with a period of 2 kicks. To be more precise, the exact transformation is

$$\tilde{\psi}(\theta, t + T) = e^{-ik\cos\theta}\tilde{\psi}(\theta + \pi, t) , \qquad (2.5.15)$$

with only two values for the quasienergies, $\varepsilon_1 = 0$ and $\varepsilon_2 = \pi$, which are infinitely degenerate. Such a degeneracy seems to be accidental; no indications for other cases have been found. From (2.5.15) one can conclude that this special resonance is related to the particular form of $V(\theta) = k\cos\theta$. Indeed, for other choices of $V(\theta)$, say, for $V(\theta) \sim \cos 2\theta$, this periodic behaviour of $\psi(\theta, t)$ disappears, and quantum resonance behaviour [$E(t) \sim t^2$ as $t \to \infty$] takes place for all values of q.

Numerically, the dependence of $\varepsilon_j(\theta_0)$ on the phase θ_0 can be investigated by diagonalization of the unitary $q \times q$ matrix (2.5.11) or (2.5.14) for different values of θ_0. The structure of the QE spectrum for some values $q \gg 1$ and different parameters k and K has been analysed in [CS85, CS86]. In particular, the sharp decrease of band widths for approximately constant values of τ, $\tau = 4\pi r/q \approx$ const. has been observed when $\tau/4\pi$ was approximated by simple rational ratios with increasing q. Previously, in [IS79, IS80] strong (exponential) decrease of the band widths was predicted for the case $k \ll q$ as a function of $q \to \infty$. Such a property is well associated with the expectation that the QE spectrum should be discrete for the nonresonant case ($\tau \approx$ const. with $r \to \infty$ and $q \to \infty$). This prediction, that the size of the bands is exponentially small for $q \gg 1$ and $k \ll q$ is clearer when we assume the analogy between our model (2.2.1) and the Anderson model (see the discussion in the previous section). Indeed, in solid state physics a relation between the localization length and the size of the band is known, which appears when the boundary conditions for the crystal are changed,

$$\Delta\varepsilon \sim \exp(-L/l_\infty) . \qquad (2.5.16)$$

Here L is the size of the crystal and l_∞ is the localization length defined as the inverse increase of EF, $\psi(x) \sim \exp(-x/l_\infty)$, for $l \ll L$. In such a definition, l is associated with l_∞ found for QE eigenfunctions of the kicked rotator (see section 2.3). It is interesting to note that, in spite of the fact that all EFs in the case of quantum resonance are definitely delocalized in momentum space [and quasiperiodic, according to (2.5.9)], it appears to be useful to investigate whether they are localized or not, on the finite scale of quasiperiodicity, for $0 \le n < q$. Then, if $l \ll q$, the size of the bands is expected to be exponentially small.

Direct numerical simulations performed by the author have revealed a clear exponential dependence,

$$\langle \ln(\Delta_j) \rangle = -\alpha q/k^2 + C_0 , \qquad (2.5.17)$$

for the quantum resonance case (for $K = 5$), where $k^2/2$ may be associated with the diffusion coefficient D_n. Numerical experiments were run for matrices $\tilde{U}_{nm}$ [see (2.5.11)] of size $q = 199$ and 401, with q being a prime number to avoid reducible fractions. It can be proved that the $\varepsilon_j(\theta_0)$ are symmetric about $\theta_0 = \pi/q$; therefore, it is sufficient to run for $0 \le \theta_0 \le \pi/N$ only. Moreover, numerical simulations have discovered that for a small ratio $k^2/q \ll 1$ only one oscillation is observed for ε_j depending on θ_0. This remarkable property symplifies very much numerical experiments since the size of each band is

essentially determined by the normalized difference in two points: $\Delta_j \approx [\varepsilon_j(\pi/N) - \varepsilon_j(0)]/2\pi$. Then, all Δ_j have to be averaged because of extremely large fluctuations in the band widths. These fluctuations seem to be very important in further investigations of the statistical properties of localized ($l \ll q$) EFs, especially in view of comparison with solid state models, where such fluctuations of Δ_j result in fluctuations of the conductivity.

It turned out, that, in spite of the large fluctuations in Δ_j, they can be effectively averaged, when averaging $\ln(\Delta_j)$, not Δ_j. The summarized data are shown in fig. 7, where $\langle \ln(\Delta_j) \rangle$ versus $1/k^2$ is plotted and the dashed horizontal lines correspond to the average spacing $\Delta_0 = 1/q$. From these data the approximate value of the coefficient α can be obtained, $\alpha \approx 2.4$, which is practically independent of the size q of the matrix. It is interesting to note that the value found for α is closer to that obtained for $l_s \approx D_n \approx k^2/2$ than to that obtained for $l_\infty \approx D_n/2 \approx k^2/4$ (see section 2.3). Such a difference may be a result of fluctuations, which are meant to be important for l_s, and not for l_∞. In any case, the obvious exponential dependence (2.5.17) is seen from the data.

Another interesting observation which can be claimed from fig. 7 is the breakdown of the exponential increase of $\langle \ln(\Delta_j) \rangle$ when the line $\langle \ln(\Delta_j) \rangle = -\ln q$ is approached. This effect can be associated with some type of repulsion between the bands when they are increased sufficiently to be comparable with the mean spacing, $\Delta_j \approx 1/q$. This behaviour is quite unexpected since only levels with the same θ_0 are known to exhibit strong repulsion with the increase of the ratio k^2/q (see, e.g., [CS85, CS86). Indeed, for k^2/q not too small, QE levels have many oscillations as a function of θ_0, resulting in the levels possibly intersecting different bands, because levels with different θ_0 correspond to different symmetries and do not feel each other. To check that such a repulsion is not a result of a specific procedure when measuring the band width only in two points, some other points θ_0 from the range $(0, \pi/q)$ have been used to estimate the size of the bands. However, repulsion seems not to disappear and further investigations are needed to understand this phenomenon.

A typical example of QE repulsion is shown in fig. 8a, where the Bloch parameter θ_0 varies for very large perturbation $k \approx 20\,000$. A strong sensitivity of the levels is seen in comparison with fig. 8b, where
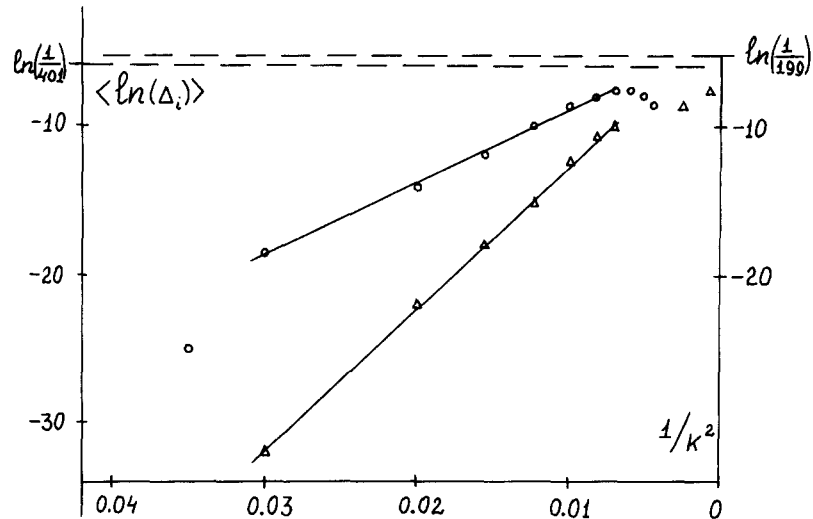

Fig. 7. Dependence of the quasienergy band width for the model (2.5.11) with $q = 199$ (circles) and $q = 401$ (triangles). The dashed line is the average spacing between quasienergies, $\Delta_0 = 1/q$.
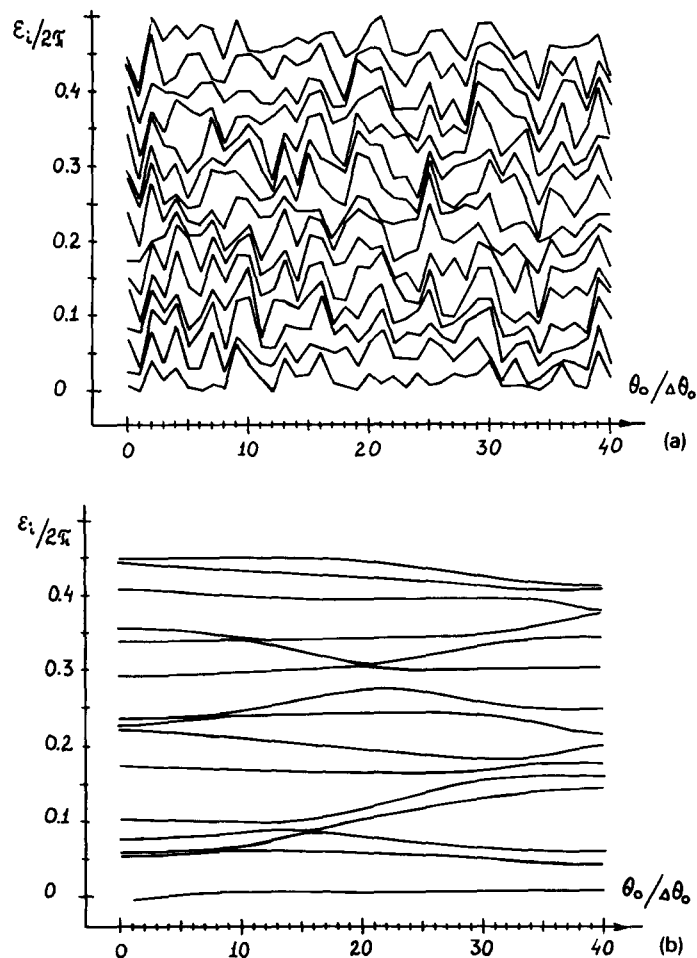
Fig. 8. The dependence of 15 quasienergy levels ε_i on the Bloch parameter θ_0 in the model (2.5.11) with the step $\Delta\theta_0 = \pi/(41q)$ for $q = 31$ and $\tau = 4\pi/q$. (a) Strong repulsion for the extremely large perturbation $k = 20\,000$; (b) weak repulsion for the relatively small value $k = 20$.

the parameter k is relatively small. A similar behaviour of the energy levels is known in autonomous quantum systems which can exhibit chaotic motion in the classical limit (see, e.g., the reviews [E88, E88a] and references therein).

It was suggested in [P73] to use such a sensitivity of the levels as a distinctive property of the irregular character of the quantum spectrum in the case of classically chaotic motion. To measure this sensitivity, the second derivative of the energy levels with respect to the perturbation strength is used. In our case of QE levels this quantity has the form

$$\kappa_k \equiv \langle \mathrm{d}^2\varepsilon/\mathrm{d}k^2 \rangle ,\tag{2.5.18}$$

where $\langle\ \rangle$ denotes averaging over the number of QE levels. As was mentioned above, an analogous quantity has been analysed in detailed simulations for some autonomous systems. However, up to now, it is not clear whether this quantity κ_k can be really used to distinguish systems with classically chaotic motion from those exhibiting regular motion (see discussion in [E88a]). Indeed, in the latter case,

avoidance of crossing occurs only in very small regions where the energy levels approach each other very closely. This happens quite rarely, when the perturbation is changing, but repulsion appears to be very strong in these small regions. In contrast, for strong chaos, the levels cannot approach each other very closely because of the strong sensitivity of the levels. Therefore, locally, the second derivative is smaller in this case, but repulsion occurs on the larger scale of perturbation. Thus, when averaging over many levels for a fixed perturbation, the quantity (2.5.18) may be of the same order for both cases. The same situation is expected in the case of averaging over the perturbation for some fixed level.

This situation is a real problem in numerical simulations with autonomous systems (see, e.g., [SS87]); therefore, more investigations are desirable. In this sense, our model (2.2.1) in quantum resonance is quite useful to shed light on this question. In contrast to autonomous systems, where the density of states typically increases with the perturbation, in our case the density of QE levels is fixed by the size of the matrix. In addition, a new parameter θ_0 arises, which can also be used as a free parameter for the investigation of level repulsion,

$$\kappa_{\theta_0} \equiv \langle \mathrm{d}^2\varepsilon / \mathrm{d}\theta_0^2 \rangle .$$
(2.5.19)

In this definition, however, the averaging over the parameter θ_0 has no sense, since $\varepsilon(\theta_0)$ is periodic in θ_0, resulting in a zero mean for κ_{θ_0} when averaging from $\theta_0 = 0$ to $\theta_0 = 2\pi/q$. For this reason, $\langle \ \rangle$ is to be taken as the average over different QE levels for some fixed value of θ_0. Such numerical experiments with the computation of (2.5.18) and (2.5.19) as a function of the classical parameter K or the quantum parameter k may be very interesting. Up to now, only qualitative results are known [CS85, CS86], which give a clear picture of the repulsion when θ_0 or k varies.

Taking into account that the spectrum of quasienergies has a continuous part, with q bands, the asymptotic expression for the energy increase $E(t)$ has been found rigorously [IS79, IS80] (for $t \to \infty$),

$$E(t) = \eta t^2 + at + b(t) + E(0) .$$
(2.5.20)

Here η and a are some coefficients which depend both on the initial state $\psi_0(\theta)$ and the dynamical parameters K and $\tau = 4\pi r/q$. Detailed analyses of expression (2.5.20) have shown, in particular, that the coefficient η vanishes in the case when all QE are independent of θ_0. This means that the asymptotic quadratic dependence $\sim t^2$ is entirely related to the continuous component in the spectrum. A special case of vanishing η has been also discovered [IS80] for a specific form of the initial wave packet $\psi_0(\theta)$, with the additional condition that at least one of the QEs does not depend on θ_0. It should be noted that the other coefficient, a, in (2.5.20), which provides the linear energy increase, turns out to be also related to the continuous component in the QE spectrum. Indeed, the complicated expressions for η and a obtained in [IS79, IS80] depend on $\varepsilon_j'(\theta_0)$ and $\varepsilon_j''(\theta_0)$, where the first and second derivatives are taken with respect to θ_0. Therefore, not only η but also a vanishes for a purely discrete spectrum.

The only time dependence for the energy in the case of a nonresonant condition $\tau/4\pi \neq r/q$ is described by some function $b(t)$, given in the form of a finite sum of terms $\exp\{i[\varepsilon_m(\theta_0) - \varepsilon_{m'}(\theta_0)]\}$ with further integration over θ_0 $(m, m' = 0, 1, \ldots, q - 1)$. A nonresonant behaviour can be obtained by making use of the limit $r \to \infty$, $q \to \infty$ $(\tau \approx \text{const.})$. In this case only a summation remains and the question of what type of time dependence is expected from $b(t)$ is entirely related to the amplitudes of terms in the infinite $(q \to \infty)$ sum. As we know, only a finite number of exact (perturbed) EFs is excited by any initial state $\psi_0(\theta)$ localized in momentum space. This leads to the fact that only a finite number of oscillating terms are effectively present in the expression for $b(t)$. Therefore, up to some finite time

t_D the time dependence of $b(t)$ will be linear. The question of the influence of the statistical properties of the QEs ε_m, $\varepsilon_{m'}$ on the dynamics is of special interest (see next section).

Both coefficients η and a in (2.5.20) appear to vanish very rapidly with the increase of $q \gg k^2$. Indeed, we may assume the simple dependence $\varepsilon(\theta_0) \approx \varepsilon_{max} \cos \theta_0$, which seems to be approximately true for exponentially small bands, see (2.5.16). Then both $\varepsilon'(\theta_0)$ and $\varepsilon''(\theta_0)$ are exponentially small too. Therefore, for the case of strong localization, when $l \sim k^2 \ll q$, the coefficients η and a are so small that they do not affect the nonresonance behaviour. This means that the resonant case can be used as a good approximate model for the nonresonant behaviour for some finite times t during which the quadratic growth of the energy can be neglected.

The opposite case of a clear quadratic increase of the energy, without visible oscillations, occurs when $k^2 \gg q$ (see fig. 9a). Some additional oscillations appear in case of small values of $k \ll q$ (see figs. 9b and 9c). The estimate for η in the case of $k \gg q$ and for a smooth initial wave packet $\psi_0(\theta)$ was obtained in [IS80, IS81],

$$\eta \sim [\varepsilon'(\theta_0)]^2_{max}/2 \approx k^2/\xi_0 q ,\qquad (2.5.21)$$

where ξ_0 is some parameter. Numerical data [IS79, IS80] are found to be in good agreement with
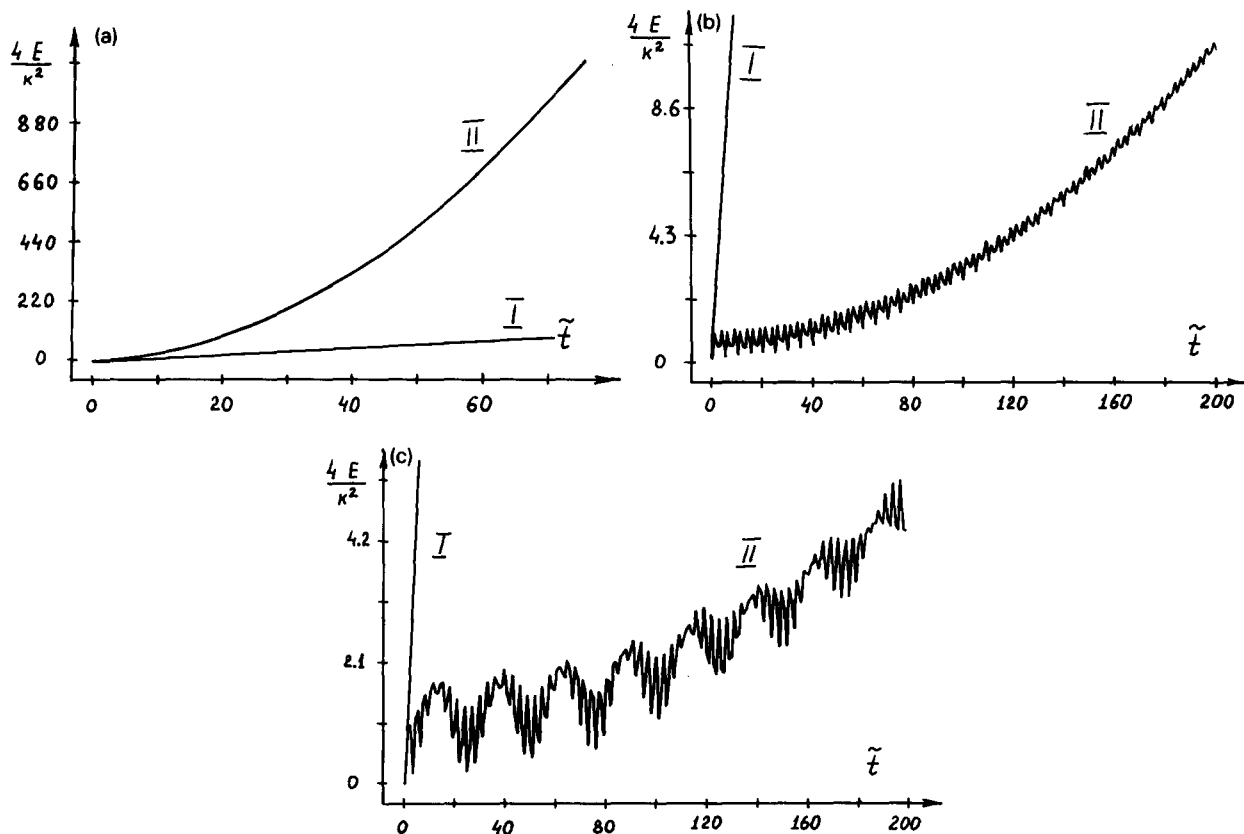
Fig. 9. The time dependence of the rotator energy E in the case of quantum resonance; the straight line (curve I) corresponds to classical diffusion, $E = k^2 \tilde{t}/4$, here $\hbar = 1$; (a) $\tau = 4\pi/17$, $k = 19$, $K \approx 14.0$; (b) $\tau = 8\pi/5$, $k = 0.5$, $K \approx 2.5$; (c) $\tau = 4\pi/3$, $k = 0.25$, $K \approx 1.0$ (after [IS79, IS80]).

(2.5.21) for different values of the parameters $q \approx 7\text{-}17$ and $k \approx 12\text{-}100$, for which the average value of $\langle \xi_0 \rangle$ appears to be $\langle \xi_0 \rangle \approx 2.4$. In the case of moderate values of $k \gtrsim q$ the numerical results may be approximated by the dependence

$$\tilde{E}(t) = E(t)/\hbar^2 = k^2 t^2 / \xi_0 q + \tfrac{1}{4} k^2 t + \tilde{E}(0) \,, \qquad\qquad (2.5.22)$$

where the quadratic term corresponds to (2.5.21).

Extensive numerical investigations have been made in [CFGV86], where attention has mainly been paid to the dynamics of the model (2.2.1) under the quantum resonance condition (2.2.14). One of the questions was how the energy growth is affected by the ratio r/q when the irrational number $\tau/4\pi$ is approximated by a sequence of rationals. Earlier, in [CG84] an interesting result was rigorously proved: for a generic choice of the potential $V(\theta)$ in (2.2.2) there is a nonempty set of nonresonant values of the period $\tau/4\pi$ for which the QE spectrum still has a continuous component. These values turn out to be very exceptional in the sense that they are extremely close to rational values (so-called Liouville numbers). Thus, the serious question arises as to the type of dynamics for the rotator for these special values of $\tau/4\pi$.

Numerical data [CFGV86] have uncovered a quite interesting dependence for the energy $E(t)$, reflecting the number properties of $\tau/4\pi$. Namely, the typical time dependence of $E(t)$ for $r/q = [m_1, m_2, m_3, \ldots]$ with $m_3 \gg m_2 \gg m_1$, represented in the form of a continuous fraction expansion, reflects the structure of r/q. It appeared that $E(t)$ consists of different time scales, with alternating regimes of long diffusive linear growth $(\sim t)$ and quadratic $(\sim t^2)$ energy growth. The durations of the diffusive regimes are related to the numbers m_1, m_2, m_3 in the continuous fraction. However, an analytical expression for this relation has not been found.

Another interesting question, in view of these exceptional values of $\tau/4\pi$, is how the structure of the EFs changes when irrational values of $\tau/4\pi$ are approached using these special numbers. It should be noted that for such transitions the localization length is expected to be approximately the same since $l \sim k^2$ and $\tau \approx \text{const}$. The only thing that will drastically change is the period q, giving the scale on which the EF is localized; however, how the EF changes on a large scale $n \gg q$ is unclear.

To conclude this section, some applications of the resonant case are worthwhile to be mentioned. As was pointed out, for rational $\tau/4\pi$ only a finite number q of phase points are mapped onto each other under the unitary transformation (2.5.5). This property has been used in [BIK88] to construct the so-called classical model of quantum diffusion,

$$p_{t+1} = p_t + [2\varepsilon_0 \sin(2(\theta_0 + 2\pi m_t/q))]_{\text{int}} \,, \qquad m_{t+1} = [m_t + 2rp_{t+1}]_q \,, \qquad\qquad (2.5.23)$$

which exhibits both classical diffusion during some time t_D and suppression for $t \gg t_D$. This model corresponds to $V(\theta_0) = \varepsilon_0 \cos 2\theta$ in (2.2.2), instead of $V(\theta_0) = \varepsilon_0 \cos \theta$, which is taken for some technical reasons connected with the fact that Wigner's function is used to describe the properties of the kicked rotator model (2.2.1). The notation $[\ ]_{\text{int}}$ indicates that the integer part is taken; therefore p_t are integer numbers. This is meant to reflect a distinctive property of a quantum model like the discreteness of the momentum. In addition, the phases m_t are also assumed to be discrete (or integer, for computational convenience, with the use of the notation $[\ ]_q$ to emphasize that the m_t are taken modulo q).

A similar model, but with continuous phases θ_t, has been used earlier in [CIS81] to demonstrate how the discreteness of the momentum leads to the suppression of the diffusion. It was found, however, that

the effect of the suppression is exhibited by this model only qualitatively, without quantitative agreement with the degree of suppression in the model (2.2.1). Indeed, the energy growth in this discrete model appeared to be somehow suppressed in comparison with the classical model (2.1.4), but true energy growth remains much faster than in the quantum model.

In contrast, in the model (2.5.23) both the momentum p_t and m_t are discrete, resulting in the complete discreteness of phase space. The free parameter θ_0 plays an important role in the model and determines the total shift of the grid from $\theta = 0$ in the classical model (2.1.5). Hence, many copies of the $q \times q$ grid on the torus with different $0 \leq \theta_0 \leq 2\pi/q$ have to be taken, averaging over the whole set of trajectories $E(t, \theta_0)$. It was unexpectedly found that the classical model (2.5.23) exhibits not only diffusion and suppression of it, but, in the case of very large $q \gg 1$, also a purely quadratic growth of the energy $(E \sim t^2)$, which is a distinctive property of quantum resonance behaviour (see details in [BIK88]). Unfortunately, it is not clear which number of copies of grids (or which number of different θ_0 in the simulation) are needed to ensure that for a given time $t \gg t_D$ a good correspondence between the discrete model (2.5.23) and the given quantum model (2.2.1) is guaranteed. However, this approach to the attempt to find a classical analogy to the quantum motion, apart from the theoretical basis, is of great interest.

2.6. Quantum diffusion and correlation functions

One of the important problems is to describe the energy growth in the model (2.2.1) both on the diffusive time scale $t \lesssim t_D$ and on the large time scale $t > t_D$, where quantum suppression occurs. As was discussed in section 2.2, the suppression of classical diffusion can be directly related to the peculiarities of quantum correlations, which, unlike the classical correlations, appear not to vanish for $t \to \infty$. As a result, the role of these residual quantum correlations increases in time, due to strong quantum effects of localization. Here we discuss the possibility of an analytical description of quantum diffusion using a phenomenological approach based on some numerical data (for details, see [BI88]).

We start with the transformation for the function ψ given in the form where the first operator is a kick and the second one is a free rotation,

$$\hat{U} = \exp[i(\tau/2)\partial^2/\partial\theta^2] \exp(-ik \cos \theta)$$

[compare with (2.5.1)]. This form appears to be more convenient to represent all correlations in the most simple expressions. Then, according to the definition of energy (2.5.3) one can obtain the transformation for $E(t)$ in one period,

$$E_{t+1} = E_t + \tfrac{1}{4}\varepsilon_0^2 - \tfrac{1}{4}\varepsilon_0^2 \langle \cos 2\theta \rangle_t + \tfrac{1}{2}\varepsilon_0 \langle \sin \theta \, \hat{I} + \hat{I} \sin \theta \rangle_t , \tag{2.6.1}$$

where $\hat{I} = -i\hbar \, \partial/\partial\theta$ is the momentum operator and the notation $\langle \ \rangle$ is used to denote the quantum-mechanical average,

$$\langle F \rangle \equiv \frac{1}{2\pi} \int\limits_0^{2\pi} \psi^*(\theta, t)\hat{F}\psi(\theta, t) \, d\theta , \quad \psi(\theta, t) = (\hat{U})^t\psi(\theta, 0) , \tag{2.6.2}$$

which is taken at the instants of time $t = \tilde{t}$, before the kicks. To compare (2.6.1) with the classical model

[see (2.1.4)] we write the classical analog of (2.6.1) taking the limit $\tau = \hbar T \to 0$ and $k = \varepsilon_0/\hbar \to \infty$ for $K = \varepsilon_0 T = \text{const.}$,

$$E_{t+1}^{(cl)} = E_t^{(cl)} + \tfrac{1}{4}\varepsilon_0^2 - \tfrac{1}{4}\varepsilon_0^2 \langle \cos 2\theta_t \rangle + \varepsilon_0 \langle p_t \sin \theta_t \rangle \,. \tag{2.6.3}$$

Here the averaging is performed over the initial distribution $\rho_0(\theta, p)$ corresponding to the initial quantum state $\psi_0(\theta)$. For example, in the case when one unperturbed state $n_0 = p_0/\hbar$ at time $t = 0$ is taken as the initial state, we have

$$\psi_0(\theta) = \exp(\mathrm{i}n_0\theta) \,, \qquad \rho_0(\theta, p) = \delta(p - p_0) \,. \tag{2.6.4}$$

It is well known that in the classical model (2.1.4) under the condition $K \gg 1$ diffusion of energy $E_t^{(cl)}$ occurs [see (2.1.10)] resulting from the very fast decay of correlations $\langle \cos 2\theta_t \rangle$ and $\langle p_t \sin \theta_t \rangle$. In contrast, the quantum correlation functions

$$F_1(t) \equiv \langle \cos 2\theta \rangle_t \,, \qquad F_2(t) \equiv \mathrm{i}\langle \sin \theta \, \partial/\partial\theta + (\partial/\partial\theta) \sin \theta \rangle_t \tag{2.6.5}$$

appear to be responsible for the suppression of diffusion. It is our purpose to clarify the role of quantum correlations in the energy growth,

$$\tilde{E}_{t+1} = \tilde{E}_t + \tfrac{1}{4}k^2 - \tfrac{1}{4}k^2 F_1(t) + \tfrac{1}{2}kF_2(t) \,. \tag{2.6.6}$$

Here, for convenience, we passed to the normalized energy $\tilde{E} \equiv E/\hbar^2$.

To investigate quantum correlations in the kicked rotator model, an approach has been developed in [BK83] where a generalized correlation function is introduced,

$$R^{(t)}(z|M_0) = \frac{1}{2\pi} \int_0^{2\pi} \psi^*(\theta, t)\, \mathrm{e}^{\mathrm{i}M_0\theta}\, \mathrm{e}^{\mathrm{i}z\tau\hat{t}}\psi(\theta, t)\, \mathrm{d}\theta \,, \tag{2.6.7}$$

which can be written in recursive form,

$$R^{(t+1)}(z|M_0) = \mathrm{e}^{\mathrm{i}\tau M_0^2/2} \sum_{m=-\infty}^{\infty} \mathrm{e}^{\mathrm{i}m\tau(z+M_0)/2} J_m\{2k \sin[\tau(z+M_0)/2]\} R^{(t)}(z+M_0|M_0+m) \,. \tag{2.6.8}$$

In eqs. (2.6.7) and (2.6.8) z and M_0 are parameters (M_0 is an integer) determining a specific correlation function. Using this definition it is possible to obtain the mean value of any variable, for example,

$$\langle \cos(M_0\theta) \rangle_t = \tfrac{1}{2}[R^{(t)}(0|M_0) + R^{(t)}(0|-M_0)] \,,$$

$$\langle \sin \theta \, \hat{I} \rangle_t = -\frac{1}{2\tau}\left(\frac{\partial}{\partial z}\,[R^{(t)}(z|1) - R^{(t)}(z|-1)]\right)_{z=0} \,. \tag{2.6.9}$$

First, let us discuss the behaviour of the correlation functions (2.6.7) on the short time scale $t \lesssim t_{\mathrm{E}}$. It was shown [BK83] that in the classical limit ($\tau \to 0$, $k \to \infty$, $K = \text{const.}$) expression (2.6.8) takes the form

$$R_{\mathrm{cl}}^{(t+1)}(z|M_0) = \sum_{n=-\infty}^{\infty} J_n[K(z+M_0)]R_{\mathrm{cl}}^{(t)}(z+M_0|M_0+n) \,. \tag{2.6.10}$$

Expression (2.6.10) can be estimated for strong chaotic motion $(K \gg 1)$ by the saddle point method (see [BK83]),

$$R_{\text{cl}}^{(t)}(z|M_0) \sim \exp(-\tfrac{1}{2}t \ln K) .$$ (2.6.11)

It gives an effective time t_E, eq. (2.2.20), for which the motion of the quantum model is expected to follow the classical behaviour in all details including the exponential time decay of correlation functions.

As was discussed in section 2.2, this time scale $0 < t \lesssim t_E$ is too short to investigate the spread of a wave packet in detail because for typical parameters used in numerical experiments the time t_E turns out to be equal to a few kicks.

After some time $t \sim t_E$ quantum effects start to affect the motion more and more and, as a result, suppression of classical diffusion occurs. Nevertheless, there is another time scale $t_E \lesssim t \lesssim t_D$ where quantum diffusion turns out to be very close to classical diffusion for parameters $K \gg 1$ and $k \gg 1$. To obtain some estimates for the correlation functions (2.6.7) on this time scale we expand the initial state $\psi_0(\theta)$ in quasienergy functions $\varphi_{\varepsilon_m}(\theta)$ [see (2.2.19)] taken at $t = 0$,

$$\psi_0(\theta) = \frac{1}{\sqrt{2\pi}} \sum_m g_m \varphi_{\varepsilon_m}(\theta, 0) .$$ (2.6.12)

Then, the generalized correlation function (2.6.7) can be written in the form

$$R^{(t)}(z|M_0) = \sum_{m_1, m_2} e^{-i(\varepsilon_{m_1} - \varepsilon_{m_2})t} \phi_{m_1 m_2}(z|M_0) ,$$

$$\phi_{m_1 m_2}(z|M_0) = \frac{1}{(2\pi)^2} \sum_{n_1, n_2} g_{m_1}^* g_{m_2} \varphi_{m_1}^*(n_1) \varphi_{m_2}(n_2) e^{i n_2 z \tau} \delta_{n_2 - n_1 + M_0, 0} ,$$ (2.6.13)

where the coefficients $\varphi_m(n)$ are determined by

$$\varphi_{\varepsilon_m}(\theta, 0) = \frac{1}{\sqrt{2\pi}} \sum_n \varphi_m(n) e^{in\theta}$$ (2.6.14)

[see (2.3.1)] and ϕ_{m_1, m_2} in (2.6.13) are the overlap integrals of the quasienergy functions. It follows from (2.6.13) that the correlation functions can be represented as

$$R^{(t)}(z|M_0) = C(z|M_0) + W^{(t)}(z|M_0) ,$$ (2.6.15)

where $C(z|M_0)$ is the time-independent part of the function $R^{(t)}(z|M_0)$, that appears in (2.6.13) for $m_1 = m_2$. The second term in (2.6.15) represents interference effects $(m_1 \neq m_2)$.

Analytical analysis of (2.6.15) for specific correlation functions turns out to be very difficult. There are two questions which arise in this context. The first concerns the level of residual quantum correlations. To give an answer on this question one needs to estimate the constant term $C(z|M_0)$ in (2.6.15). Such an estimate has been obtained analytically only for the simplest correlation function $\langle \sin \theta \rangle$ (see [BK83]). Using the quantum resonance case with high values of $q \gg 1$, an exponentially small value for the time-independent term of $\langle \sin \theta \rangle$ has been found; therefore, for $t \to \infty$ residual correlations vanish. Unfortunately, for the more important correlations F_1 and F_2, eq. (2.6.5), there are no analytical estimates and the main information available comes only from numerical simulations (see further).

Another question concerns the rate of decrease of quantum correlations. This rate is determined by the second, time-dependent term in (2.6.15). Some rough analytical estimate can be made in the following way. For simplicity, we restrict ourselves to the case $z = 0$ in (2.6.15). In what follows we write $W^{(t)}(0|M_0) \equiv W^{(t)}(M_0)$. Some of the most important peculiarities can be understood from a simple qualitative analysis. Indeed, since the initial state (2.6.12) consists of a final number δm of exact eigenstates $\varphi_m(\theta)$ [according to (2.3.8), $\delta m \sim k^2$], the number of not too small terms in the sum (2.6.13) is also finite and approximately equal to $\delta m_1 \sim \delta m_2 \sim k^2$. Therefore, typical minimal frequencies in (2.6.13) are of the order of $1/k^2$. The latter means that on the time scale $t \lesssim t_D$ in the system (2.2.1) relaxation occurs, related to the fact that on this time scale the spectrum of the motion can be regarded as continuous. However, for $t \gtrsim t_D$, the discrete nature of the spectrum starts to reveal itself and leads to almost periodic oscillations, the rate of which is determined by a finite number $\delta m_1 \, \delta m_2 \sim k^4$ of terms.

Using (2.6.13) we can write $W^{(t)}(M_0)$ as

$$W^{(t)}(M_0) = \sum_{m_1 \neq m_2} e^{is_{m_1,m_2}t} \phi_{m_1 m_2}(M_0) , \tag{2.6.16}$$

where $s_{m_1,m_2} \equiv \varepsilon_{m_2} - \varepsilon_{m_1}$ stands for the spacings (taken modulo 2π) between the quasienergies. For further consideration it is convenient to represent the sum (2.6.16) in the form

$$W^{(t)}(M_0) = \sum_m e^{is_{m,m+1}t} \phi_{m,m+1}(M_0) + \sum_m e^{is_{m+1,m}t} \phi_{m+1,m}(M_0) + \sum_{m_1 \neq m_2 \pm 1} e^{is_{m_1 m_2}t} \phi_{m_1,m_2}(M_0) , \tag{2.6.17}$$

where the terms with nearest neighbour spacings of quasienergies are subtracted from the total sum. These terms are responsible for the time behaviour of the correlation function $W^{(t)}(M_0)$ on the scale $t_E \lesssim t \lesssim k^2$. To estimate the contribution of these terms we pass from the sum to an integration,

$$\sum_m e^{is_{m,m+1}t} \phi_{m,m+1}(M_0) \rightarrow \int_{(m)} e^{is_{m,m+1}t} \phi_{m,m+1}(M_0) \, dm \approx \phi_m^{(1)}(M_0) \int e^{ist} P(s) \, ds . \tag{2.6.18}$$

Here we introduce $P(s) = dm/ds$ as the distribution function of nearest neighbour spacings. It is also assumed in (2.6.18) that the overlap integrals $\phi_{m,m+1}(M_0)$ are only slightly dependent on the state number m. The latter conjecture seems to be correct as follows from numerical results.

Thus, we assume $\phi_{m,m\pm1}(M_0) \approx \phi^{(1)}(M_0)$ is, approximately, independent of m and therefore the integral in (2.6.18) can be easily evaluated, provided the function $P(s)$ is known. As was shown in [188], the level spacing distribution $P(s)$, under the condition of strong classical diffusion $(K \gg 1)$, is determined by the degree of overlap of eigenfunctions in the unperturbed basis. In our case all eigenfunctions, which are excited in accordance with (2.6.18), have a finite localization length $l \approx D_n \sim k^2$ and, as a result, they overlap only partly (see also [BIV87]). This situation can be approximately described by a distribution $P(s)$ which is intermediate between the Poisson and the Wigner ones. As we discussed above (section 2.4), the first one is known to be good for localized states while the latter is expected to appear in the limiting case of completely extended chaotic states. For our purpose we may use the following form of $P(s)$ (see details in section 4.1):

$$P(s) = As^\beta e^{-Bs^2 - Cs} , \tag{2.6.19}$$

where A, B and C are normalization constants and the parameter β is related to the degree of repulsion of nearby levels. Using (2.6.19), the integral in (2.6.18) can be estimated as

$$\int_0^{\infty} e^{ist} P(s) \, ds \sim 1/t^{1+\beta} , \quad t \gtrsim t_C .$$

(2.6.20)

It follows from (2.6.20) that on some time scale $t_E < t_C \lesssim t \sim t_D$ the decay of the correlation function $W^{(t)}(M_0)$ has the form

$$W^{(t)}(M_0) \propto 1/t^{1+\beta} , \quad t \gtrsim t_C .$$

(2.6.21)

Here t_C stands for some characteristic time corresponding to the lower limit of t in (2.6.21).

As a result, we may conclude that on the scale $t_E < t_C \lesssim t \sim t_D$ the typical behaviour of correlation functions can be represented as

$$R^{(t)}(z|M_0) \approx C(z|M_0) + \tilde{W}^{(t)}(z|M_0)/t^{1+\beta} ,$$

(2.6.22)

where $\tilde{W}^{(t)}(z|M_0)$ is some oscillating function and the time-independent part $C(z|M_0)$, in general, is not equal to zero.

To check the prediction (2.6.22) we analyse some data of numerical simulations (see [BI88]). First, we consider the correlation function $F_1(t)$, which reflects the correlations between the phases θ only. The typical behaviour of $F_1(t)$ as a function of the dimensionless time t/T is shown in fig. 10. The initial decrease of $F_1(t)$ appears to be so sharp that it is completely invisible. This fact corresponds to the
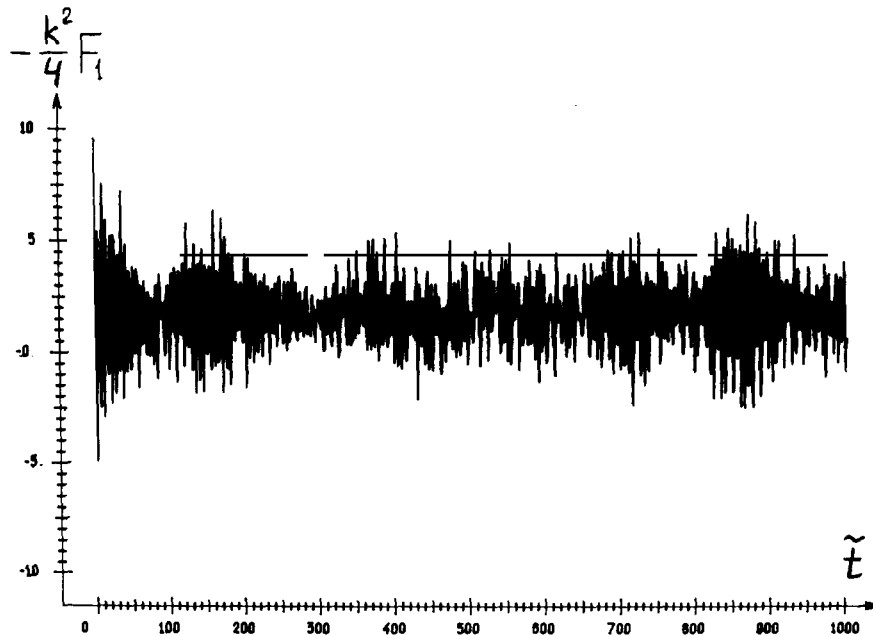
Fig. 10. Time dependence of $F_1(t)$ [see (2.6.5)] for $K = 5$ and initial state $\psi_0(\theta) = 1/\sqrt{2} + \cos 2\theta$. The averaging is performed over 10 trajectories for close values of k around $k = 10$ with step $\Delta k = 0.1$; the number of unperturbed states is $N = 2048$ (after [BI88]).

prediction of exponential decrease on the shortest time scale $t \lesssim t_E$ (we should recall that t_E is approximately equal to one or two kicks for the parameters used in the simulations). Another result, clearly seen in fig. 10, is that there is some nonvanishing value of $\langle \cos 2\theta \rangle$ around which quite large fluctuations occur. From numerical data a rough estimate can be obtained for the constant term of F_1, namely, $\bar{F}_1 \sim 1/k$.

Unlike F_1, a different behaviour is found for the correlation function F_2, eq. (2.6.5). This function reflects the correlations between the phases θ and the momentum p. It turns out that F_2 increases in time, having some limit as $t \to \infty$. Typical behaviour of F_2 is presented in fig. 11, where for convenience the constant term $k/2$ was subtracted from F_2. To reduce fluctuations, the averaging was performed, both for F_1 and F_2, over ten curves with slightly different values of k. It is seen from the data [BI88] that after some time $t > t_D \sim k^2$ the function F_2 exhibits steady-state fluctuations around some value which can be roughly approximated by $(F_2)_{max} = k/2 + \Delta_0$. Here, the relatively small term Δ_0 stresses that the time-independent term $\bar{F}_1$ has to be compensated by Δ_0 in the limit $t \to \infty$. A rough comparison of these two terms, $\bar{F}_2$ and $\bar{F}_1$, shows that the first one, $\bar{F}_2$, is about k^2 times larger than $\bar{F}_1$, $\bar{F}_2 / \bar{F}_1 \sim k/(1/k) \sim k^2$. It means that the most essential role in the suppression of classical diffusion is played by the correlations between θ and p.

It is interesting to note the quite unexpected behaviour of the correlation function F_2. First, for the shortest time scale, $t < t_E$, it starts to decrease very fast and then grows up to $F_2 \sim k$. The rate of this increase has to be essentially dependent on k, to provide the classical limit, according to which F_2 is expected to increase less and less slowly as $k \to \infty$.

It is of special interest to determine the parameter β for F_2 from the numerical data. As is seen, this parameter is related to the repulsion of the QE levels. Such a relation seems to be very important for further investigations. The most interesting peculiarity is that for repulsion ($\beta > 0$) decay of correlations is expected to occur slightly faster than $1/t$. Another intriguing conclusion of (2.6.6) is that two
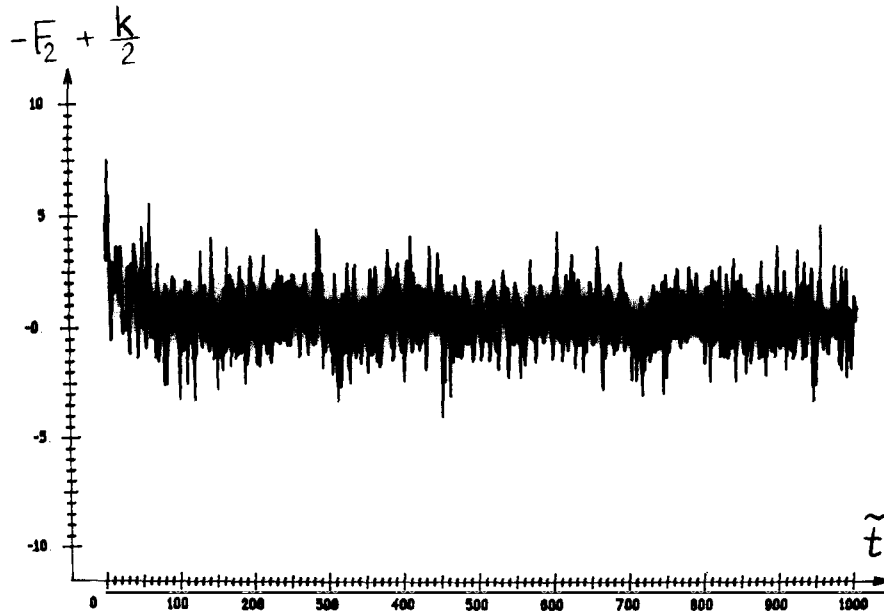

Fig. 11. Time dependence of $F_2(t)$ [see (2.6.5)] for the same parameters as in fig. 10; for convenience of comparison, the constant term $k/2$ was subtracted (after [BI88]).

different correlation functions have to cancel each other, on average, $\langle \sin^2\theta \rangle + (k/2)F_2 \approx 0$ as $t \to \infty$. Moreover, for the time-independent terms of these correlations, the above relation has to be exact if the suppression of diffusion is complete. This fact may be associated with the existence of some dynamical integral of the motion. The latter should be related, somehow, to the localization length l.

As follows from (2.6.1), quantum diffusion is directly related to the character of the time behaviour of the correlation functions (2.6.5). This allows us to obtain, in the framework of our kicked rotator model, an approximate analytical expression for the dependence of the mean energy to describe both classical diffusion and the quantum suppression of diffusion.

Using expression (2.6.22) and taking into account that at small times classical diffusion occurs, we assume the average increase of the energy per step can be written in the form

$$\Delta \tilde{E}_t \equiv \tilde{E}_{t+1} - \tilde{E}_t = A_0/(t + t^*)^{1+\beta} , \tag{2.6.23}$$

where t^* is some characteristic time up to which ΔE_t corresponds to classical diffusion. The numerical data in fig. 12 present ΔE_t (in units $\Delta \tilde{E} = \hbar^{-2} \Delta E$) versus time for the model (2.2.1). The constant A_0 in (2.6.23) can be found from the condition that ΔE_t correspond to the classical expression $\Delta \tilde{E}_t^{(cl)} = D_{cl}(K)/(2T^2)$, where $D_{cl}(K)$ is determined in (2.1.9); therefore, $\Delta \tilde{E}_t^{(cl)} \approx k^2/4$. Integrating (2.6.23) over time we obtain

$$\tilde{E}_t = \frac{D_{cl}(K)}{2\tau^2} \frac{t^*}{\beta} \left(1 - \frac{1}{(1 + t/t^*)^\beta}\right) . \tag{2.6.24}$$

Expression (2.6.24) contains two unknown parameters, β and t^*, one of which may be found from a comparison of (2.6.24) with the expression for the energy of stationary oscillations [CS86, CIS88] as $t \to \infty$,
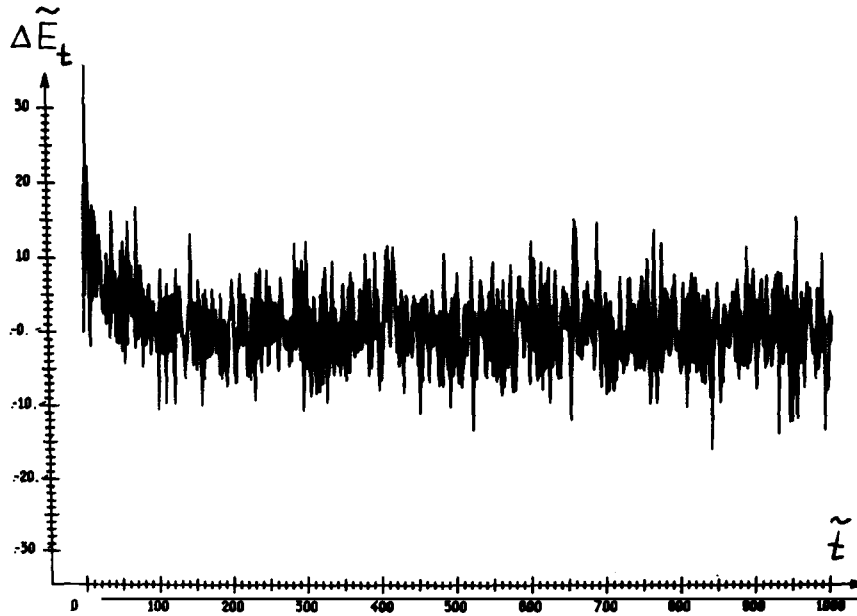

Fig. 12. Time dependence of $\Delta \tilde{E}_t$ [see (2.6.6)] for the parameters of fig. 10 with the same averaging (after [BI88]).

$$\tilde{E}_\infty = D_{cl}^2(K)/2\tau^4 .$$ (2.6.25)

This relationship was verified numerically in [CS86, CIS81] over a wide range of parameters. The energy $\tilde{E}_\infty$ represents the time averaged energy after classical diffusion has stopped $(t \gg t_D)$ and only fluctuations remain, due to the finite number of excited eigenstates. In fact, $\tilde{E}_\infty$ is determined by the degree of localization of eigenfunctions in the unperturbed basis of the system (see discussion in section 2.3). With account of (2.6.25) one can write

$$\tilde{E}_t = \frac{D_{cl}^2(K)}{2\tau^4} \left(1 - \frac{1}{[1 + \tau^2 t/D_{cl}(K)\beta)]^\beta} \right) ,$$ (2.6.26)

where only the unknown parameter $\beta > 0$ remains, which is determined by the correlations between excited states. If we do not take into account repulsion [$\beta = 0$ in (2.6.19) and (2.6.22)] logarithmic growth of the energy appears, which can be suppressed only by the additional assumption that the number of perturbed states is finite (see [C83]).

To check the prediction (2.6.26) for the energy growth, numerical experiments with the model (2.1.1) have been made [BI88] in the range of the quantum parameter $10 \le k \le 40$ and for a constant classical parameter $(K = 5)$. It is convenient to write expression (2.6.26) in dimensionless units,

$$Y = 2 \left\{ 1 - \frac{1}{(1 + X/2\beta)^\beta} \right\} , \quad Y \equiv \frac{4\tilde{E}_t \tau^4}{D_{cl}^2(K)} , \quad X \equiv \frac{2\tau^2 t}{D_{cl}(K)} ,$$ (2.6.27)

where Y is the dimensionless energy and X is the new dimensionless time. Typically, averaging for $Y(X)$ was performed over ten close values of k to reduce the fluctuations $(\Delta k \ll k)$. The result is presented in fig. 13, where for comparison three analytical calculations of Y according to eq. (2.6.27) are shown for three values of the degree of repulsion $\beta = 0.1, 0.2, 0.3$. It is seen that the function (2.6.27) quite well describes the numerical data.

It should be noted that the fluctuations for the energy $\tilde{E}_t$ as a function of k are inevitable due to the strong sensitivity of the motion to the value of $\tau = K/k$. It is known that even a slight change of τ can lead to a noticeable change in the $\tilde{E}_t$ behaviour (see, e.g., [CFGV86]). One reason is that τ can be close to some rational value, for which quantum resonance takes place. In addition, the expansion of the
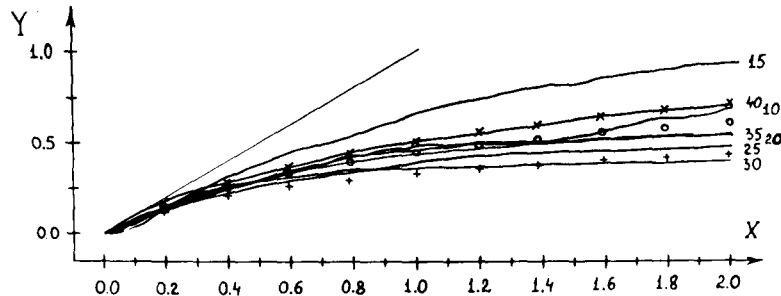

Fig. 13. The energy growth in the normalized variables Y and X [see (2.6.27)], for $K = 5$. The averaging is performed over 10 trajectories with different k around $k = 10, 15, 20, 25, 30$; as for $k = 40$, the only one trajectory has been examined. The initial state is $\psi_0(\theta) = 1/\sqrt{2} + \cos 2\theta$ with $N = 2048$ [for $k = 40$ the initial state is $\psi_0(\theta) = \exp(i\theta)$, $N = 8192$]. The values of Y are presented according to expression (2.6.27) for three values of β: $(\times)$ $\beta = 0.3$, $(\bigcirc)$ $\beta = 0.2$, $(+)$ $\beta = 0.1$. The straight line shows classical diffusion $Y = X$ (after [BI88]).

initial state $\psi_0(\theta)$ in exact EFs is sensitive to the value of k and τ. Nevertheless, the values of β does not fluctuate very much $(0.1 \lesssim \beta \lesssim 0.3)$ when k changes in the range $10 \leq k \leq 40$. It is important to note that the correspondence of the numerical data to (2.6.27) is also confirmed at large times, see an example in fig. 14.

It is now interesting to compare our analytical dependence (2.6.26) for $\tilde{E}_t$ with other results. For example, in [FGP87] the question of the scaling behaviour of E_t is investigated for the case when the classical parameter K is slightly above the global stability border $(K \gtrsim K_{cr} \approx 1)$. This border corresponds to the destruction of the last invariant curve that restricts unbounded diffusion in momentum space (see section 2.1). In particular, some scaling was found for the time t^*, which characterizes the crossover from classical to quantum behavior of the energy. The statement is that as the quantum parameter $\hbar$ scales to larger values then the crossover time t^* scales as $t^* \propto \hbar^{-1/\gamma}$. For the energy growth it gives [FGP87]

$$E_t = t\tilde{D}(\hbar^{1/\gamma}t) , \tag{2.6.28}$$

where $\tilde{D}$ is some function which depends on the quantity $\xi = \hbar^{1/\gamma}t$ only [for fixed classical parameters ε_0 and T in (2.2.1)]. Using a renormalization group approach, the value $\gamma \approx 3$ was found analytically. Numerical data [FGP87] for $K = 1.5$ on the short time scale, when the deviations of E_t from the classical behaviour are not very large, have been treated as a confirmation of the analytical prediction (2.6.28). To compare our result with (2.6.28) we rewrite (2.6.26) in the form

$$E_t = [D_{cl}(K)/2T^2]f(\tilde{\xi}) \approx \tfrac{1}{4}\varepsilon_0^2 tf(\tilde{\xi}) , \tag{2.6.29}$$

where the classical expression $D_{cl}(K)/(2T^2)$ stands in front of some function $f(\tilde{\xi})$,

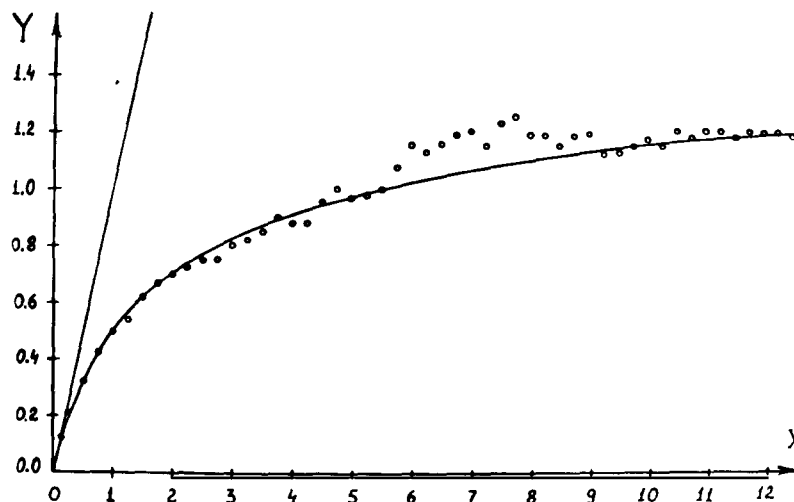$$f(\tilde{\xi}) = \frac{1}{\tilde{\xi}}\left(1 - \frac{1}{(1 + \tilde{\xi}/\beta)^\beta}\right) , \tag{2.6.30}$$

Fig. 14. Energy growth of the kicked rotator for large time $\tilde{t}_{max} = 4800$ and the parameters $K = 5$ and $k = 40$; the initial state is $\psi_0(\theta) = \exp(i\theta)$. The straight line is classical diffusion $(Y = X)$; the smooth curve corresponds to (2.6.27) with $\beta = 0.3$ and $D_{cl} = K^2/2$ (after [BI88]).

which depends only on the parameter $\tilde{\xi}$,

$$\tilde{\xi} = \frac{\tau^2 t}{D_{cl}(K)} = \frac{K^2 t}{D_{cl}(K)k^2} = \frac{T^2 \hbar^2 t}{D_{cl}(K)} .$$

(2.6.31)

This result is in apparent contradiction with [FGP87] because it gives a different scaling, $t^* \sim \hbar^{-2}$. It is important to note that the same scaling (2.6.31) corresponds to the known relation (2.2.16) with $\alpha = 2$ between the characteristic time t^* and the quantum parameter k ($t^* \sim k^2 \sim \hbar^{-2}$, see discussion in section 2.2). Since in the simulations [BI88] only the value $K = 5$ has been used, an additional comparison can be performed between (2.6.29) and the data of [FGP87] taking into account that the diffusion coefficient $D_{cl}(K)$ for $K = 1.5$ is determined by the second term in expression (2.1.9) [$D_{cl}(K) \approx 0.3(K - K_{cr})^3$]. The analysis shows that even in the region of incomplete classical chaos ($K = 1.5$) the dependence (2.6.29) is in good correspondence with the numerical data, giving $\beta \approx 0.2$ and $\beta \approx 0.35$ for the two most representative cases given in [FGP87]. Therefore, the scaling $t^* \sim \hbar^{-2}$ seems to be true over a wide range of K. From this point of view, the result of [FGP87] leads to the problem of the transition from one type of scaling, eq. (2.6.28), to another, eq. (2.6.31) when passing from $K \gtrsim 1$ to $K \gg 1$.

3. Maximal quantum chaos and its statistical properties

3.1. The quantum rotator model with a finite number of states

In the previous sections a model was discussed which has restricted statistical properties for any finite perturbation. In particular, the statistics of the quasienergy spectrum turns out to be very close to uncorrelated statistics with a Poissonian distribution for the spacings between nearest levels. Also, all eigenfunctions are generically localized in the unperturbed momentum space of the system. It was found that classical chaos manifests itself only in a special way, namely, in the random character of the eigenfunctions on a scale less than the localization length and in the level repulsion of those eigenstates which are significantly overlapping. Therefore, such a model cannot be used to study either maximal statistical properties of quantum dynamical systems or the transition from one limit case of regular motion to another one with completely chaotic motion. For this reason we pass here to a new model which seems to be richer in describing all interesting situations.

This model corresponds to the standard mapping (2.1.4), which is now assumed to be on a torus, rather than on a cylinder. Therefore, the phase space is now restricted both in phase θ and momentum p. As is known [C79, LL83], the local properties of the classical model (2.1.1) are the same for these two models due to the periodicity of momentum space [with period of $2\pi/T$ for (2.1.4) or 2π for (2.1.5)]. Nevertheless, the global properties are different since the phase space for the model on the torus is bounded in momentum resulting in the restriction of diffusion in the case of strong enough perturbation ($K > 1$). To quantize the standard mapping on the torus we follow the approach [I86, CIS88, I89] which is essentially based on the concept of quantum resonance (see section 2.5). Indeed, the quantum resonance condition appears when we require that the bounded momentum space is discrete and the total number N of states is integer,

$$N = 2\pi m_0/T\hbar = 2\pi m_0/\tau .$$

(3.1.1)

Here $2\pi m_0/T$ is the total size of phase space in momentum p with m_0 being the number of classical cells of period $2\pi/T$. It means that the momentum space is closed after m_0 periodic phase cells of the classical model (2.1.4). Comparing (3.1.1) with the quantum resonance condition (2.2.14) we obtain the relation $m_0 = 2rN/q$. For convenience, in what follows we consider only odd values of q [see (2.2.14)]; therefore, $N = q$ and m_0 is an even integer. Here, we just note that to quantize the classical model with m_0 odd we need to use a slightly different procedure which requires even values of q. Then, for quantum resonances with q an even integer, half of the eigenfunctions $\varphi(\varepsilon)$ turn out to be periodic in momentum space with period $N = q/2$, which is twice smaller than q. It allows us to construct the matrix U_{nm} of size $N \times N$ corresponding to odd values of m_0. The classical limit in such models means $k \rightarrow \infty$, $\tau \rightarrow 0$, $K = k\tau = $ const. with the additional conditions $N\tau = $ const. and $N \rightarrow \infty$.

Thus, according to the results of section 2.5, the behavior of the quantum rotator on the torus can be described by some finite unitary matrix U_{nm} of dimension $N \times N$. For the kicked rotator on the cylinder this matrix is known to depend on some parameter (Bloch number θ_0) which is related to the boundary conditions for the eigenfunctions [see (2.5.9)]. It is clear that in our new model this parameter has to be chosen as $\theta_0 = 0$. In this case all eigenfunctions are periodic in momentum with period $N = q$, resulting in the periodicity of the dynamics of the model under consideration. Finally, our model can be given by the matrix [I87]

$$U_{nm} = e^{i\tau n^2/4} \frac{1}{N} \sum_{l=-N_1}^{N_1} e^{-ik \cos(2\pi l/N)} e^{-2\pi i l(n-m)/N} e^{i\tau m^2/4} , \qquad (3.1.2)$$

where $n, m = -N_1, \ldots, N_1$ and $N = 2N_1 + 1$. Here $\tau = 4\pi r/N$ and the summation over l is shifted to obtain the most symmetric form of U_{nm} [compare with (2.5.12)–(2.5.14)].

This procedure of quantization of the standard mapping on the torus can be easily generalized for two-dimensional mappings of the form

$$p_{t+1} = p_t + \varepsilon_0 f(\theta_t) , \qquad \theta_{t+1} = \{\theta_t + Tp_{t+1}\} , \qquad f(\theta) = -V'(\theta) , \qquad (3.1.3)$$

with periodic potential $V(\theta + 2\pi) = V(\theta)$. The special case $f(\theta) = \theta$ and $\varepsilon_0 = 1/T$ is well known as the so-called "cat map" (see, e.g., [AA68, LL83]), which was, for the first time, quantized and studied in [HB80]. Recently, new results have been obtained for this model [R87a, FMR89]. In particular, it was found that the behaviour of the quantum cat map can be exactly described by the classical model on a discrete grid in phase space. This remarkable property is closely related to the linear character of the force $f(\theta)$ and can be regarded as exceptional. As was shown in [BIK88], for the general case of a nonlinear function $f(\theta)$ such a correspondence seems to be impossible.

The model (3.1.2) can be generalized by introducing nonzero values of the Bloch number θ_0. In this case the symmetry of the system under consideration turns out to be dependent on θ_0. This very important fact stems from the study of the properties of the unitary matrix U_{nm}. Indeed, for the kicked rotator on the cylinder the evolution operator $\hat{U}$ [see (2.2.3)] is invariant with respect to the change $\theta \rightarrow -\theta$ provided both $H_0 = -\frac{1}{2}\hbar^2 \, \partial^2/\partial\theta^2$ and $V(\theta) = \cos \theta$ have the same invariant properties $[H_0(\theta) = H_0(-\theta)$ and $V(\theta) = V(-\theta)]$. This implies the existence of an additional integral, which is parity. Correspondingly, the quasienergy functions $\varphi_\varepsilon(\theta)$ in the phase representation have to be either even or odd $[\varphi_\varepsilon(\theta) = \pm\varphi_\varepsilon(-\theta)$, see section 2.2]. In the momentum representation this property has the form $\varphi_n(\varepsilon) = \pm\varphi_{-n}(\varepsilon)$. It can be seen that such a symmetry of the eigenfunctions corresponds to the symmetry

$$U_{nm} = U_{-n,-m}$$ (3.1.4)

of the infinite matrix in (2.2.10). The same symmetry can be shown to exist for the model (3.1.2) in the case of parity conservation. It is easy to obtain that the relation (3.1.4) holds only for $\theta_0 = 0$ or $\theta_0 = \pi/N$ [see (2.5.12)–(2.5.14)] and is violated for other values $0 \le \theta_0 < 2\pi/N$. Therefore, the model with a finite number of states with $\theta_0 \ne 0$ can be regarded as some new dynamical system on the torus where parity conservation may be broken by the perturbation $[V(\theta) \ne V(-\theta)]$.

Another generalization of the model can be obtained by modifying the unperturbed Hamiltonian as

$$H_0 = -\tfrac{1}{2}\hbar^2 \, \partial^2/\partial\theta^2 + i\gamma\hbar \, \partial/\partial\theta , $$ (3.1.5)

where a new term is added which is linear in the momentum $\hat{p} = -i\hbar \, \partial/\partial\theta$. This term may be treated as a magnetic field with the corresponding strength parameter γ. Since the Hamiltonian (3.1.5) now is not real but complex, this results in the absence of the basis in which the eigenfunctions can be represented in real form. As is known, a system with a complex Hamiltonian has no time reversal invariance. This may not only affect the eigenfunctions but also the statistics of the spectrum [P65, BFFMPW81]. As a result, the generalized quantum system is determined by the unitary matrix

$$U_{nm} = \frac{1}{N} \exp[i(\tau n^2/4 - \gamma\tau n)] \sum_{l=-N_1}^{N_1} \exp[ik \cos(2\pi l/N + \theta_0)] \exp[-2\pi i l(n-m)/N]$$

$$\times \exp[-i\theta_0(n-m)] \exp[i(\tau m^2/4 - \gamma\tau m)] , $$ (3.1.6)

where both parity conservation and the time reversal invariance can be broken depending on θ_0 and γ. It can be shown that the time reversal invariance for the model (3.1.6) corresponds to the relation

$$U_{nm} = U_{-m,-n} , $$ (3.1.7)

which reflects an additional symmetry of the matrix elements [compare with (3.1.4)].

It should be noted that the above approach to obtain a model with a finite number of states is not a simple truncation of the evolution matrix (2.2.3) which breaks unitarity (see discussion in section 2.2). The procedure of construction of the finite unitary matrix (3.1.6) can be regarded as a new method to quantize nonlinear two-dimensional mappings of the type (3.1.3). Other approaches which also lead to finite unitary matrices can be found in [BBTV79, BB79, HB80, BV87, BV89] (see also references in [E88]). The most studied model of this kind is the so-called kicked top [FM86, HKS86, HKS87], which represents a three-dimensional quantum top subjected to periodic pulses. The relevant dynamical variables are the three components of angular momentum operator $\hat{J}$. Since the squared angular momentum is conserved, there is a good quantum number j defined by $\hat{J}^2 = j(j+1)$. It allows one to reduce the dynamics to some two-dimensional quantum map as in the above example. It is clear that the quantization in such models is natural provided the number of states is given by $N = 2j + 1$.

One should note that the potential richness of the model (3.1.6) is far from being exhausted. As was pointed out in [CIS88], this system may also be treated as a model of conservative dynamics. Indeed, in the classical limit a two-dimensional mapping of the type (3.1.3) is related to some conservative system of two degrees of freedom (see, e.g., [LL83]). Thus, such a mapping can be used to describe the local dynamics on the energy surface. To some extent, this should be true for the quantum model (3.1.6) as well.

Our main interest in the next two sections is the question of the maximal statistical properties of the model (3.1.6). Unlike the previous model (2.2.1) with an infinite number of states, the model (3.1.6) is expected to show strong statistical properties under some conditions. It is also of great importance to find the conditions for the appearance of such properties.

3.2. Limiting statistics of the quasienergy spectrum

In this section we shall discuss the maximal statistical properties of the quasienergy spectrum for the model (3.1.6). Unlike the kicked rotator model on a cylinder (2.2.1), we may expect now much stronger chaotic properties due to the possibility of full overlap for all eigenstates. This was not possible in the model (2.2.10) since all eigenstates are localized in the unbounded momentum space for any finite value of the perturbation k. In view of the above discussion one can assume that the strongest quantum chaos appears when the quantum parameter k is larger than the size of momentum space, $k \gtrsim N$, provided the classical chaos is also strong ($K \gg 1$). In this case the evolution matrix U_{nm} is expected to be of a very complicated structure; therefore, it is natural to compare its statistical properties with those of random unitary matrices. As was mentioned in section 2.4, the statistical properties of such matrices are well investigated by random matrix theory (RMT) and one of the commonly used quantities to characterize the spectrum is the distribution $P(s)$ of spacings between nearest quasienergy levels situated on a unit circle. This distribution is known to be closely related to the underlying symmetry of the matrix. For example, for symmetric matrices (circular orthogonal ensemble, COE) $P(s)$ is approximately described by the Wigner surmise (2.4.1) with $\beta = 1$. Correspondingly, for matrices which are not restricted by any symmetries (circular unitary ensemble, CUE) the repulsion parameter is $\beta = 2$. Coming back to our matrix (3.1.2) one should note that it has a symmetric form; therefore, the possible maximal repulsion of the quasienergy levels is linear ($\beta = 1$).

First numerical experiments [I84] with a model of the type (3.1.6) proved that with increasing perturbation $k \gg 1$ (for strong classical chaos, $K \gg 1$) the distribution $P(s)$ changes from Poisson-like [see (2.4.3)] to the Wigner distribution (2.4.1) with $\beta = 1$. A more detailed analysis of $P(s)$ depending on the symmetry of the evolution matrix has been performed in [I86], where the model (3.1.6) was studied in the θ-representation. As far as only irrational values $\tau \neq 4\pi r/N$ have been used in [I86], it is doubtful whether a corresponding classical system can be found especially with nonzero θ_0 and γ. For this reason, such a generalized model is meant as a generic quantum model which can demonstrate statistical properties under some conditions. We would again like to stress that all chaotic properties of these models are intrinsic in the sense that there are no random parameters and the behaviour is only determined by two dynamical parameters, one of which is classical while the other one is of a pure quantum nature. From this point of view, our interest is not in the exact correspondence to some classical model but in the investigation of statistical properties of the quantum model depending on these parameters. Since it was found that the general properties of the model (3.1.6) do not depend on whether the values of $\tau/4\pi$ are irrational or rational (if r/N is irreducible) we discuss here the main results of [I86] in the framework of our model (3.1.6).

First, we start with the symmetric case $\theta_0 = \gamma = 0$, which corresponds to the space reflection invariance of the system $[H_0(\theta) = H_0(-\theta)$ and $V(\theta) = V(-\theta)]$. As was noted, in this case the quasienergy functions $\varphi_\varepsilon(\theta)$ have to be either even or odd, $\varphi_\varepsilon(\theta) = \pm\varphi_\varepsilon(-\theta)$. This means that there are two sets of quasienergies which are independent of each other. Hence, the quasienergy spectrum should be treated independently for even-parity and odd-parity states. Extensive numerical data have shown that the distribution $P(s)$ is well described by the Wigner distribution (2.4.1) with $\beta = 1$. The

correspondence of the data to this analytical expression is confirmed by using the statistical χ^2 approach (see [I86]). To improve the statistical significance NG matrices U_{nm} have been used with slightly different parameters k. Because of the strong sensitivity of the quasienergy levels to small changes in the parameter k (with step $\Delta k \ll k$), these sequences of levels can be regarded as mutually independent. Also, the distributions $P(s)$ for even and odd eigenfunctions have been summed. As a result, the total number M of spacings in [I86] was quite large ($M = 1990$ with $N = 199$) to assert good correspondence to the RMT prediction. In this simulation the extremely large value $k \approx 20\,000$ was taken as a limit case of the strongest perturbation (the classical parameter is also very large $(K \approx k)$, but this is not very important since for $K \gtrsim 5$ the result is not sensitive to the value of K). As was said above, in this case the model (3.1.6) is not only space reflection invariant but time reversal invariant as well. Correspondingly, the matrix U_{nm} turns out to be symmetric about two main diagonals [see (3.1.4) and (3.1.7)], which reduces the total number of independent matrix elements by a factor of $1/4$. It means that each set of eigenfunctions (odd and even parity) are described by some unitary matrices of size $N/2 \times N/2$ which should be symmetric. This makes clear why the distribution $P(s)$ corresponds to $\beta = 1$.

The distribution $P(s)$ with linear repulsion has been found to appear also when only the unperturbed motion is space reflection invariant, $H_0(\theta) = H_0(-\theta)$ and $V(\theta) \neq V(-\theta)$. In the model (3.1.6) it corresponds to the values $\theta_0 \neq 0$ or π/N (with $\gamma = 0$); this breaks the parity (3.1.4) but the system remains time reversal invariant. According to the condition (3.1.7) the matrix U_{nm} halves the number of independent elements and, therefore, can be represented in symmetric form. Again, this case is expected to correspond to a circular orthogonal ensemble (COE). Indeed, the numerical data [I86] showed the same Wigner dependence for $P(s)$ with $\beta = 1$.

The most interesting result has been obtained for the case of $H_0(\theta) \neq H_0(-\theta)$ but $V(\theta) = V(-\theta)$ [$\theta_0 = 0$ and $\gamma \neq 0$ in the model (3.1.6)]. It was unexpectedly found that $P(s)$ again corresponds to (2.4.1) with $\beta = 1$. This result is in clear contradiction with Dyson's prediction, which claims that in the case of broken time reversal invariance such systems with very complex behaviour should be described by the circular unitary ensemble (CUE) with $\beta = 2$ for $P(s)$. Nevertheless, our model turns out still to have some additional symmetry, which is clearly seen from the structure of U_{nm}. Indeed, in spite of the broken parity in the unperturbed part of the Hamiltonian $(H_0 = -\frac{1}{2}\hbar^2 \, \partial^2/\partial\theta^2 + i\gamma\hbar \, \partial/\partial\theta)$ due to the additional linear term in momentum, some symmetry of the form

$$U_{nm} = U_{mn} \,,$$
(3.2.1)

remains. Then again the number of independent elements is twice less than in the case of CUE. Such an effect has been found also for some autonomous models [SV85, SV85a] where $P(s)$ appeared to correspond to $\beta = 1$. In the general case this result has been explained in [RB86, BR86], where a theory was developed based on the existence of a special type of symmetry not taken into account in Dyson's approach. We observe the appearance of this symmetry (so-called antiunitary symmetry) in our model (3.1.6) for $\theta_0 = 0$ and $\gamma \neq 0$. The physical meaning of this symmetry is the conservation of TP invariance for the system under the transformation $t \rightarrow -t$ together with $\theta \rightarrow -\theta$.

Finally, for the model in which the symmetries in both H_0 and V are broken [$H_0(\theta) \neq H_0(-\theta)$ and $V(\theta) \neq V(-\theta)$, or $\theta_0 \neq 0$, π/N and $\gamma \neq 0$], a distribution $P(s)$ is obtained with quadratic $(\beta = 2)$ repulsion (see fig. 15). In this case no additional symmetries exist and the matrix U_{nm} is of general form with $N \times N$ independent complex matrix elements.

The above results show that the maximal statistical properties of the quasienergy spectrum are well described by random matrix theory. This fact is far from trivial because our model (3.1.6) is not random
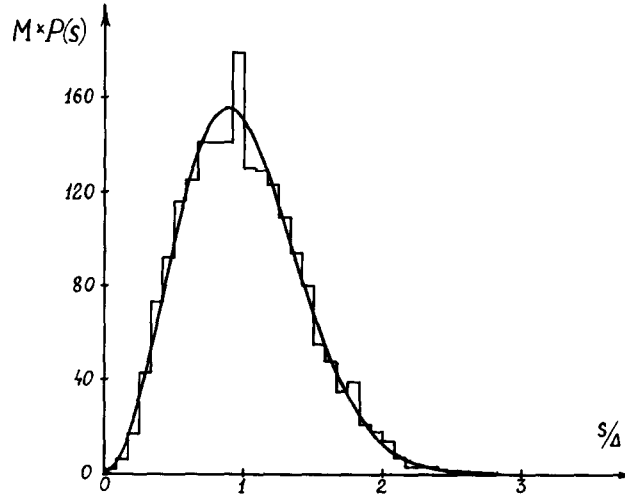
Fig. 15. Distribution $P(s)$ for the model (3.1.6); s is the distance between the nearest eigenvalues ε_i on the unit circle; Δ is the mean spacing; $\theta_0 \approx 8 \times 10^{-4}$, $\gamma = 1/\sqrt{2}$, $\tau = 1/\sqrt{3}$, $k = 20\,000$, $N = 199$, $M = N \cdot NG = 1990$. The smooth curve gives the analytical dependence (2.4.1) with $\beta = 2$; the numerical data show quite good correspondence ($\chi^2_{27} \approx 18.9$ with $P_w \approx 65\%$ confidence level) (after [I86]).

and only when both K and k are large enough do the spectral characteristics [at least the spacing distribution $P(s)$] appear to be the same as for random unitary matrices. One of the important questions is to find the conditions under which such properties appear. As was noted, the values of the parameters K and k used in [I86] were very large. Now our interest is to find a parameter which characterizes the proximity of our model to the limit case of a random matrix. As a related physical parameter one can take the parameter Λ which was introduced in section 2.4,

$$\Lambda = l_\infty/N \approx k^2/4N ,$$

(3.2.2)

which is the ratio of the localization length l_∞ to the size of the system in momentum p. Let us note that l_∞ is determined for the eigenstates in the model with infinite momentum space; therefore, for the model with bounded momentum space it has the sense of a localization length only when $l_\infty \ll N$. According to our approach, this parameter shows that in the case of large $\Lambda \gg 1$ one may expect that all eigenfunctions fully overlap in the momentum space of the model (3.1.6). This fact seems to be most important for the appearance of strong statistical properties. Of course, it is also assumed, here and in the following, that the condition of strong classical chaos holds ($K \gg 1$).

Indeed, numerical data show [I86, I87, CIS88] that for $\Lambda \gg 1$ the spacing distribution $P(s)$ is close to the Wigner distribution. A typical example is given in fig. 16 [I87], where the distribution $P(s)$ has been obtained for the model (3.1.6) of size $N = 199$ with $K \approx 11.4$ and $k \approx 60$. The symmetrical case is used, $\theta_0 = 0$ and $\gamma = 0$, with the resonant value $\tau = 12\pi/N$. The histogram is obtained by the same procedure as described above (by summing over a number of different histograms $P(s)$ with slightly different k for odd- and even-parity states). The correspondence of the data to the theoretical dependence (2.4.1) with $M = 995$ is quite good (the χ^2 value for 24 subintervals is $\chi^2_{24} \approx 20.1$, with a high confidence level, $P_w \approx 30\%$). The value of Λ is $\Lambda \approx 6.5$ provided the localization length is found in accordance with the classical relation (2.1.9). Let us note that here l_∞ should be compared with $N_1 = (N - 1)/2$, not with N, because of the symmetry about $n = 0$ (see fig. 4).
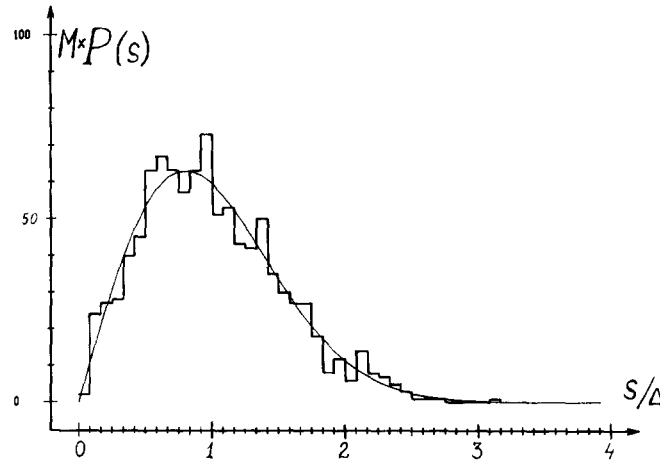
Fig. 16. Distribution $P(s)$ for the model (3.1.6) with $\theta_0 = \gamma = 0$, $\tau = 12\pi/N$, $K \approx 11.4$, $k = 60$, $\Delta k = 1.0$, $N = 199$, $N_1 = 99$, $NG = 5$. The total number of eigenvalues is equal to $M = 990$; here the mean spacing is equal $\Delta = 1/N_1$ due to parity conservation. The χ^2 value for $\beta = 1$ in relation (2.4.1) gives $\chi_{24}^2 \approx 20.1$ with $\approx 30\%$ confidence level (after [I87]).

With decreasing Λ the distribution $P(s)$ starts to deviate from the Wigner law and approaches the Poisson dependence. According to the numerical data, values of $\Lambda \approx 5$–10 seem to be critical for the closeness of $P(s)$ to the limiting form. With this parameter Λ it is possible to predict the appearance of strong statistical properties. The importance of Λ is confirmed by recent simulations [FM88] for the model (3.1.6) with different N. The data showed the existence of two extreme regimes for the spacing distribution $P(s)$, the Poisson and Wigner laws. However, it turned out to be very difficult to analyse the result without the parameter Λ indicating under which conditions one may expect the Wigner distribution (see the discussion of these data in [FFGP88, FM88a]).

Recently [S89a] the model (3.1.6) was generalized by assuming that the particle (rotator) has half-integer spin. Therefore, the unitary matrix U_{nm} appears to be of symplectic form, with total number of matrix elements $2N \times 2N$. As is known from RMT, the spacing distribution $P(s)$ for unitary symplectic random matrices should be of the form (2.4.1) with quartic repulsion between neighbouring levels ($\beta = 4$). Therefore, such a distribution is also expected in this half-integer spin model. The numerical simulation [S89a] confirmed this prediction.

To conclude this section, it should be mentioned that there are similar results with the kicked top model [KSH87, SDKHB88], for which the distribution $P(s)$ of the quasienergy level spacings also manifests all these limiting types of distribution with $\beta = 1$, 2, 4 depending on the symmetry of the model. Also, there are many results concerning autonomous systems where the statistics of the energy spectrum was thoroughly investigated (see, e.g., the reviews [E88, E88a]).

3.3. Chaotic structure of the quasienergy eigenfunctions

Unlike the spectral statistics, little is known about the structure of the eigenfunctions for quantum systems which are strongly chaotic in the classical limit. As we could see, for the kicked rotator on a cylinder (2.2.1) the only more or less rigorous results are the exponential localization of all eigenfunctions $\varphi_n(\varepsilon)$ as $|n| \to \infty$ (see section 2.3) and an estimate of the average localization length l_∞. As for the structure of the eigenfunctions on a scale less than l_∞, numerous data show that it seems to be chaotic. Nevertheless, up to now, there are no clear results on this subject.

The above model (3.1.6) with a finite number of states appears to be more suitable to study the structure of the eigenfunctions (EF) as a function of the parameters of the system. This is related to the possibility of investigating the full transition from localized states to maximal quantum chaos, for $K \gg 1$ and $\Lambda \gg 1$. From the point of view of the EF properties the latter conditions (for nonresonant values of $\tau/4\pi$) mean that all EFs are completely delocalized (extended) in the bounded momentum space of the system provided strong classical chaos occurs in the corresponding classical model. This case is treated as a limiting one with the expectation of maximal statistical properties for the EFs. The only rigorous statement for this limiting case is Shnirelman's theorem [S74] (see also [B77, V79]), which claims that the eigenfunctions should be ergodic in the whole phase space of the system when the corresponding classical system is chaotic. By the ergodicity for quantum systems we mean that there exists only one integral of the motion, the energy, and the EFs in the Wigner representation uniformly fill an energy band of finite width corresponding to the energy surface in the classical limit (see the reviews [P84, E88, E88a]). Also, there is some conjecture about the Gaussian character of fluctuations for the eigenfunction components [B77]. There are also a number of papers where these properties are discussed for autonomous systems (see, e.g., [BGR82, SG84, MK88] and the review [SH84]), but as for the time-periodic models, the study of the statistical properties of quasienergy eigenfunctions is still at the beginning.

In this section we present the main results concerning the structure of the eigenfunctions for the model (3.1.6) in the limiting case, for $K \gg 1$ and $\Lambda \gg 1$, when the statistics of the spectrum shows very nice correspondence to the predictions of RMT (see previous section). A typical example of an EF under such conditions is presented in fig. 17, where the probability $w_n = |\varphi_n(\varepsilon)|^2$ of the EF with some quasienergy ε is plotted in the unperturbed basis n. First, we discuss the data concerning the ergodicity of the EF.

Before we pass to the data, one should note that there is the delicate question about the basis in which we study the EF structure. It is clear that there exist bases in which the eigenfunctions are very well localized for any values of the parameters (in our model, for any K and k). Indeed, there is a special basis where all EFs are completely localized, namely, the basis where the matrix U_{nm} is diagonal. Therefore, there is some measure in N-dimensional Hilbert space corresponding to the bases which are close to diagonal. It means that all results concerning the statistical properties of EFs, strictly speaking, are not invariant with respect to the choice of the basis. However, the answer is that this measure is negligibly small in N-dimensional space; hence, it is very unlikely that we choose such a special basis in advance; for this reason we can treat these bases as exceptional ones. We could recall that the same problem appears also in random matrix theory, without any serious consequences. Nevertheless, for physical applications we should be careful since, actually, the choice of the basis very often is associated with the basis in which the unperturbed Hamiltonian has a diagonal form. It means that the basis in some cases is physically defined and only for strong enough perturbation does this choice seem to be unimportant.

For convenience, only odd-parity eigenstates φ_n were examined in the model (3.1.6), namely, $\varphi_n = -\varphi_{-n}$. Then, as was noted in the previous section, the total number of components is $N_1 = (N-1)/2$ (N is an odd integer). Under the condition $l_\infty \gg N_1$ it is natural to expect (for $K \gg 1$) that all probabilities $w_{nm} = |\varphi_{nm}|^2$ are equal on average [here $\varphi_{nm} \equiv \varphi_n(\varepsilon_m)$ with ε_m as the quasienergy]. To be more precise, we define ergodicity by the relation
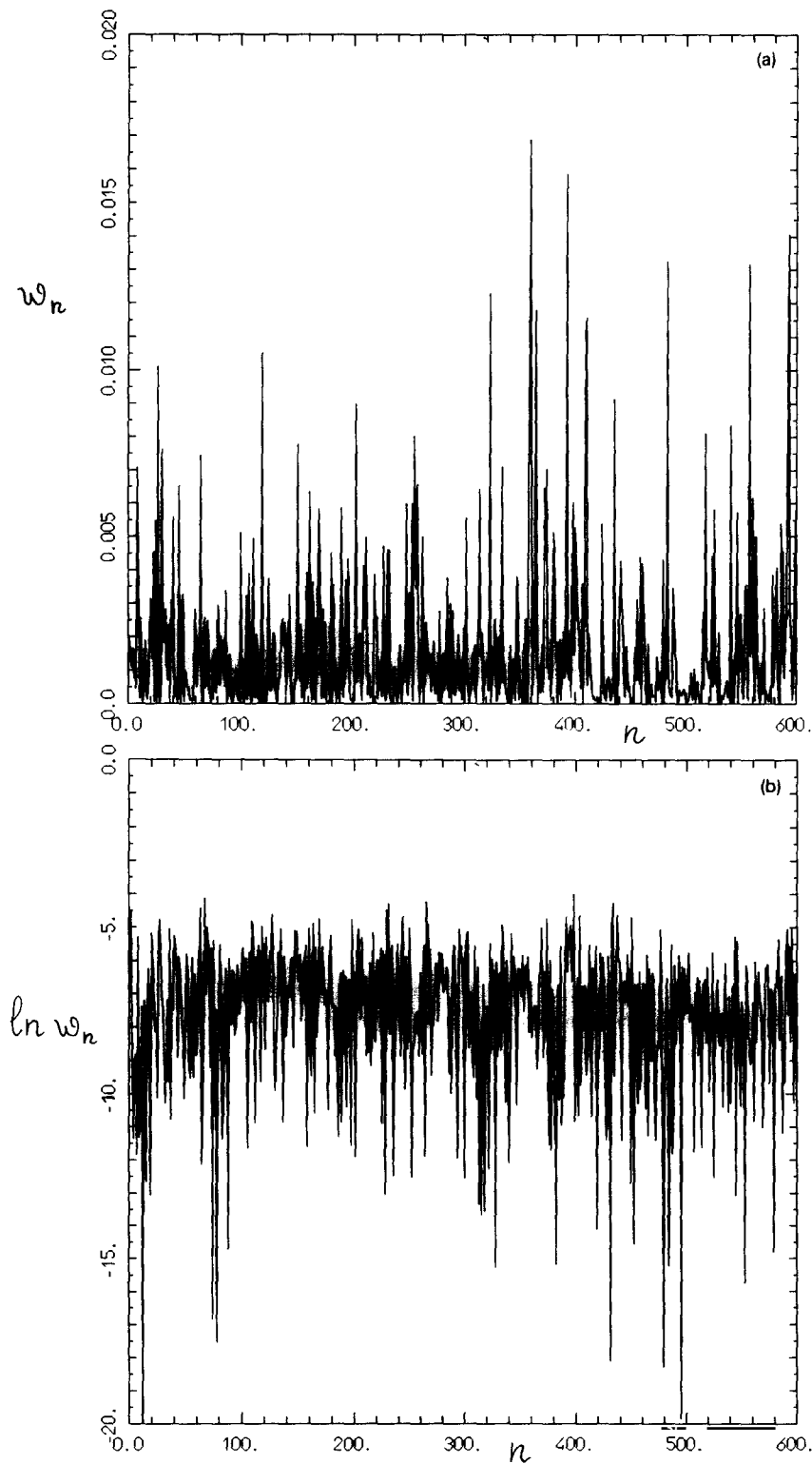
$$\langle w_{nm} \rangle = 1 , \tag{3.3.1}$$

Fig. 17. Typical eigenfunction in the unperturbed basis for the model (3.1.6) is shown for $\theta_0 = \gamma = 0$, $\tau = 8\pi/1201$, $k = 240$, $K \approx 5$, $N_1 = 600$, $N = 1201$, $\Lambda = k^2/(4N_1) \approx 24$. (a) On the vertical axis the probability $w_n = |\varphi_n|^2$ is plotted; (b) the same as (a), on a logarithmic vertical scale.

with the normalization condition $\sum_{n=1}^{N_1} w_{nm} = N_1$. The averaging in (3.3.1) is performed over the elements of the same eigenfunction or over different eigenfunctions in the same matrix U_{nm}, or over a number of matrices U_{nm} with different parameters of the model (3.1.6). Such a definition is in accordance with the RMT (see, e.g., [BFFMPW81]). Other equivalent definitions of ergodicity are discussed in [S74, B77, V79]. It should be noted that the matrix φ_{nm} not only represents the transformation from the unperturbed basis to the basis where the matrix U_{nm} is diagonal (the basis of eigenfunctions) but the transformation back to the unperturbed basis as well. This results from the fact that the matrix φ_{nm} is orthogonal. As a result, the relation $\sum_{m=1}^{N_1} w_{nm} = N_1$ also holds; therefore, the averaging over all elements w_{nm} automatically gives $N^{-2} \sum_{n,m}^{N_1} w_{nm} = 1$. For this reason, the averaging in (3.3.1) has to be done over those elements which belong to the same matrix.

Some data are summarized in table 1 for $N = 51$ (correspondingly, $N_1 = 25$) and $\tau/4\pi = 4/N$, $m_0 = 8$. The average values $\langle w_{nm} \rangle$ were found in the following way. Each of N_m matrices with close values of k was divided into N_s equal squares of size $L \times L$. Then, for each of these squares with index $i = 1, 2, \ldots, N_s$ the sum

$$S_i = \frac{1}{L^2} \sum_{n,m}^{L} w_{nm} \qquad (3.3.2)$$

was computed. The numerical data discovered very strong fluctuations for the element w_{nm} in the case $l_\infty \gg N_1$. Therefore, as an indication of the ergodic character of the EF, the decay of the dispersion σ^2 can be taken for the deviation of the sum S_i from its average value, when the number of terms in (3.3.2) is increased. The dispersion for S_i is found in the usual way,

$$\sigma^2(L) = \frac{1}{N_s} \sum_{i=1}^{N_s} (S_i - \langle S \rangle)^2, \qquad \langle S \rangle = \frac{1}{N_s} \sum_{i=1}^{N_s} S_i. \qquad (3.3.3)$$

The quantity (3.3.3) has been found in the simulation for three values of L: for each element of the matrix ($L = 1$) and for the sums S_i obtained by dividing the matrix in such a way that $L = 5$ and $L = 12$. For each variant, in turn, two sorts of averaging have been done: over the elements of one matrix ($N_m = 1$) and over the elements of 20 matrices ($N_m = 20$) with different k (with step $\Delta k \ll k$). The data show that the values of $\langle S \rangle$ are close to 1, in accordance with the ergodicity conjecture. In addition, the values of σ^2 for $\Lambda > 1$ appear to decay very fast with decreasing L.

A theoretical value for σ^2 can be found from the distribution of the elements of a random matrix taking into account the correlations between the matrix elements due to the finite size of the matrix

Table 1
Numerical data for the dispersion σ^2. $N = 51$, $N_1 = 25$, $\tau/4\pi = 4/N$, $m_0 = 8$

					Dispersion σ^2		
					$L = 1$	5	12
K	k	Λ	Δk	N_m	$N_s = 625$	25	4
19.7	20.0	5	–	1	1.74 ± 0.14	0.038 ± 0.014	0.0041 ± 0.0010
~20	~20	5	0.2	20	0.88	0.022	0.0028
5.0	5.0	0.25	–	1	2.80 ± 0.58	0.215 ± 0.057	0.0015 ± 0.0012
≈5.0	≈5.0	0.25	0.1	20	1.18	0.044	0.005
theory (3.3.4):					1.77	0.05	0.0036

(see, e.g., [BFFMPW81]),

$$(\sigma^2)_{\rm T} = 2(N_1 - L)^2/L^2(N_1 - 1)(N_1 + 2) .$$ (3.3.4)

To derive this expression, a specific form of the fluctuations for the matrix elements φ_{nm} of a unitary random matrix was taken into account. In this sense, comparison of (3.3.4) with the numerical data for σ^2 allows one to obtain some information about both the ergodicity and the character of the fluctuations for φ_{nm}.

Let us first discuss the case of large k, $k \approx 20$, when the localization length $l_\infty \approx 130$ is much larger than the maximal dimension N_1 of the EF. From table 1 it is seen that the dispersion σ^2 for one matrix $(N_m = 1)$ is in good agreement with the expected value (3.3.4). The mean squared value given in table 1 is obtained from 20 different matrices with close k (see the line with $N_m = 20$). At the same time, the averaging over 20 matrices $(N_m = 20)$ does not give the expected decrease (by a factor of 20) compared with the averaging only over one matrix. This may mean that the change in the parameter k is not large enough to make the eigenfunctions of the different matrices completely independent.

For comparison, now we discuss the opposite case, when l_∞ is much less than N_1 (two bottom lines in table 1). It is seen that the nonergodic character of the EFs found for $N_m = 1$ is also confirmed by the data for $L = 1$ and $L = 5$ [all values of σ^2 are larger than the theoretical ones, $(\sigma^2)_{\rm T}$]. Meanwhile, one should note the anomalous (small) value of σ^2 for $L = 12$. This result can be explained as follows. As is seen, the localization length l_∞ is of the same order as the size L over which the averaging is performed. This means that some specific EF may be essentially concentrated within the averaging interval. Correspondingly, in the other intervals there are many small values of w_{nm}, which results in additional correlations between the sums S_i. On the whole, the data for $\Lambda \approx 0.25$ indicate that there is a strong deviation from the ergodic character of the EF in comparison with $\Lambda \approx 5$. The clearest evidence for this is given by the dispersion found from the averaging over blocks of size $L = 5$.

A more interesting question concerns the type of fluctuations of the components of the EF, φ_{nm}. The Gaussian form of the fluctuations, in general, has been analysed in several papers [B77, BGR82, SG84, MK88] and seems to be the strongest chaotic property of the eigenfunctions. Here we discuss some of the results [CIS88] for the model (3.1.6).

Because the matrix U_{nm} for $\theta_0 = 0$ and $\gamma = 0$ is symmetric, the real and imaginary parts of $\varphi_n(\varepsilon)$ coincide. Hence, it is sufficient to study only the real part of the EF. For this, it is convenient in a numerical simulation to pass from the matrix U_{nm} to its real part, $\mathrm{Re}(U_{nm})$, whose EFs are the real parts of the EFs of $\varphi_n(\varepsilon)$. This property is due to the symmetry and unitarity of our matrix U_{nm}. Also, only odd-parity EFs are considered, for which the maximal dimension in N-dimensional Hilbert space is N_1, not N. A typical result for the case of completely delocalized $(\Lambda \gg 1)$ and chaotic $(K \gg 1)$ states is shown in fig. 18, where the histogram of the components of the EF in the unperturbed $(k = 0)$ basis is given. To improve the statistics, NG matrices of size N have been considered for different values of k (with step $\Delta k \ll k$). The total number of φ_n components is equal to $M = NG \cdot N_1 \cdot N_1 = 12\,500$.

At first glance, we may conclude that the data correspond to a Gaussian distribution,

$$w(\varphi_n) = \sqrt{N_1/2\pi} \, e^{-\varphi_n^2 N_1/2} ,$$ (3.3.5)

assuming ergodicity, $\langle \varphi_n^2 \rangle = 1/N_1$ and $\langle \varphi_n \rangle = 0$. Nevertheless, this conclusion is wrong since the χ^2 value points to an extremely bad correspondence to a Gaussian law. Indeed, $\chi_{38}^2 \approx 98$ (for 38 intervals), which gives a negligible confidence level $<10^{-6}$. Hence, in spite of the Gaussian-like shape of $w(\varphi_n)$, the fluctuations are certainty not Gaussian.
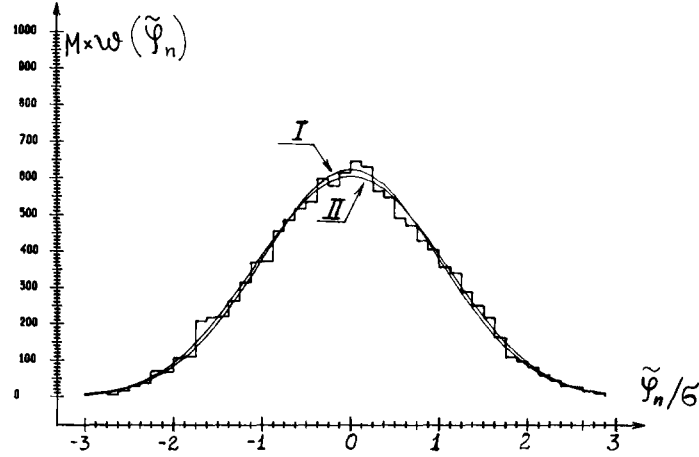
Fig. 18. Distribution of the components φ_n of the EF for the model (3.1.6) with $N = 51$, $NG = 20$, $\tau = 16\pi/N$, $K \approx 5$, $\Delta k = 0.1$, $l_\infty \approx 130$, $\Lambda \approx 5.2$. Curve II is the Gaussian distribution (3.3.5), curve I is the distribution (3.3.6) with $N_1 = 25$; here $\tilde{\varphi}_n^2 = N_1\varphi_n^2$, $M = N_1^2 \cdot NG$.

The explanation of this surprising disagreement relies upon the finite dimension, N_1, of the eigenfunctions. As a result, φ_n fluctuations are strictly bounded by the condition $\varphi_n^2 \leq 1$; therefore, an exact Gaussian distribution appears only in the limit $N_1 \to \infty$. In the spirit of RMT, instead of (3.3.5) we should assume that the EFs are to be invariant under rotation of the N_1-dimensional basis. Then the distribution takes the form [BFFMPW81]

$$w_{N_1}(\varphi_n) = \frac{\Gamma(N_1/2)}{\sqrt{\pi}\Gamma((N_1 - 1)/2)} (1 - \varphi_n^2)^{(N_1-3)/2} , \tag{3.3.6}$$

where Γ is the gamma function. This distribution is also shown in fig. 18 (curve I), which looks very similar to the Gaussian distribution (3.3.5). However, the χ^2 criterion ($\chi_{38}^2 \approx 56$ with 3% confidence level) clearly indicates a much better agreement of the numerical data with (3.3.6). This means that the φ_n fluctuations are the same as those predicted by random matrix theory. With increasing N the deviation of $w_{N_1}(\varphi_n)$ from a Gaussian distribution decreases (see fig. 19), in agreement with (3.3.6). Universality of the eigenvector statistics has recently been found also for the kicked top [KMH88].

The above result is quite instructive from the point of view of a quantitative comparison of numerical data with analytical predictions. As we could see, the χ^2 approach turns out to be very useful in such situations. It is interesting to note that the use of the χ^2 value allows one to determine the effective dimension N_1 of the EF. As numerical data show, when the parameter N_1 in (3.3.6) is changed, the χ^2 value discovers the minimum exactly for the actual maximum value $N_1 = (N - 1)/2$.

An additional check of the distribution (3.3.6) consists of the calculation of the moments m_k, normalized to unity in the limit of a Gaussian distribution. For the parameters of fig. 16 the three first even moments m_2, m_4 and m_6 are

$$\langle m_2^{exp} \rangle = \langle \varphi_n^2 \rangle = 0.999 , \quad \sigma_2 = 0.012 ,$$

$$\langle m_4^{exp} \rangle = \langle \varphi_n^4 \rangle = 0.888 , \quad \sigma_4 = 0.030 , \tag{3.3.7}$$

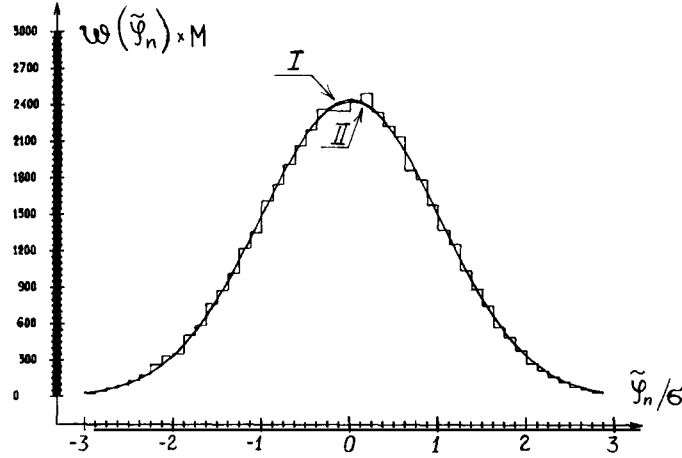$$\langle m_6^{exp} \rangle = \langle \varphi_n^6 \rangle = 0.703 , \quad \sigma_6 = 0.068 .$$

Fig. 19. The same as in fig. 18 for the parameters of fig. 17. Comparison of the data with the Gaussian distribution (3.3.5), curve II, gives $\chi^2_{48} \approx 56.7$ with $P_w \approx 36\%$ confidence level; correspondingly, for the distribution (3.3.6), $\chi^2_{48} \approx 50.0$ with $P_w \approx 20\%$.

The mean squared values σ_k, which are also given, were found by averaging over 20 different matrices U_{nm}. Since some correlations may exist between the different U_{nm}, the dispersion for the means, in general, is not equal to $\sigma_k/\sqrt{20}$. Nevertheless, if one assumes that the mean deviation is of the order of σ_k, then it is seen that the differences of $\langle m_4^{exp} \rangle$ and $\langle m_6^{exp} \rangle$ from 1.0 are not accidental. The theoretical values for m_k can be found from (3.3.6),

$$m_2 = 1 , \qquad m_4 = N_1/(2 + N_1) \approx 0.926 , \qquad m_6 = \frac{1}{(1 + 2/N_1)(1 + 4/N_1)} \approx 0.798 . \qquad (3.3.8)$$

These data also prove that the deviations from the Gaussian distribution are in agreement with random matrix theory.

All above results discussed in sections 3.2 and 3.3 give strong evidence that our dynamical model shows in some limit statistical properties which are known for random matrices. One interesting conclusion is that the matrix U_{nm} can be treated as pseudorandom, depending only on two parameters, K and k. Therefore, we have some approach to construct pseudorandom unitary matrices of different symmetries. This might be useful in some applications.

A serious question arises when comparing these results with those known for autonomous systems. It was found [H84, STB84, CB85, CH88] that the eigenfunctions in some quantum models (for example, in the billiard model) have so-called "scars", which seems to be in contradiction with the conjecture of the random character of the EFs in the classical limit. These scars appear for some eigenfunctions in the coherent state representation (or in the Wigner representation) in the form of increased density in the regions of phase space where unstable periodic trajectories of low periods are situated. This property of EFs in the semiclassical limit seems to be generic for many autonomous models (see, e.g., the review [G89]). Now it is understood that this effect is not in contradiction to Shnirelman's theorem, since this theorem proves the ergodicity of the EF in integral form. This means that an increased density is allowed in some narrow regions of phase space of size $\sim \hbar$. Since the thickness of these scars appears to be proportional to $\hbar$, it is clear that after averaging over the energy surface the scars disappear. However, the structure of the EFs in the coherent state representation cannot be treated as random since the regions with increased density are well predicted from the consideration of periodic orbits of

the corresponding classical system. Again, it should be noted that only strongly chaotic models are here discussed, without significant stable regions in the classical phase space.

Recently, new results have appeared [BV89] concerning some quantum maps, where the scars were also found. Thus, the quasienergy eigenfunctions seem to have the same scar properties. This poses the very interesting question whether the correlations caused by the existence of these scars can be detected in the distribution $w(\varphi_n)$ or if they are "washed off" when passing from the coherent state representation to the θ-representation. To get the answer to this question, more detailed simulations are needed.

4. Statistical properties of quantum chaos in the presence of localization

4.1. Intermediate statistics of the spectrum and Dyson's Coulomb gas

Now we pass to the study of so-called intermediate quantum chaos, by which the restricted statistical properties of quantum systems are meant while the corresponding classical model is strongly chaotic. As we could see, for the model with a finite number of states (3.1.6) this situation arises when the classical parameter K is large ($K \gtrsim 5$) but quantum localization effects suppress the chaotic properties. It was shown above that the relevant parameter Λ for the prediction of such a situation is the ratio of the average localization length l_∞ to the total number of states. In particular, the level spacing distribution $P(s)$ in this case appears to be different from the limiting Wigner distribution (2.4.1) and approaches the other limiting case of uncorrelated Poisson statistics when Λ decreases.

Our conjecture is that the statistics of the quasienergy spectra can be quantitatively related to the EF structure. We should note that here we are discussing only the relatively simple case when classical chaos is strong; therefore, all effects essentially depend only on the degree of localization, or on the quantum parameter k. The general situation, when the classical parameter K also affects the spectral statistics ($K \lesssim 1$), is much more difficult because the features of classical dynamics then should be taken into account (see discussion in section 5). For this reason, we restrict ourselves only to an analysis of strong classical chaos, when K is fixed and large enough ($K \gtrsim 5$).

To relate the level spacing distribution to the degree of localization, first we need some analytical description of $P(s)$. In the literature one can find two analytical formulae in the description of the transition from Poisson to Wigner statistics (see, e.g., the reviews [E88, E88a]), one of which is the well-known Berry–Robnik dependence [BR84, R87]. This dependence is commonly used to describe the intermediate statistics of the spectrum for the situation when the corresponding classical system has significant regions of stable motion in phase space. The only parameter in the Berry–Robnik dependence is exactly the ratio of the area with stable motion to that of chaotic motion. It is clear that for our case of strong classical chaos this formula is not valid. In some sense, the Berry–Robnik expression deals with a situation which is opposite to our case. Namely, the deviation of the Berry–Robnik distribution from the limiting Wigner distribution is entirely caused by the classical effect (the existence of stable regions), while in our case the intermediate statistics is of a pure quantum nature (localization).

Another known expression for $P(s)$ is the so-called Brody distribution [B73], which is nothing but some approximate dependence with the only fitting parameter α,

$$P(s) = As^\alpha e^{-Bs^{1+\alpha}} , \quad A = 1 + \alpha , \quad B = [\Gamma((2 + \alpha)/(1 + \alpha))]^{1+\alpha} . \tag{4.1.1}$$

Here Γ is the gamma function and the repulsion parameter α varies in the range $0 \le \alpha \le 1$. Since this formula has no physical basis, it is useless for our purpose. In addition, the dependence (4.1.1) is wrong for $\alpha > 1$, which is important for us in view of application to models discovering stronger repulsion ($\beta = 2, 4$, see section 3.2).

For this reason, we need some new approach in deriving the distribution $P(s)$ (see also [I87, I88]). The proposed way to construct $P(s)$ is associated with the theory of unitary random matrices developed by Dyson [D62, P65]. The core of this theory is the physical model of a two-dimensional gas of N equally charged particles moving on the unit circle, with positions denoted by the angles θ_j and interacting via a Coulomb force. The partition function of such a gas with inverse temperature $\beta = 1/T$ is

$$Z_N(\beta) = \frac{1}{(2\pi)^N} \int_0^{2\pi} e^{-\beta W} \, d\theta_1 \cdots d\theta_N ,$$ (4.1.2)

where the potential energy W is given by

$$W = - \sum_{1 \le j < k \le N} \ln \left| e^{i\theta_j} - e^{i\theta_k} \right| .$$ (4.1.3)

Then, the joint distribution of the angles θ_j is

$$Q_{N\beta}(\theta_1, \theta_2, \ldots, \theta_N) = \frac{1}{Z_N(\beta)} \prod_{1 \le k < k \le N} \left| e^{i\theta_j} - e^{i\theta_k} \right|^{\beta} .$$ (4.1.4)

Here the trivial part of the partition function, which depends on the momentum, is omitted. It turns out that for the specific values $\beta = 1, 2$ and 4, expression (4.1.4) is exactly the same as the joint distribution of the eigenphases of the circular ensembles of random matrices [with the normalization constant $Z_N^{-1}(\beta)$]. Therefore, by investigation of this physical model it is possible to deduce some quantities describing the statistical properties of random matrices. In this way many results have been obtained [D62, P65]; however, the exact analytical form of the spacing distribution $P(s)$ has not been found due to great mathematical difficulties. Later, by making use of Mehta's approach [P65, M67], $P(s)$ was found numerically to a great accuracy (see also recent results [DH90]). Comparison of the exact data for $P(s)$ with the Wigner surmise (2.4.1) has shown that the latter dependence is very close to the exact one and can be used in almost all real situations [D62].

In Dyson's approach the thermodynamics of the Coulomb gas with the partition function (4.1.1) was studied for any temperature $T = 1/\beta$ but not only for the specific values $\beta = 1, 2$ and 4. It was noted that for intermediate β no analogy with matrices has been found. The main point of our conjecture is the statement that the above discussed intermediate quantum chaos to a good accuracy can be described by the Coulomb gas model (4.1.1) with arbitrary $\beta \le 4$. This allows us to obtain some analytical expressions by using the model (4.1.1). Unfortunately, such a characteristic of quantum chaos as the level spacing distribution appears to be one of the most complicated, from the point of view of deriving analytical estimates. As was mentioned, even for the specific values $\beta = 1, 2$ and 4 it is questionable if one can obtain appropriate analytical expressions. However, it seems to be possible to construct some approximate formulae using Dyson's results. In particular, the limit case of large spacings has been thoroughly investigated by Dyson for any temperature $T = 1/\beta$ and the asymptotic behaviour (for

$\beta s \gg 1$) was rigorously found [D62, P65, M67],

$$P(s) \sim \exp[-\tfrac{1}{16}\pi^2\beta s^2 - \tfrac{1}{2}\pi(1 - \tfrac{1}{2}\beta)s] \,. \tag{4.1.5}$$

This allows us to construct the approximate expression for $P(s)$ [I87, I88],[*]

$$P_\beta(s) = A(\tfrac{1}{2}\pi s)^\beta \exp[-\tfrac{1}{16}\beta\pi^2 s^2 - (B - \tfrac{1}{4}\pi\beta)s] \,, \tag{4.1.6}$$

where the two normalization parameters, A and B, are determined from the normalization conditions

$$\int\limits_0^\infty P_\beta(s) \, ds = 1 \,, \qquad \int\limits_0^\infty sP_\beta(s) \, ds = 1 \,, \tag{4.1.7}$$

with $s = 1$ being the mean distance between neighbouring levels. The dependence (4.1.6) has a form that approximately takes into account the rigorous asymptotic expression for $P(s)$ for $s \to \infty$, namely, the exponential decrease $\exp(-\tfrac{1}{16}\beta\pi^2 s^2)$. Also, the behaviour of $P(s)$ for small $s \ll 1$ corresponds to repulsion $\sim s$, $\sim s^2$ and $\sim s^4$ for $\beta = 1$, 2 and 4, respectively. In addition, for $\beta = 0$ the dependence is exactly Poissonian. Comparison of (4.1.6) with the expressions given by the Wigner surmise (2.4.1), namely,

$$P_1(s) = \tfrac{1}{2}\pi s \, e^{-\pi s^2/4} = A_1^W(\tfrac{1}{2}\pi s) \, e^{-\pi s^2/4} \,, \quad A_1^W = 1 \,,$$

$$P_2(s) = (32/\pi^2)s^2 \, e^{-4s^2/\pi} = A_2^W(\tfrac{1}{2}\pi s)^2 \, e^{-4s^2/\pi} \,, \quad A_2^W = 8(2/\pi)^4 \approx 1.314 \,, \tag{4.1.8}$$

$$P_4(s) = (64/9\pi)^3 s^4 \, e^{-64s^2/9\pi} = A_4^W(\tfrac{1}{2}\pi s)^4 \, e^{-64s^2/9\pi} \,, \quad A_4^W = 6(8/3\pi)^7 \approx 1.905 \,,$$

shows a quite good correspondence. As an example, in fig. 20 expressions (4.1.6) and (4.1.8) are shown for $\beta = 1$, together with the numerical data of RMT [P65, M67]. It is seen that the deviation of the approximate formula (4.1.6) does not exceed 5% for the most essential region $s \approx 1$–2 (from a practical point of view). This means that the dependence (4.1.6) can be regarded as a good approximation if the total number N of levels does not exceed $N \approx 10^4$. A much better correspondence occurs for $\beta = 2$ (see fig. 21), Also, for $\beta = 4$ expression (4.1.6) is very close to (4.1.8) with the same accuracy. Thus, we may expect that for intermediate values $0 < \beta < 4$ the dependence (4.1.6) is good in describing the intermediate statistical properties of the Coulomb model (4.1.1). Figure 22 shows the dependence of A and B in (4.1.1) on β for the range of largest physical interest. The values of A and B for $\beta = 1, 2, 4$ are given in table 2 together with A^W, eq. (4.1.8), and A^{RMT} (exact value, predicted by RMT [M67]). The value of $(2/\pi)B_D$ corresponds to Dyson's asymptotic expression (4.1.5).

An extensive Monte Carlo simulation of the Coulomb gas model (4.1.1) was performed in [IS88, SI90] for β in the range $0.1 \le \beta \le 4.0$. The thermodynamical properties of a gas with N particles (like energy and specific heat) were found to be in good agreement with Dyson's theoretical predictions. Also, the computations of $P(s)$ for the known cases $\beta = 1$, 2, 4 showed reasonable agreement with (4.1.6). The main data concern intermediate values of β, for which the actual distribution $P(s)$ was compared with the dependence (4.1.6). The comparison was done by minimizing the deviation (χ^2

[*] Very recently a similar expression with the same properties was found by the author, which for $\beta = 1, 2, 4$ corresponds much better to the data of RMT than the Wigner surmise (2.4.1) (to be published).
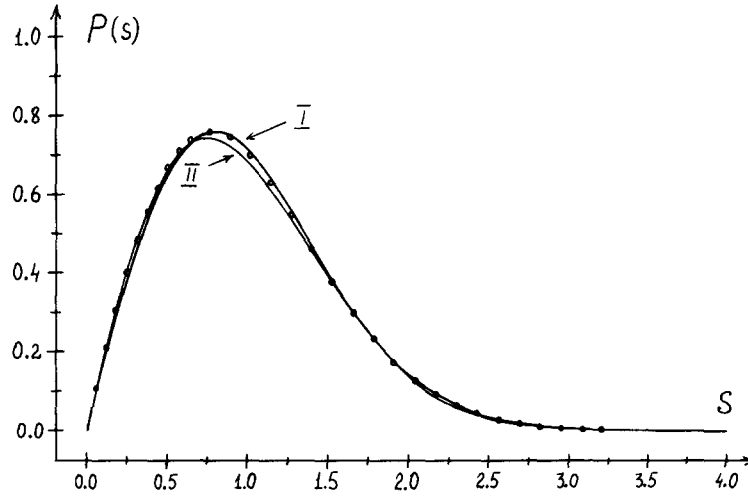
Fig. 20. The level spacing distribution $P(s)$ for $\beta = 1$. Curve I is the Wigner surmise (2.4.1); circles represent the numerical result of RMT; curve II is the approximate dependence (4.1.6) (after [189]).

value) of $P(s)$ from the experimental data with the fitting parameter $\beta = \beta_{histo}$. The data show that it is possible to fit all experimental spacing distributions over the whole range of physically interesting β values with sufficiently small deviations when using the proposed distribution (4.1.6).

The main result is presented in fig. 23 for the dependence of β_{histo} upon the inverse temperature $\beta = \beta_{therm}$. As a good approximation $\beta_{histo} \simeq \beta_{therm}$ holds and can be used for practical purposes if the exact $\beta = \beta_{therm}$ is unknown, as is usually the case. Two deviations from this simple relation can be noticed upon close inspection. One is a slight underestimation of the true β when using β_{histo} for large values of β. The other is a slight deviation for small values of β, which amounts to gauging the experimental results for β_{histo} to find β with accuracy $\Delta\beta \approx 0.2$. Thus, fig. 23 shows that the proposed spacing distribution (4.1.6) can be used over the whole range of physically relevant β values to obtain
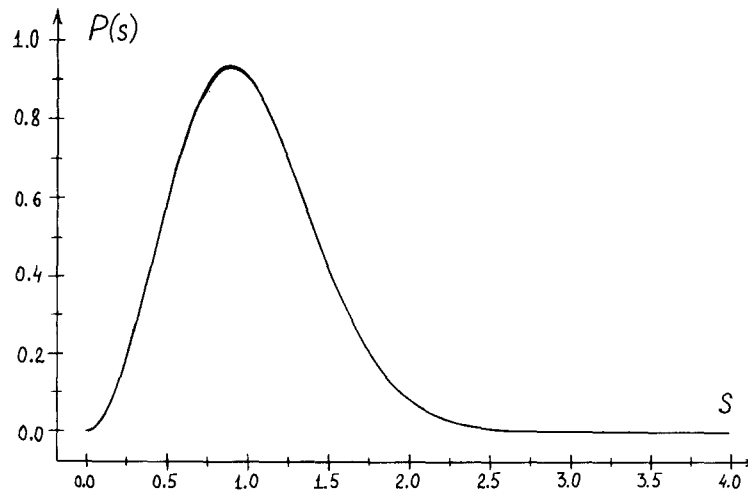
Fig. 21. The distribution $P(s)$ for $\beta = 2$. The two expressions (2.4.1) and (4.1.6) give a very similar dependence (the discrepancy for $s \approx 1$ does not exceed 0.7%) (after [189]).
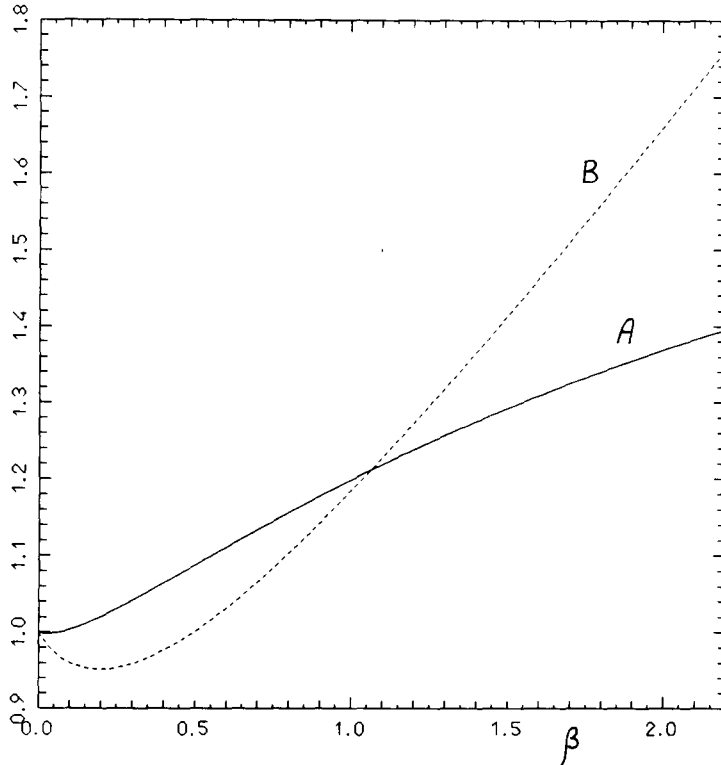
Fig. 22. Dependence of the constants A (full line) and B (dashed line) of the spacing distribution (4.1.6) upon β (after [SI90]).

an approximation β_{histo} that describes the physics behind the spacing distribution. It is interesting to note that it is also possible to find an approximation β_{delta} to the inverse temperature $1/T = \beta$ from the spectral stiffness (measured by Δ_3 statistics) of the particle positions of the gas with the help of the conjecture $\Delta_\beta(L) \sim \beta^{-1} \ln(L) + \text{const.}$ (see [SI90]). The approximation β_{delta} is inferior to β_{histo} but nevertheless comparable in its deviations from β.

Before comparing the proposed spacing distribution (4.1.6) with the numerical data for the model (3.1.6) we shall discuss, in the next section, the structure of chaotic localized eigenfunctions. This structure is assumed to be closely related to the repulsion parameter β in (4.1.6).

4.2. Localized chaotic eigenstates

Now we discuss the structure of EFs when the parameter k varies while classical chaos is strong and fixed ($K = 5$). Typical shapes of EFs are given in fig. 24, where ten randomly chosen EFs out of a total number $N = 398$ are plotted in the unperturbed basis. For the convenience of numerical computations, a unitary matrix U_{nm}^{a} has been used which describes only odd-parity states ($\varphi_n = -\varphi_{-n}$). This matrix can

Table 2

β	A	A^{W}	A^{RMT}	$(2/\pi)B$	$(2/\pi)B_{\text{D}}$
1	1.198	1.000	$\frac{1}{3}\pi \approx 1.047$	0.753	1.0
2	1.369	1.314	$\frac{4}{3} \approx 1.333$	1.055	1.0
4	1.551	1.905	$\frac{256}{135} \approx 1.896$	1.726	1.0
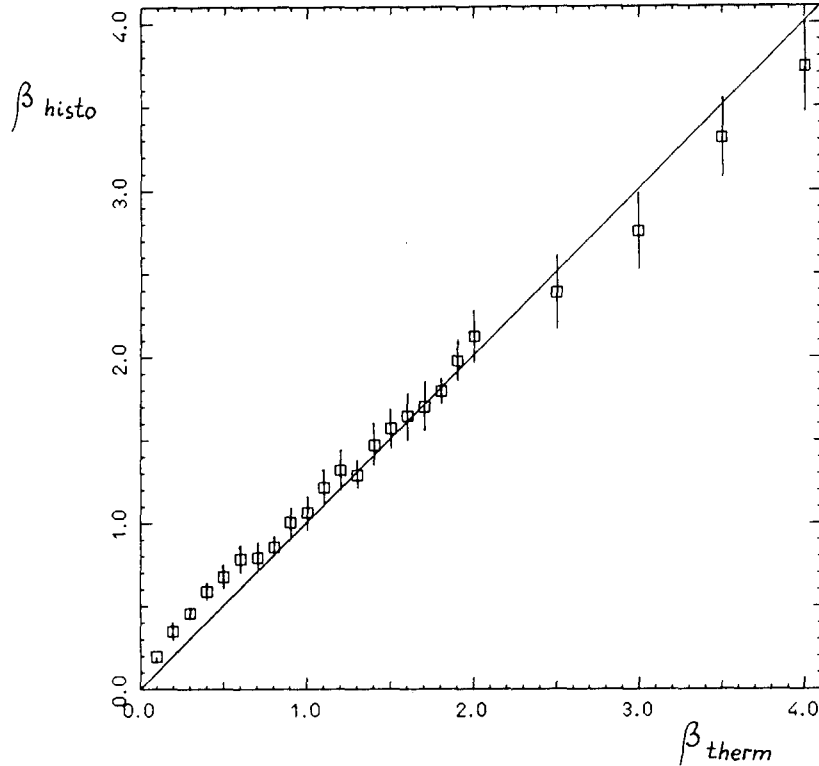
Fig. 23. Relation between β_{histo}, obtained from a minimum χ^2 fit of the experimental histogram using the conjectured spacing distribution (4.1.6), and β_{therm}. The bars correspond to 1% confidence fitting (after [IS89, SI90]).

be deduced in the same way as the matrix (3.1.6), the only difference being that the unperturbed basis is now taken in the form $\sin(n\theta)$, unlike (3.1.6), where the unperturbed basis is $\exp(\pm in\theta)$. Therefore, the even-parity states corresponding to the basis $\cos(n\theta)$ are automatically dropped. This can be done only when the model (3.1.6) has parity conservation. In the sine representation all components of the EFs can be independent, compared with (3.1.6), where we get valuable information only about half of the components of the EFs. The exact expression of U^a_{nm} for $\theta_0 = 0$ and $\gamma = 0$ has the form [I88, I89]

$$U^a_{nm} = \frac{1}{2N+1} e^{i\tau(n^2+m^2)/4} \sum_{l=1}^{2N+1} \{\cos[(n'-m')2\pi l/(2N+1)] - \cos[(n'+m')2\pi l/(2N+1)]\}$$

$$\times \exp\{-ik \cos[2\pi l/(2N+1)]\}, \tag{4.2.1}$$

where $n, m = 1, 2, \ldots, N$ and N has the same sense as N_1 in (3.1.6). Here the dimensionless period is $\tau = 4\pi r/(2N+1)$, in accordance with the quantum resonance condition for $q = 2N + 1$. The eigenvectors $\varphi_n(\varepsilon)$ of the unitary matrix (4.2.1) represent half of the components of the EF for the full matrix (3.1.6) with positive (or negative) values of the unperturbed momentum $n > 0$.

Two main features of the EFs can be easily observed in fig. 24. The first is some sort of localization, which means that a finite number of unperturbed states, less than N, are essentially occupied by each EF (see fig. 24a). Unlike the common definition of the localization length l_∞ from the decay of φ_n in the tails (as $|n| \to \infty$), in our model (3.1.6) the EF localization is restricted by the total number of states, N.
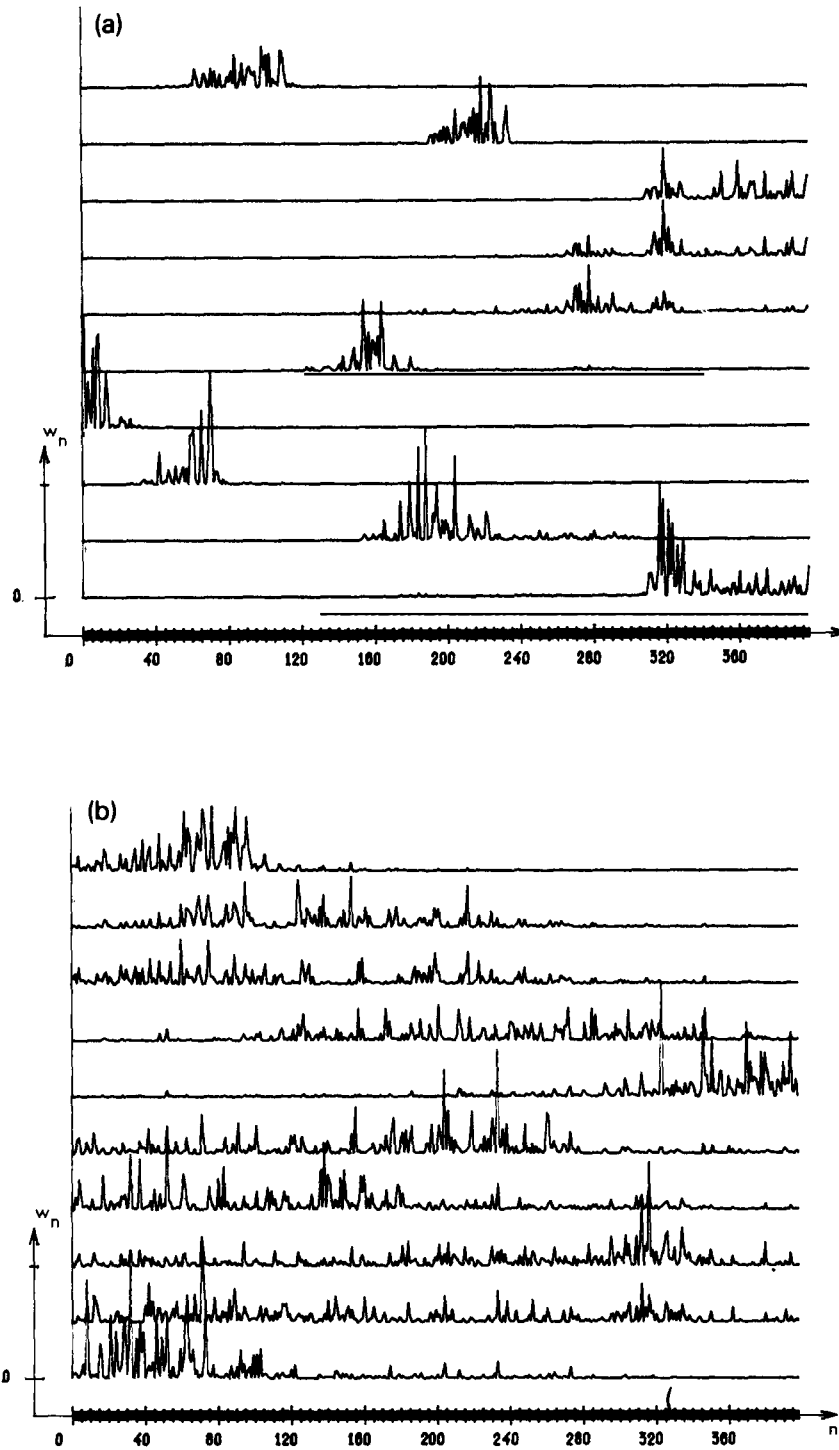
Fig. 24. Ten out of $N = 398$ eigenfunctions in the unperturbed basis, n, for the model (4.2.1) are shown. On the vertical axis the probability $w_n = |\varphi_n|^2$; on the horizontal axis the number of the unperturbed state, n. The parameters are (a) $K \approx 5$, $k \approx 10.6$, $\tau \approx 0.473$, $\Lambda \approx 0.07$; (b) $K \approx 5$, $k \approx 32.0$, $\tau \approx 0.158$, $\Lambda \approx 0.64$.
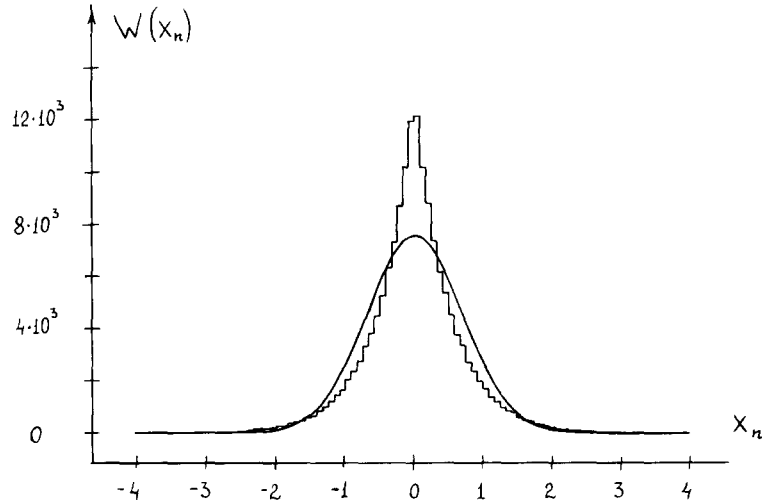
Fig. 25. The distribution of the components φ_n for the EFs of the model (4.2.1) for the parameters of fig. 24b; $X_n = \tilde{\varphi}_n/\sigma$.

Another feature is the more or less random character of the amplitudes φ_n on a scale less than the size of the localization (especially when the localization is large, see fig. 24b). Also, there is clear evidence of very strong fluctuations in the size of the localization both for $\Lambda \approx 0.07$ and $\Lambda \approx 0.64$. The latter peculiarity seems to reflect the specific form of the EF fluctuations; this will be discussed later. To compare with the Gaussian distribution of the components φ_n (see figs. 18, 19) in the case of complete delocalization, the distribution of φ_n is given in fig. 25 for the case when some of the EFs are not completely extended (the data correspond to those of fig. 24b). Such a shape of $w(\varphi_n)$ with a deviation from the Gaussian distribution has been also observed in other physical models [SG84, MKZ88] and seems to be typical in the case of quantum localization.

On the whole, numerical data show that in the case of strong classical chaos all EFs are characterized by a finite size of localization on which large fluctuations of the EF components occurs. In what follows such eigenstates will be termed "localized chaotic eigenstates". Then, the very important problem of the quantitative description of such EFs arises. First, in spite of the strong fluctuations for the size of the EF, it seems possible to introduce some quantity for the degree of localization, which is restricted by the maximal number of unperturbed states. The second question is how to describe the degree of chaos inside an EF on the length of their localization. Also, it is of importance to study the fluctuation properties of EFs. All these questions appear also in solid state physics in the investigation of the localization in a random potential for finite samples. As in our case of dynamical chaos, for such solid state models the parameter Λ plays a significant role in describing the general properties of the systems. The only (but principal) difference is the different mechanisms of the chaos in dynamical and random systems (see discussion in section 2.3). It is reasonable to assume that the chaotic properties of the spectra and eigenfunctions of dynamical models under the additional condition of strong classical chaos are very close to those of pure random systems. For this reason, the study of chaotic localized EFs in the model (3.1.6) [or (4.2.1)] seems quite instructive.

We start now with the relatively simple question of the definition of the localization length for systems with a finite number of states (finite samples). It is desirable to define the localization length of localized chaotic states in such a way that it is equal to the total number of states N in the limit of completely extended states. Also, in such an approach our definition is assumed to be related to the

chaotic structure of the EFs. According to [I88, I89], for each N-dimensional eigenvector of the matrix U_{nm}^a we introduce the information entropy

$$\mathcal{H}_N(u_1, \ldots, u_N) = -\sum_{n=1}^{N} w_n \ln w_n, \quad w_n = u_n^2, \quad u_n = \operatorname{Re} \varphi_n, \quad \sum_n u_n^2 = 1, \tag{4.2.2}$$

It is seen that $\mathcal{H}_N$ is essentially the logarithm of the number of sites significantly populated by the given eigenstate $\varphi(\varepsilon)$. If all sites were equally populated, then $\mathcal{H}_N$ would be $\ln N$. If, instead, u_n were exponentially localized around some site n_0 with a localization length $1 \ll l \ll N$, then $\mathcal{H}_N = 1 + \ln l + O(1/l)$. In general, the quantity $\exp(\mathcal{H}_N)$ is proportional to the effective number on nonzero components u_n of the EF and can be taken as some measure of localization.

This definition of localization length, $l = \exp(\mathcal{H}_N)$ has already been used before. For example, among others, this quantity was studied in the application to some two-dimensional solid state models [Y80]. For the quantum dynamics of classically chaotic systems this definition has been applied, for the first time, in [BS84, BS84a], where the quasienergy eigenfunctions of the hydrogen atom under strong microwave perturbation were investigated.

It is important to note that for chaotic states the above definition gives a value which is only proportional to the "actual" localization. For example, for the limiting case of extended chaotic states ($\Lambda \gg 1$) this definition gives $\approx N/2$ for the localization length while the actual size is N. Thus, to have a more rigorous correspondence, we need some factor which takes into account the chaotic structure of the EF. This factor was introduced in [I88] in the following way. Let us consider the limiting case of random matrix states of size N. As is known, these states have an invariant distribution over the surface of the N-sphere of radius one, with the probability density for each component given by (3.3.6). As was noted, in the large-N limit this distribution becomes Gaussian, eq. (3.3.5), a signature of the random nature of the eigenvectors. The entropy (4.2.2) of such an eigenvector takes the average value

$$\mathcal{H}_N^{\mathrm{GOE}} = \psi(\tfrac{1}{2}N + 1) - \psi(\tfrac{3}{2}) \approx \ln(\tfrac{1}{2}N\alpha) + O(1/N), \quad \alpha \approx 4/\exp(2 - \gamma) \approx 0.96, \tag{4.2.3}$$

where ψ is the digamma function and γ is the Euler constant. Finally, we define the "entropy localization length" l_H,

$$l_H = N \exp(\mathcal{H}_N - \mathcal{H}_N^{\mathrm{GOE}}). \tag{4.2.4}$$

It is clear that with the normalization parameter $\exp(-\mathcal{H}_N^{\mathrm{GOE}})$ this definition gives, on average, the exact limiting value $l_H = N$ for completely chaotic states.

This quantity (4.2.4) has large fluctuations from one EF to another, in agreement with numerous observations, see, e.g., fig. 24. This remarkable property is well illustrated in fig. 26, where the distribution of l_H, eq. (4.2.4), for an individual EF is given for three values of Λ, $\Lambda \approx 63$, 0.3 and 7×10^{-3} ($k \approx 317$, 21.1 and 3.3, respectively) with the horizontal scale being the ratio of l_H to the total number of states N. Here, the entropy localization length l_H is computed for the model (3.1.6) with u_n being the real part of the EF only, due to the symmetry of the form $\operatorname{Re} \varphi_n = \operatorname{Im} \varphi_n$ (see section 3.1). It is seen that the largest fluctuations correspond to the value $\langle l_H \rangle / N \approx 0.5$. In this case there are both strongly localized states ($l_H \ll N$) and almost extended states ($l_H \approx N$). It is a very interesting problem to find an approach to an analytical explanation of these fluctuations. This problem seems to be closely related to that of the fluctuations of the conductivity in finite samples with random potentials (see also section 4.4).
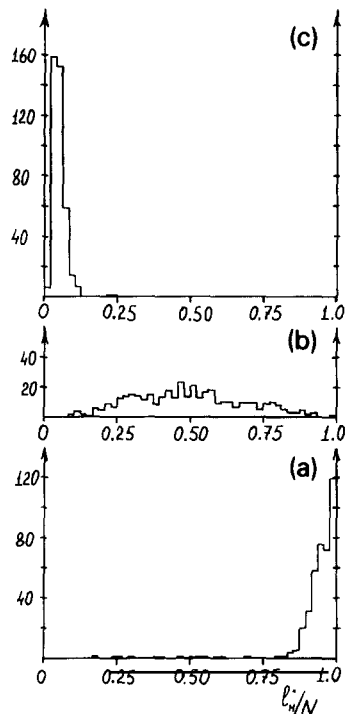
Fig. 26. Three examples of the distribution of the localization length l_H of an EF for the matrix (4.2.1) with different values of k and the fixed value $K \approx 5$. The right-hand side of the distribution $(l_N > N)$ is omitted. Here $\tau = 4\pi r/(2N + 1)$ and the other parameters are (a) $r = 1$, $k \approx 317$, $\Lambda \approx 63$, $\langle l_H \rangle \approx 0.95N$; (b) $r = 15$, $k \approx 21.1$, $\Lambda = 0.3$, $\langle l_H \rangle \approx 0.5N$; (c) $r = 95$, $k \approx 3.3$, $\Lambda \approx 7 \times 10^{-3}$, $\langle l_H \rangle \approx 0.05N$ (after [189]).

To reduce the fluctuations we pass to a more appropriate quantity, namely, the mean localization length $d \equiv \langle l_H \rangle$, which is computed by averaging over all eigenvectors of the same matrix (or over an ensemble of similar matrices),

$$\langle l_H \rangle = N \exp(\langle \mathcal{H}_N \rangle - \mathcal{H}_N^{GOE}) .$$ (4.2.5)

Here the averaging is performed for the entropy $\mathcal{H}_N$, not for the localization length. There is another possibility to define the mean value of l_H by averaging for the localization length, $\langle l_H \rangle = N \langle \exp(\mathcal{H}_N - \mathcal{H}_N^{GOE}) \rangle$ (see [187, 188]). It turns out that the latter definition gives a slightly larger (about 5–10%) value for the mean localization than (4.2.5). It is not clear which definition is more appropriate; however, for our purposes of an approximate description it seems not important. The quantity $\langle l_H \rangle$ may be associated with the dimensionality $d \leq N$ of the subspace of the N-dimensional Hilbert space in which all EFs are spanned. It turns out that, in spite of strong fluctuations for the localization length (4.2.4), the average quantity $\langle l_H \rangle$ is quite good in describing the general properties of EFs. Indeed, the dependence of $\langle l_H \rangle$ on the quantum parameter k with the fixed value $K = 5$ has a quite smooth form (see fig. 27). It is interesting to compare the entropy localization length $\langle l_H \rangle$ with the common definition l_∞ [see (2.3.9)] for small values $1 \ll \langle l_H \rangle \ll N$. Assuming an exponential shape of the EF, $\varphi_n \sim \exp(-|n - n_0|/l_\infty)$, we obtain from (4.2.4)

$$\langle l_H \rangle \approx \frac{2l_\infty e}{\alpha} \approx 2.8l_s \approx 1.4k^2 ,$$ (4.2.6)
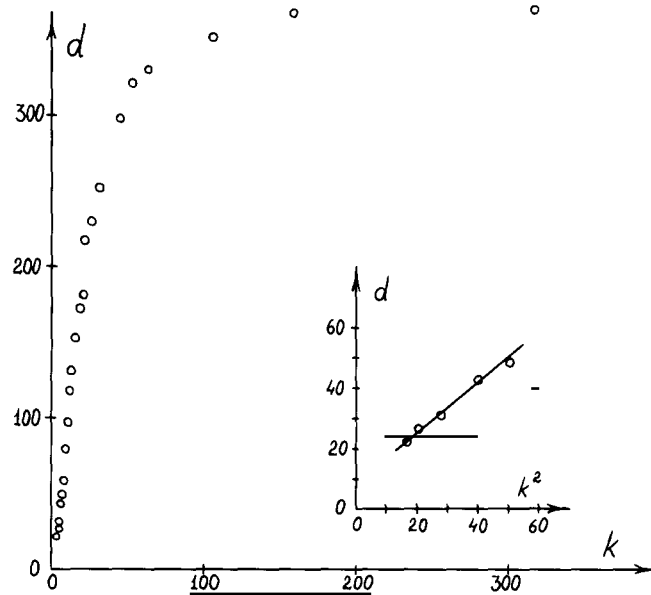
Fig. 27. The mean entropy localization length $d = \langle l_H \rangle$ against the quantum parameter k for fixed $K = 5$ is given. The inset shows the region of small $l_H \ll N$ with the linear dependence $\langle l_H \rangle \approx 0.87 k^2$, $N = 398$ (after [189]).

where l_s is the localization length found from the stationary distribution after the diffusion in the kicked rotator model (2.2.1) has stopped (see section 2.3). The inset in fig. 27 allows one to estimate the actual proportionality, $\langle l_H \rangle \approx 0.87 k^2$, which can be used to establish the correspondence between $\langle l_H \rangle$ and l_∞ in the region $1 \ll l_H \ll N$ where both definitions are valid. It should be noted that in (4.2.6) unknown fluctuations of l_H are not taken into account. Additional numerical data are certainly needed to clarify this problem.

It is important to note that our definition (4.2.4), (4.2.5) is in good agreement with the common meaning of localization length as the effectve size of the range in which the main probability of the EF in the given basis is concentrated. This is confirmed by the data in fig. 28, where the entropy localization length $\langle l_H \rangle$ is plotted against "the probability localization length", l_w. The latter has been computed as the number of unperturbed states carrying most (95%) of the normalization of the EF. There is a good correspondence between these two quantities, especially when large fluctuations of the individual EFs are taken into account.

4.3. Relation between spectrum fluctuations and localization

In the previous section some characteristic of the degree of localization for chaotic localized states has been introduced. As is seen from numerous data, when $\langle l_H \rangle$ has the maximal value N, the spacing distribution $P(s)$ has the limiting form of the Wigner distribution (2.4.1) with the maximal repulsion $\beta = 1$ (here, we discuss the symmetric case only, $\theta_0 = 0$ and $\gamma = 0$ in (3.1.6); other cases will be discussed later). Also, when $\langle l_H \rangle$ is much smaller than N, the distribution $P(s)$ approaches the Poisson law with vanishing repulsion, $\beta \rightarrow 0$. In [188, 189] some conjecture has been proposed according to which the relative localization of EFs is associated with the repulsion of quasienergy states. Namely, the quantity β was introduced which is the ratio of the mean entropy localization length to the total number
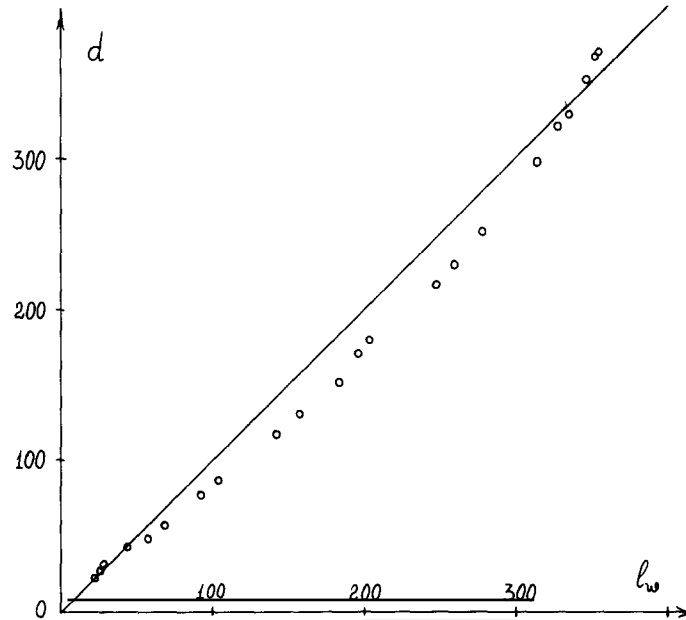
Fig. 28. Relation between the mean entropy localization length $d = \langle l_H \rangle$ and the mean probability localization length, l_w. The quantum parameter k varies and the classical one is fixed ($K \approx 5$). The size of the matrix is $N = 398$. The averaging is over all EFs of the same matrix U_{nm}^a, (after [189]).

of states,

$$\beta = \langle l_H \rangle / N .$$ (4.3.1)

It is seen that this quantity varies from zero for completely localized states to one for fully extended states. This conjecture allows one to relate, quantitatively, the statistical properties of spectra to the chaotic structure of eigenfunctions. Now we discuss some numerical data for the model (4.2.1) which have been generated to check this conjecture. Again, we deal with the situation corresponding to strong classical chaos, $K \gg 1$. This is assumed to provide a chaotic structure of the EFs on a scale smaller than the localization scale.

First, let us compare actual spacing distributions $P(s)$ with the analytical dependence (4.1.6), where the parameter β is determined by (4.3.1) through the mean localization length (4.2.5). For this, the latter quantity $\langle l_H \rangle / N$ and the spacing distribution $P(s)$ have been computed independently over a wide range of the quantum parameter k with fixed $K = 5$. To improve the statistics, the distributions $P(s)$ for a number ($NG = 4$) of matrices U_{nm}^a of size $N = 398$ have been summed with slightly different values of k ($\Delta k \ll k$). As usual, the spacings $s_j = \varepsilon_{j+1} - \varepsilon_j$ were found from the eigenvalues $\lambda_j = \exp(i\varepsilon_j)$ of the unitary matrix U_{nm}^a. Typical examples of $P(s)$ are given in fig. 29 for three values of k. The full lines correspond to the expression (4.1.6) with β computed in accordance with the above definition (4.3.1). Good agreement between the numerical data and (4.1.6) is clearly seen, which is also supported by the χ^2 approach. Specifically, for $\Lambda \approx 1.0$, 0.28 and 0.05 ($\beta \approx 0.76$, 0.48 and 0.22, respectively), the χ^2 values for 23 subintervals are $\chi_{23}^2 \approx 15.6$, 27.2 and 28.5, which gives for the confidence levels 90%, 30% and 35%, respectively.

More data are presented in fig. 30, where the confidence levels for different values of β are shown not only for β in (4.1.6) taken from the definition (4.3.1), but also for some other relations. Namely, two different expressions, $\beta = (\langle l_H \rangle / N)^2$ and $\beta = (\langle l_H \rangle / N)^{1/2}$ have been examined to check whether
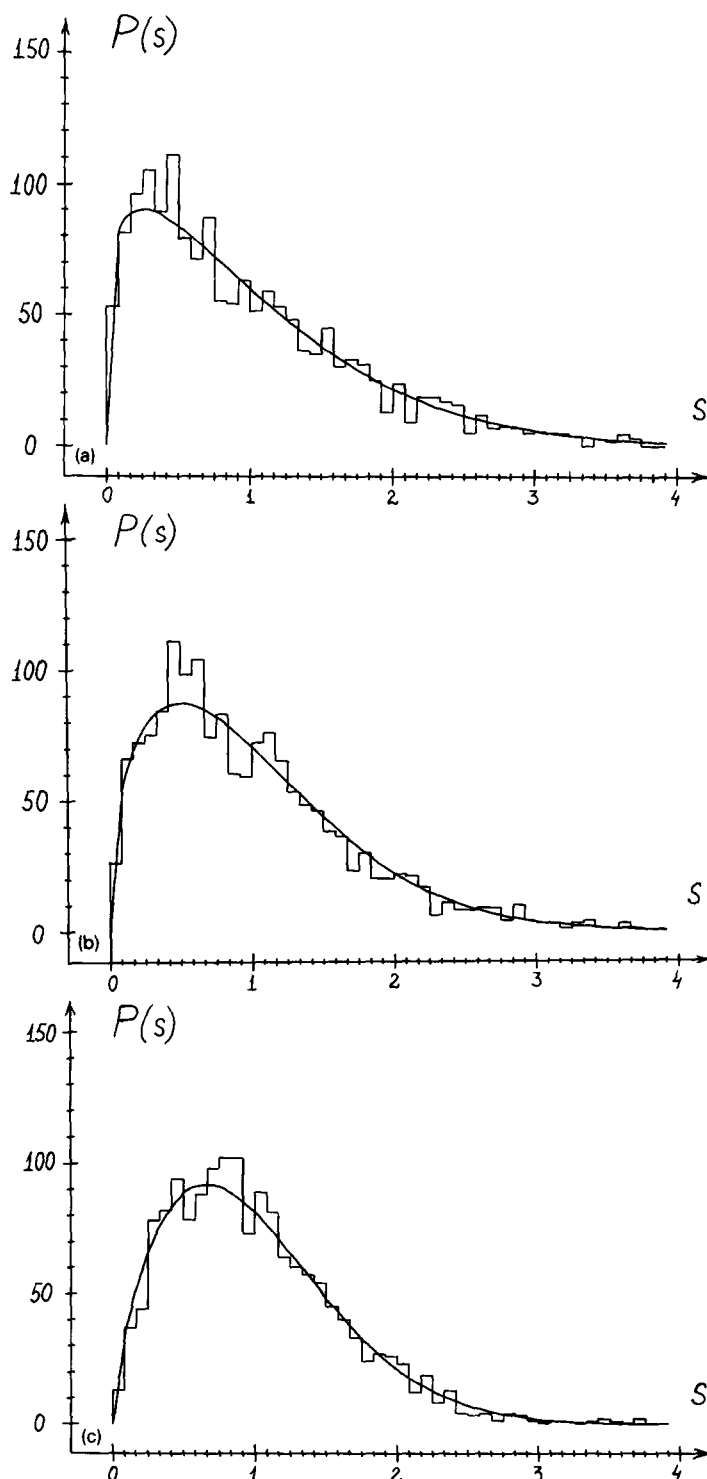
Fig. 29. Three examples of intermediate statistics for $P(s)$ for the model (4.2.1) with $N = 398$ and $K = 5$. Four matrices U_{nm} with slightly different values of k ($\Delta k \ll k$) have been studied, with the total number of quasienergy levels $M = N \cdot NG = 1592$. The histograms are the numerical data, the smooth curves are relation (4.1.6) with $\beta = d/N$ ($d = \langle l_H \rangle$). Here s is measured in units of the mean spacing, $\Delta = 1/N$. (a) $k \approx 39.8$, $\beta \approx 0.76$, $\chi_{23}^2 \approx 15.6$; (b) $k \approx 21.1$, $\beta \approx 0.48$, $\chi_{23}^2 \approx 27.2$; (c) $k \approx 9.1$, $\beta \approx 0.22$, $\chi_{23}^2 \approx 28.5$ (after [189]).
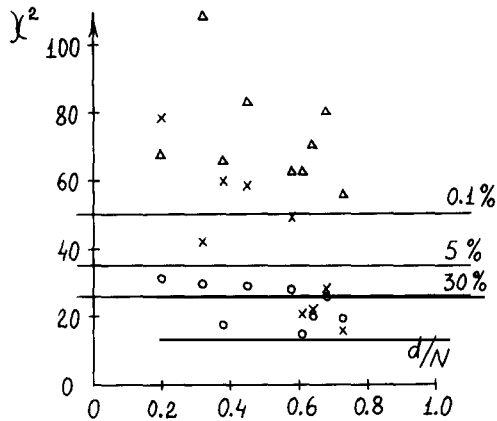
Fig. 30. The χ^2 values for the comparison of numerical data with the conjectured relation (4.1.6), with 24 subintervals in s. The circles are for $\beta = d/N$ in (4.1.6) ($d = \langle l_H \rangle$), the triangles for $\beta = (d/N)^2$, the crosses for $\beta = (d/N)^{1/2}$; χ^2_{23} values corresponding to 0.1%, 5%, 30% confidence levels are also shown (after [189]).
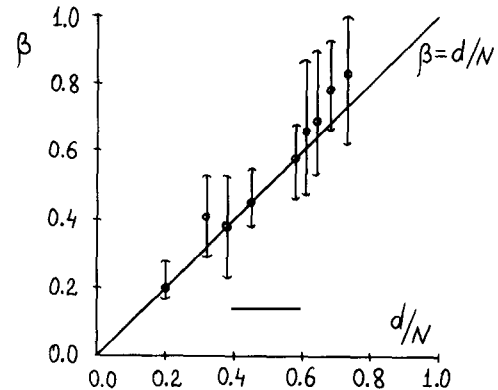
Fig. 31. The fit parameter β in (4.1.6) as a function of d/N. Circles are values of β corresponding to the minimum values of χ^2_{23}; the bars indicate the 5% confidence level (after [189]).

the linear dependence $\beta = \langle l_H \rangle / N$ is the actual relation between β and $\langle l_H \rangle$. It is seen from fig. 30 that the linear relation can be easily distinguished by the χ^2 approach. Therefore, the above conjecture about the repulsion parameter as the ratio (4.3.1) is supported by the data.

A more accurate comparison was carried out in the following way. The expected dependence (4.1.6) has been used to fit all numerical data for $P(s)$ by making use of the χ^2 approach. Then, the parameter β found by the best fit was compared with the ratio (4.3.1). The result is given in fig. 31, where the error bars for β correspond to the fitting of actual distributions $P(s)$ with 5% confidence level. As a result, we can see that all the data for $P(s)$ are well described by the linear relation $\beta = \langle l_H \rangle / N$. It is interesting to note that the spread of β in fig. 31 decreases when $\beta \to 0$. This means that the actual level spacing distribution becomes more sensitive to the analyical form of $P(s)$ when the repulsion is small and $P(s)$ approaches the Poisson law.

All data discussed above for intermediate statistics were obtained for not too small values of β ($\beta \gtrsim 0.2$). It is of interest to study the region of small β. However, numerical simulations for $\beta \ll 1$ are quite difficult because it is necessary to increase significantly the size of the matrix U^a_{nm}. This is related to the fact that the quantum parameter k has to be large, $k \gg 1$, to provide a good semiclassical condition. In other words, to treat EFs as random on a scale $\lesssim l_H$, the mean localization length $\langle l_H \rangle$ needs to be large, $\langle l_H \rangle \gg 1$.

It is very important that the definition of the repulsion parameter as the ratio of the mean entropy localization length to the total number of states can be generalized for the models where the maximal value of β is $\beta_{max} = 2$ or $\beta_{max} = 4$. The latter cases correspond, in the limit of extended chaotic states, to the CUE and CSE ensembles (see section 3.1). To generalize the meaning of β, we should note that the maximal number of independent elements of eigenvectors in the case of unitary asymmetric random matrices (CUE ensemble) is equal to $2N$, due to the fact that the real and imaginary parts are independent. Also, for symplectic matrices each EF has $4N$ independent elements.

To extend our definition of β to other models, let us now discuss the model (3.1.6) with broken parity conservation and broken time reversal invariance ($\theta_0 \neq 0$ and $\gamma \neq 0$). In this case, the unitary matrix U_{nm} has no symmetries and its EFs have different real and imaginary parts. For this reason, the

mean entropy localization length $\langle l_H \rangle$ for asymmetric matrices U_{nm} was defined in [I89] in the same way as in (4.3.1) with the only exception that the sum in (4.2.2) runs over both the real and imaginary parts of the EF. Correspondingly, the total number of components in the sum (4.2.2) is equal to $2N$, with the normalization [I89]

$$\sum_{m=1}^{2N} w_m = 1 , \quad w_m = \begin{cases} (\mathrm{Re}\ \varphi_m)^2 , & m = 1, \ldots, N , \\ (\mathrm{Im}\ \varphi_m)^2 , & m = N+1, \ldots, 2N . \end{cases} \tag{4.3.2}$$

Therefore, the definition of $\langle l_H \rangle$ takes now the form

$$\langle l_H \rangle = \tilde{N} \exp(\langle \mathcal{H}_{\tilde{N}} \rangle - \tilde{\mathcal{H}}_{\tilde{N}}) , \quad \tilde{N} = \beta_m N , \tag{4.3.3}$$

where β_m stands for the maximal value of β in the model according to its symmetry. As a result, the repulsion parameter β varies for this model in the range $0 \le \beta \le 2$. The most important question which arises immediately is whether it is possible to describe the level spacing distribution $P(s)$ by the same expression (4.1.6) with β determined from (4.3.3) and (4.3.1). A preliminary investigation [I89] indicates that the dependence (4.1.6) seems to be still valid. One interesting conclusion then follows from this result. Namely, it is clear that it is possible to find a value of k such that it corresponds to $\beta = 1$ while the maximum value of beta is $\beta = 2$. This means that intermediate statistics (with $\beta = 1$) in such a model is expected to be of the same form as the limiting Wigner distribution which occurs in models with $\beta_{\max} = 1$ (GOE-like ensembles). A special numerical simulation [I89] has been performed to clarify this question. The data are shown in fig. 32 for the model (3.1.6) with $\beta \approx 1$, the total number of spacings being $M = 1592$. The full line gives the best fit for relation (4.1.6) while dashed lines correspond to (4.1.6) with β giving a 1% confidence level according to the χ^2 approach. The fitting values of β are in the range $0.9 \le \beta \le 1.2$, with the best value 1.06, while the value found from the mean localization length $\langle l_H \rangle$ is $\beta \approx 1.15$.

The above result shows that the Wigner distribution with $\beta = 1$ can appear not only as a limit case of random matrices but also in the intermediate situation for some systems with broken time reversal invariance. However, this fact does not mean that all other statistical properties for the chosen parameters in the model should also correspond to the limit case of unitary random matrices with $\beta = 1$. For example, the Δ_3 statistics has been checked for this case, with a remarkable result (see fig. 33). The full line in this figure shows the relation which arises for the CUE (or GUE) ensemble (see, e.g.. [P65, M67]). This relation is known to appear also in a number of dynamical models with strong classical chaos, see, e.g., the reviews [E88, E88a]). Also, this behaviour holds in the symmetric model (3.1.6) with $\gamma = \theta_0 = 0$. From fig. 33 one can see that for relatively small L, $L \le 12$, the data follow the analytical prediction (it should be pointed out that for very small L, $L \sim 1$, this analytical dependence is not correct). However, with increasing L the data start to deviate from the smooth analytical curve. From the physical point of view, the absence of a strong correspondence for large L is not surprising. Indeed, in general, the EFs are not fully extended; therefore, they do not completely overlap. This results in the decay of correlations for large L. For comparison, the straight line in fig. 33 corresponds to uncorrelated statistics (Poisson level spacing distribution). It is interesting to note that the deviation of the numerical data for the Δ_3 statistics goes in a direction which is opposite to that known in autonomous systems. Namely, for the latter case the numerical data for large L are usually below the theoretical curve; this effect is well explained by Berry's theory [B85a].
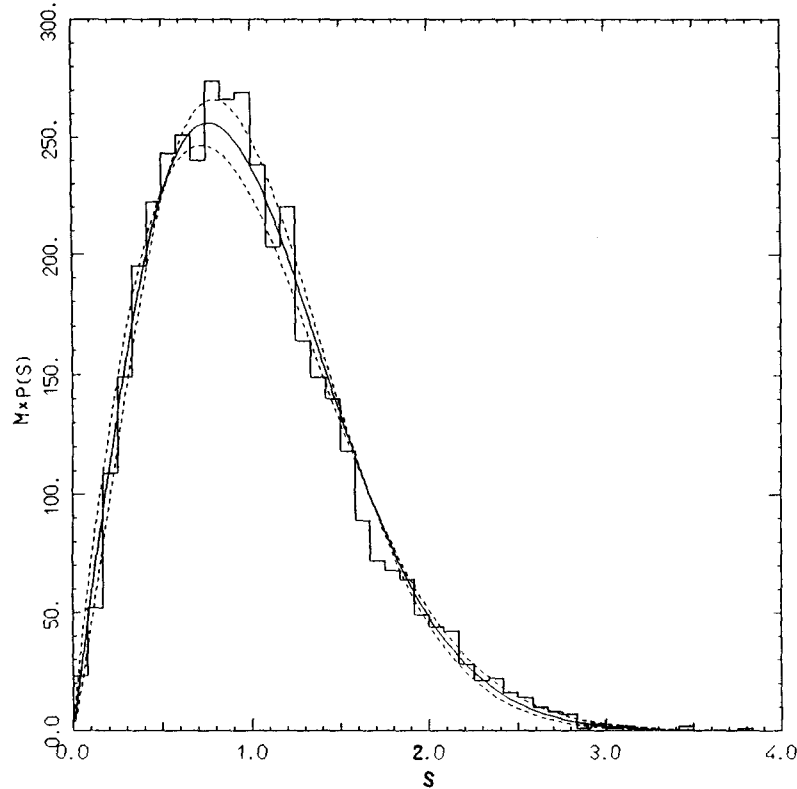
Fig. 32. Distribution $P(s)$ for the model (3.1.6) with nonzero values of θ_0 and γ. The parameters which provide intermediate statistics with $\beta \approx 1$ are: $N = 404$, $\tau = 16\pi/N \approx 0.123$, $K \approx 5$, $k \approx 40.7$. Ten matrices U_{nm} have been examined with different values of θ_0 and γ.

Recently, the approach to determine the mean entropy localization length $\langle l_H \rangle$ has been applied to the generalized kicked rotator model with spin $1/2$ [S89a]. The unitary matrix for this case is simplectic, resulting in $4N$ elements for each EF. Correspondingly, the definition of $\langle l_H \rangle$ is modified to take into account this peculiarity.

4.4. Scaling properties of eigenfunctions and spectra

In section 4.2 a definition of the localization length l_H has been introduced in such a way that it applies both for localized and completely delocalized eigenfunctions. The normalization parameter in (4.2.4) is chosen to provide the correct limit $\langle l_H \rangle = N$ for fully extended states by taking into account the random character of EFs. In the other limit, for exponentially localized states $(1 \ll l_H \ll N)$, the new quantity l_H is proportional to the usual definition of localization length, $l_H \approx 5.66 l_\infty$. It is interesting now to compare the properties of l_H for our model (4.2.1) with some results known in solid state physics for one-dimensional models with random potentials. Indeed, as was discussed above, the kicked rotator can be associated with some solid state model of the type (2.3.20) by making a special type of transformation from ψ_n to u_n. As a result, the model (2.3.20) has been derived, which can be treated as some solid state model with real Hamiltonian determined by the matrix elements W_r and ϕ_n. Correspondingly, all matrix elements are assumed to be real, in contrast to the original model (2.2.10) [or (4.2.1)]. Nevertheless, we may also regard our kicked rotator as a solid state model, conjecturing
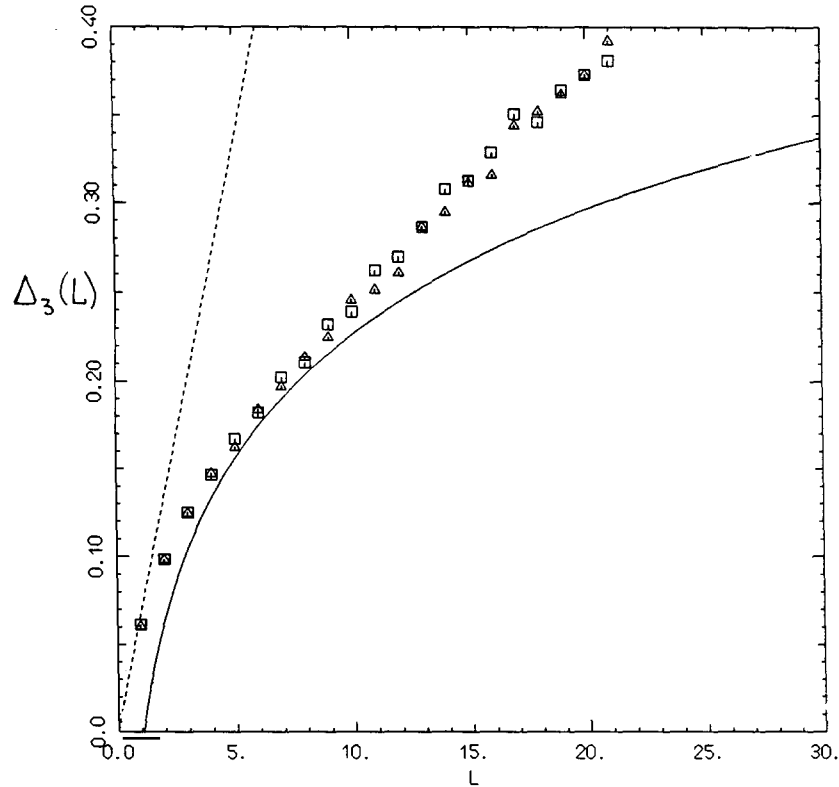
Fig. 33. The Δ_3 statistics for the parameters of fig. 32. The full curve is the theoretical prediction of GOE for $\beta = 1$; the dashed straight line corresponds to uncorrelated (Poisson) statistics; squares and triangles are data for two matrices with different values of θ_0 and γ.

that its statistical properties are of general form. In such an approach, the interaction between neighbouring "atoms" is determined by off-diagonal elements U_{nm} with $n \neq m$ and the number of atoms involved in the direct interaction is given by the band size, which is approximately equal to $\approx 2k$. Then, we have a model in which the randomness of the interaction is entirely related to the classical parameter K, and the quantum parameter k determines the range of this interaction. Since we study here only the case with strong classical chaos, $K \gg 1$, the effective potential appears to have strongly chaotic properties. In view of this, we now briefly discuss some recent numerical results [CGIS89], which may be compared with those known for tight-binding models of the solid state.

The concept of localization length in solid state physics is of great importance due to its relevance to the conductivity. According to the well-known approach (see, e.g., [LR85, P86]), the localization length in finite samples is closely related to the residual conductance of the samples itself. One of the most interesting results in this field is a scaling relation of the localization length ξ_N defined for a finite sample, to the localization length ξ_∞ in the same sample when $N \to \infty$ [P86],

$$\xi_N/N = \mathcal{F}(z), \quad z = N/\xi_\infty. \tag{4.4.1}$$

Here ξ_N is defined by means of the transfer matrix formalism. It is a characteristic length of exponential decay of EFs in a finite sample of size N; therefore, $\xi_N \to \xi_\infty$ for $N \to \infty$. In the known approach [P86] the above expression (4.4.1) is equivalent to postulating the existence of some function $\mathcal{F}(z)$, which can

be related to the scaling function g for the conductivity. Leaving apart the problem of the relation between the localization length and the conductivity, we analyse here the possibility to relate this scaling theory to our model of the kicked rotator on the torus.

Indeed, instead of ξ_N we also have a definition of the localization length l_H which in the limit $N \to \infty$ is proportional to l_∞. The important difference between ξ_N and l_H is that the latter is bounded by N, unlike ξ_N, which goes to infinity when the EF becomes a completely extended state. Nevertheless, this peculiarity seems not to be important since it reflects a specific choice of normalization. As a result, in our variables a similar scaling law is assumed, with the form

$$\beta = f(D_n/N), \quad D_n \approx 2l_\infty \sim k^2, \quad \beta \equiv \langle l_H \rangle / N, \tag{4.4.2}$$

where the diffusion coefficient D_n stands instead of l_∞ due to expression (2.3.14). The important difference with (4.4.1) is that the scaling (4.4.1) was assumed to be valid only for states with a fixed energy. Since in our case all quasienergies are determined modulo 2π, there is no smooth dependence of the localization length l_H on the quasienergy. In solid state models there is a particular dependence of ξ_N on the energy corresponding to this state. For this reason, we use the average localization length $\langle l_H \rangle$, which is related to the parameter β (see previous sections).

In order to check this scaling behaviour for β, an extensive numerical simulation with the model (4.2.1) has been performed [CGIS89]. For this, the eigenfunctions of the matrix U^a_{nm} were computed for several values of N and k in the ranges $200 \le N \le 860$ and $1 \le k \le 239$. In all cases the classical parameter was taken as $K \approx 5$, which implies $D_n \approx k^2/2$. Numerical data for β as a function of $x \equiv k^2/N$ are shown in fig. 34, which also includes a magnification of the part corresponding to the localized
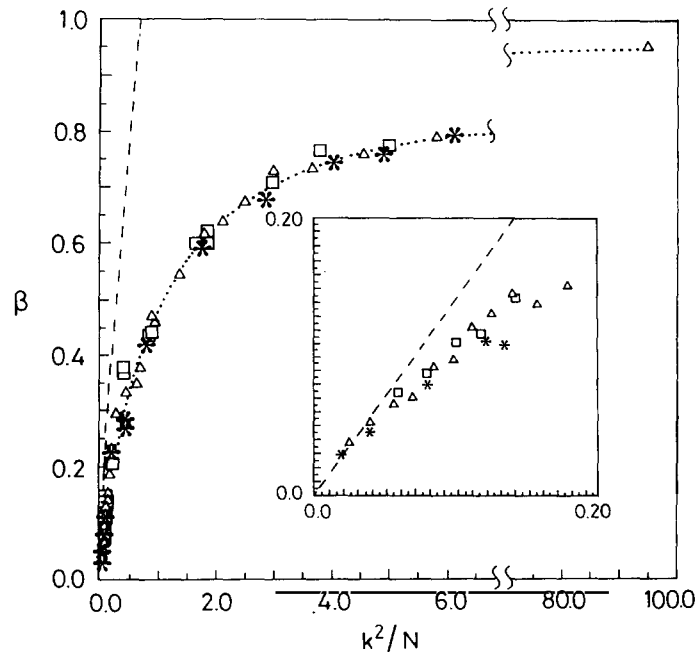

Fig. 34. The parameter β versus the variable $x = k^2/N$ for $N \approx 400$ (squares), $N \approx 600$ (triangles) and $N \approx 800$ (asterisks) is plotted for the model (4.2.1). In the inset a magnification of the region of strong localization $x \ll 1$ is shown. The dashed lines correspond to the analytical expression (4.2.6). The dotted curve gives the fit in the intermediate region when passing from localized to delocalized states. (After [CGIS89].)

states. In spite of very large fluctuations of l_H for individual EFs, all the data for β show a very good scaling on average. To compare with the localization length l_∞, relation (4.2.6) is also given (dashed line). It should be noted that the deviations from (4.2.6) for $\beta \ll 1$ have two explanations. First, relation (4.2.6) is itself approximate, since it does not take into account the fluctuations of l_H which are unknown. Secondly, in the numerical simulation the localization length l_H decreases ($l_H \rightarrow 1$) when β approaches zero; therefore, the condition $l_H \gg 1$ breaks down (see discussion in section 4.2).

Of special interest is the dependence of β in the region where the assumption of exponential localization is no longer valid ($\beta \lesssim 1$). Until now, there is no analytical approach to describe this dependence in the whole range $0 < \beta \leq 1$. Some attempt to fit the dependence $\beta(x)$ in the intermediate region $0.5 \lesssim x \lesssim 6.0$ has been made in [CGIS89], where the law $\beta \approx 1 - 0.53(k^2/N)^{-1/2}$ was found to be in good agreement with the numerical data (see the dotted line in fig. 34). However, a theoretical explanation for such a dependence still does not exist.

Another very important region, in view of the prediction of the scaling theory for solid state models (see [FPG89]) is the region $\beta \lesssim 1$. To study the character of the approach of β to 1, it is convenient to introduce the variables

$$\ln[\beta/(1-\beta)] \equiv \ln y , \qquad \ln(k^2/N) \equiv \ln x . \qquad (4.4.3)$$

Then, the asymptotic behavior of β can be seen more clearly in both its limits, $\beta \rightarrow 0$ and $\beta \rightarrow 1$. The data for β close to unity in the new variables (4.4.3) are shown in fig. 35, where, in addition to the data of fig. 34, additional points are given, mainly for $\beta \lesssim 1$. These data confirm the conjecture of the scaling behaviour for β, except, possibly, in a small region around $x \approx 0.5$. Here, the points have some dispersion, showing a slight dependence on N. The reason for such a strange behaviour is not yet understood. One possible explanation is the occurrence in this region of a change in the typical shape of
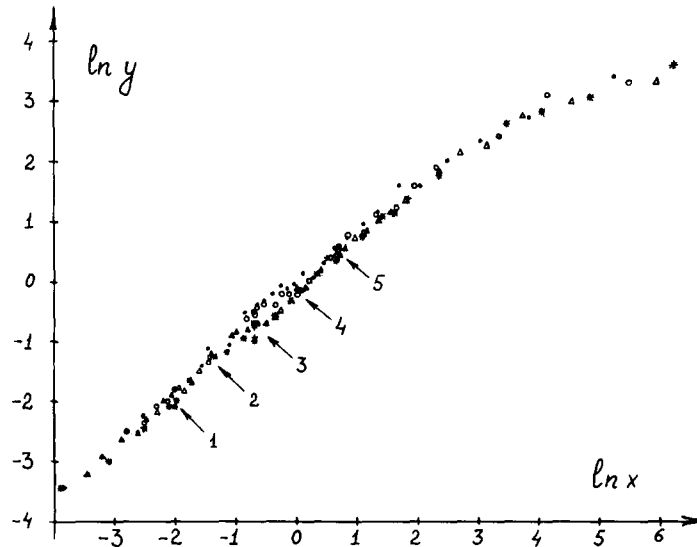

Fig. 35. ln y is plotted versus ln x [see eqs. (4.4.3)] for the model (4.2.1) with additional data compared to fig. 34. The size N of the matrix U^a_{nm} varies in the range $300 \leq N \leq 860$; full circles stand for $300 \leq N \leq 350$, open circles for $380 \leq N \leq 404$, squares for $453 \leq N \leq 534$, triangles for $575 \leq N \leq 618$, plusses for $663 \leq N \leq 711$, asterisks for $761 \leq N \leq 860$. The arrows indicate the groups of points corresponding to the values of $x \approx 0.125$ (1), 0.25 (2), 0.5 (3), 1.0 (4) and 2.0 (5).

the EF, which is not taken into account in the definition of β (see section 4.2). This fact may be related to the specific form of EFs which are symmetric about $n = 0$ due to parity conservation in the model (4.2.1) (see fig. 4). It is interesting that two very nearly linear dependences $\ln y \sim \ln x$ with a very good scaling behaviour below and above the critical point $x \approx 0.5$ are clearly seen in fig. 35. As an additional check of the scaling behavior, five values of x ($x \approx 0.125$, 0.25, 0.5, 1.0, 2.0) have been carefully examined with different N and k (these points are shown in fig. 35 by the arrows. For all values of x (except $x \approx 0.5$) remarkable clustering of β values was found, which supports the scaling conjecture.

It is important to note that scaling holds even for extremely large values of β ($\beta \rightarrow 1$), in the region which is very close to the region of unitary random matrices. As is known from solid state physics, this region is associated with the universal law of conductivity fluctuations (see, e.g., [MP87, ZP88]) and seems to be very interesting to study. However, to describe the relation $\beta(x)$ in the region $\beta \rightarrow 1$ analytically, one needs to know the character of the fluctuations for eigenstates in the matrices which are close to random.

In the previous section the possible relation between the average localization length $\langle l_H \rangle$ and the repulsion parameter in the spacing distribution $P(s)$ was discussed. Numerical data give good evidence in favour of such a relation. Therefore, it is natural to expect some sort of scaling behaviour also for the statistical properties of the quasienergy spectrum. Namely, we expect that the distribution $P(s)$ of
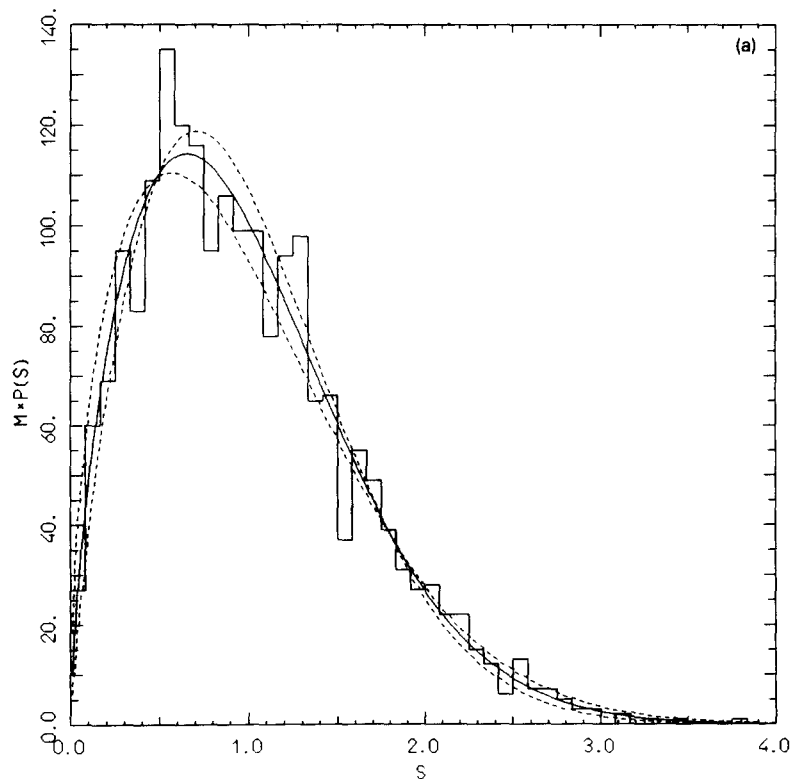

Fig. 36. The spacing distribution $P(s)$ for the model (4.2.1) with different sizes of the unperturbed basis, N. The solid lines correspond to the best fit to relation (4.1.6) by the χ^2 approach. The dashed lines are 1% deviations (for the χ^2 value) from the best fit. In all cases classical chaos is fixed ($K \approx 5$); also $k^2/N \approx 2.5$. The value of β found from the spectral entropy [see (4.2.5)] is denoted by β_H. NG matrices were used to improve statistics, with slightly different values of k. The value of the rescaled period τ is equal to $\tau = 4\pi r/(2N + 1)$. (a) $N = 200$, $k \approx 22.8$, $r = 7$, $\beta \approx 0.70$, $\beta_{min} \approx 0.55$, $\beta_{max} \approx 0.86$, $\beta_H \approx 0.71$, $NG = 10$; (b) $N = 398$, $k \approx 31.2$, $r = 11$, $\beta \approx 0.77$, $\beta_{min} \approx 0.59$, $\beta_{max} = 0.96$, $\beta_H \approx 0.63$, $NG = 5$; (c) $N = 600$, $k \approx 35.0$, $r = 14$, $\beta \approx 0.67$, $\beta_{min} \approx 0.50$, $\beta_{max} \approx 0.83$, $\beta_H \approx 0.63$, $NG = 3$.
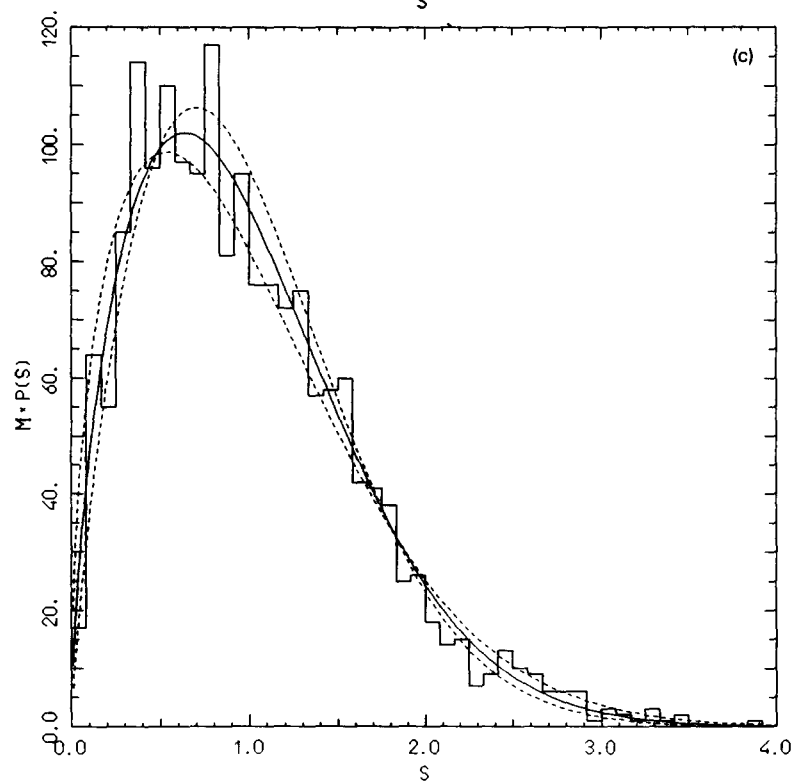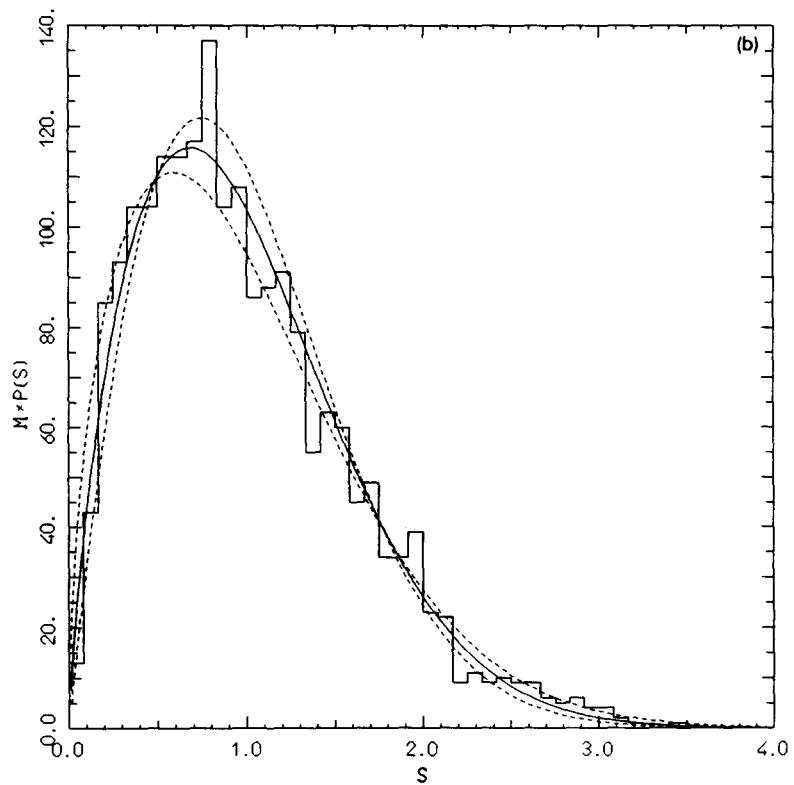
Fig. 36b, c.

nearest-level spacings is also a scaling function of the same parameter x. To check this conjecture, $P(s)$ has been studied for different values of N and k in the model (4.2.1) with a fixed degree of classical chaos ($K \approx 5$). In this study, the distributions $P(s)$ are compared for the three values $N \approx 200$, 400 and 600 with different values of the quantum parameter k chosen in such a way that x is approximately constant. To obtain a qualitative comparison, the fit of $P(s)$ has been made taking (4.1.6) as the analytical relation. In all cases, except the small critical region around $x \approx 0.5$, quite good scaling has been found. As an example, numerical data for $P(s)$ are shown in fig. 36, together with the fitting curves representing the best fit and the fits with 1% deviation for the χ^2 value. To improve the statistics, the common procedure was used to sum $P(s)$ for slightly different values of k.

The numerical data show that the fit repulsion parameter β in relation (4.1.6) is approximately the same for all cases of fig. 36. As a result, one can conclude that the level spacing distribution $P(s)$ appears to depend only on the ratio k^2/N and not on the parameters N and k separately. Of course, these data cannot be treated as a rigorous proof of the scaling behaviour of $P(s)$; however, these results seem to be a good indication of the existence of such a scaling.

To conclude this section, one should note again that all the data concern a fixed and sufficiently large value of the classical parameter K. Then the interesting problem arises whether some sort of scaling behaviour holds for $K \lesssim 1$ when in the corresponding classical model large regions with stable motion exist in phase space. Another problem, which seems to be simpler, is to obtain some evidence that the true scaling parameter is D_n/N and not k^2/N. As was discussed above, the diffusion coefficient D_n is slightly dependent on the classical parameter K (see section 2.1); therefore, additional investigation is needed with the variation of K.

All these results may also be regarded as some indication that not only β and $P(s)$ show scaling behaviour but that all statistical properties of intermediate quantum chaos (for $K \gg 1$) depend on the scaling parameter $D_n/N \approx 4l_\infty/N$ only.

4.5. Band random matrices as a model of intermediate quantum chaos

As was discussed above, in the angular momentum representation the unitary matrix U_{nm} giving the time evolution of the kicked rotator (2.2.1) has a band-like structure with an effective size of the band approximately equal to the strength parameter of the perturbation, k. Outside of the band, the matrix elements decrease exponentially fast while inside the band, under the additional condition of strong classical chaos ($K \gg 1$), the matrix elements seem to be close to random numbers. As follows from numerical experiments, the statistical properties of the spectra and EFs [the level spacing distribution $P(s)$ and the scaled localization length of EFs, d/N] essentially depend on the scaling parameter $x = k^2/N$. This fact allows one to assume that the scaling properties found for the kicked rotator model are general for random matrices with a band structure. Band random matrices (BRM) may be regarded as good models for quantum systems with a finite range of interaction between the unperturbed states. From this point of view, BRMs can be used to describe the statistical properties of real quantum systems such as atoms, nuclei and solid state models (see, e.g., [C85, LGP82, FLP89]).

A particular case of band matrices (so-called "bordered matrices") has been considered by Wigner [W55, W57]. The matrix elements in this model are defined by integers $-2, -1, 0, 1, 2, \ldots$ for the diagonal elements and by the value $\pm h$ for matrix elements inside a band of size b, with the sign of h chosen at random. In the tridiagonal case the model appears to have an analytical solution, with a semicircular distribution of the eigenvalues in the limit b and $h \gg 1$, with h^2/b finite. Other cases of band-like structures have also been considered in [SVZ85, FLP89], where a smooth decrease of the off-diagonal elements is assumed when moving away from the diagonal.

In this section we briefly discuss the statistical properties of BRMs in comparison with the above numerical results for the kicked rotator on the torus [CIM90]. We define a BRM ensemble as a set of real symmetric $N \times N$ matrices with random elements A_{ij} for $|i - j| < b$, and $A_{ij} = 0$ outside the band of size b. Therefore, $b = 1$ for diagonal matrices, $b = 2$ for tridiagonal matrices and $b = N$ for GOE (Gaussian Orthogonal Ensemble). Due to the symmetry of the matrices, the number of independent elements in a BRM is given by $F = b(2N - b + 1)/2$. All matrix elements are assumed to be independent random numbers with mean equal to zero, and the probability density for one matrix A in the ensemble is defined as

$$\mathscr{P}(A) = \mathrm{e}^{-\omega \, \mathrm{Tr} \, A^2} = \prod_{i=1}^{N} \mathrm{e}^{-\omega A_{ii}^2} \prod_{i<j}^{N} \mathrm{e}^{-2\omega A_{ij}^2} . \qquad (4.5.1)$$

From this expression one easily computes the ensemble average $\langle \mathrm{Tr} \, A^2 \rangle = F/(2\omega)$, which determines the variance of the matrix elements. It is seen that the ensemble is fully characterized by the parameters N, b and ω. The last one, ω, does not affect the statistical properties of the spectra and eigenvectors since it only changes the scale for all energy levels as well as of eigenvectors. In numerical experiments this parameter ω was specified by the relation $\langle \mathrm{Tr} \, A^2 \rangle = N$, which determines, in the limit case of GOE ($b = N$), the range $(-2, +2)$ for the distribution of eigenvalues. It is well known that this distribution takes the form of a semicircular dependence for fully random matrices. Our preliminary numerical data show that a semicircular dependence also holds for BRMs, in the limit of large $b \gg 1$ and $N \gg 1$. In the chosen definition of ω the radius of this distribution is also equal to 2, independently of b and N. The appearance of the semicircular law in the case of BRMs is far from trivial, although it seems to be a general feature of random matrices [KPW88]. At present, no rigorous results concerning BRMs are known. The main difficulty is the lack of rotational invariance for BRM ensembles under orthogonal transformations, unlike the common theory of fully random matrices [P65, M67]. The development of BRM theory seems to be a very interesting mathematical problem.

In analogy with the kicked rotator model, we introduce the parameter

$$\tilde{x} = b^2/N ,$$

and investigate the statistical properties of BRMs depending on $\tilde{x}$. We should note that the analogy between $\tilde{x}$ for BRMs and x for the kicked rotator is meaningful only for not too large b (actually, for $b \leq N/2$), since b is bounded by N, unlike k, which can be arbitrarily large.

The main result of our study [CIM90] concerns the mean entropy localization length defined by (4.2.5). As was shown for the kicked rotator (see section 4.2), this quantity gives a measure of the localization which applies both for localized and extended chaotic states. The typical structure of eigenvectors of BRMs appears to be similar to that for the kicked rotator. For example, in the two extreme cases $\tilde{x} \ll 1$ and $\tilde{x} \gg 1$ the eigenvectors of BRMs look like the EFs in figs. 4 and 17 for the kicked rotator (apart from the symmetry around $n = 0$). The dependence of the quantity $\beta = d/N$ on the parameter $\tilde{x}$ is given in figs. 37 and 38. To compute d, the average over all the eigenvectors of a number of matrices with a given b and N has been taken. The simulation with N ranging between 200 and 1000 showed a remarkable scaling behaviour for $\beta(\tilde{x})$. Indeed, all points in fig. 37 fall on a smooth curve to a high accuracy. To illustrate the scaling dependence, it is convenient to use the variable
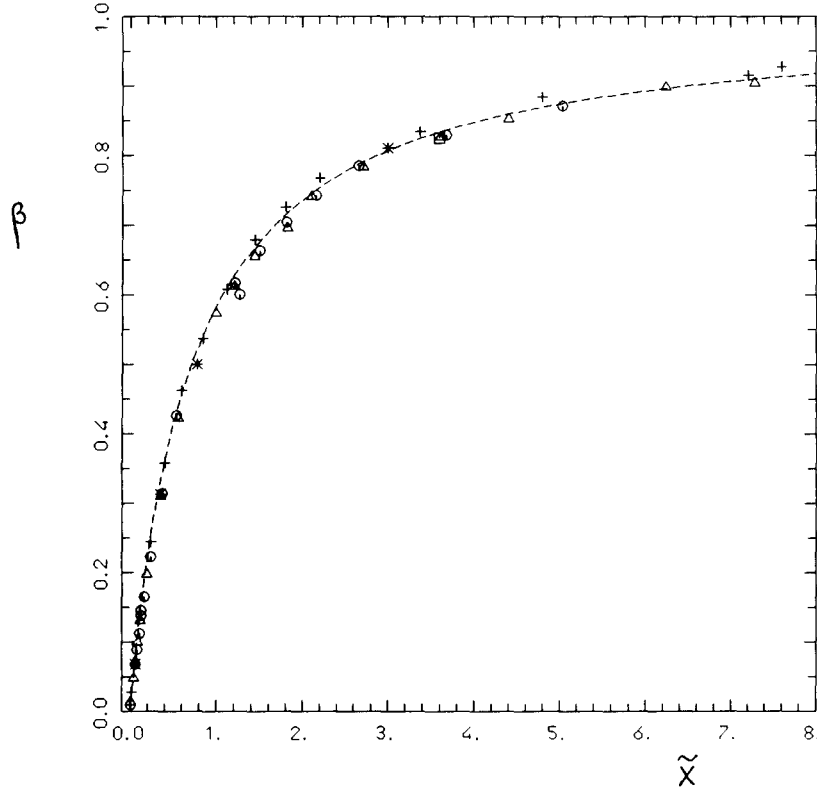
$$y = \beta/(1 - \beta) , \qquad (4.5.3)$$

Fig. 37. The scaled localization length $\beta = d/N$ versus $\tilde{x} = b^2/N$ for $N = 200$ (plusses), $N = 400$ (triangles), $N = 600$ (circles), $N = 800$ (asterisks) and $N = 1000$ (squares). The dashed curve corresponds to expression (4.5.4). (After [CIM90].)

which was introduced in section 4.4. In the variables $\ln y$, $\ln \tilde{x}$, the behaviour of β can be analysed both for $\tilde{x} \ll 1$ and $\tilde{x} \gg 1$. From fig. 38, the linear dependence is clearly seen over a very large range $\tilde{x} \leq 10$. A fit of the numerical data in this range of $\tilde{x}$ gives $\ln y = \alpha \ln x + C$ with $\alpha \approx 1$ and $C \approx 0.35$. For $\beta(\tilde{x})$ this corresponds to the relation

$$\beta = \gamma \tilde{x}/(1 + \gamma \tilde{x}), \quad \gamma \approx 1.4.$$ (4.5.4)

This curve is also plotted in fig. 37, where the correspondence of the numerical data to the analytical relation (4.5.4) is very impressive. It is important to stress that for $\tilde{x} \ll 1$ we have $\beta \approx 1.4\tilde{x}$, which exactly corresponds to relation (4.2.6) for the kicked rotator (in fig. 35 the above relation corresponds to the range $x < 0.5$). This fact gives strong evidence for the similarity of the BRM model to the kicked rotator.

For $\tilde{x} \gg 1$ ($\tilde{x} \gtrsim 10$) the numerical data deviate from the straight line behaviour (see fig. 38); however, they indicate that the scaling behaviour still holds. At present, there is no approach to give a theoretical description of $\beta(\tilde{x})$ in the limit $\tilde{x} \to \infty$. It should be noted that the connection of β scaling for BRMs with the known results on the scaling behaviour of the localization length in solid state physics (see, e.g., [LR85, P86, FPG89]) is not clear. First, all those results mainly deal with tridiagonal matrices (Anderson model or Lloyd model [FPG89]), unlike our model with a bandwidth $b \gg 1$. Also, the relation of the mean entropy localization length d to that defined by means of Thouless' formula [T72] or by the transfer matrix method [PS81] is rather vague in the limiting case $\beta \to 1$.
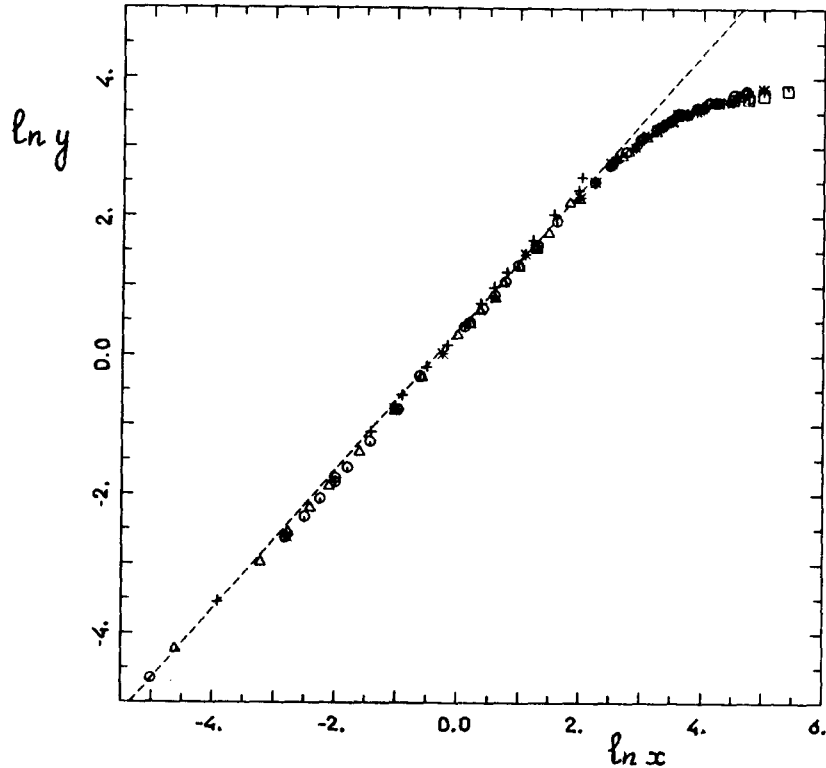
Fig. 38. A ln–ln plot of the data of fig. 37 in the variables $\tilde{x} = b^2/N$ and $y = \beta/(1 - \beta)$, together with additional numerical results for $\tilde{x} > 8$. The dashed line corresponds to $y = \gamma\tilde{x}$ with $\gamma = 1.4$. (After [CIM90].)

As was pointed out, for $b \gtrsim N/2$ the comparison with the kicked rotator model is not correct. The numerical data show that for this case the scaling behaviour breaks down and the points in fig. 38 deviate more and more from the scaling curve when b approaches N. Also, in this region the fluctuations of ln y are very strong due to small denominators in y.

To compare with the kicked rotator model, spectral fluctuations have also been studied for BRMs. Namely, the spacing distribution $P(s)$ for the eigenvalues E_i was analysed as a function of the parameter $\tilde{x}$. According to preliminary numerical results, scaling also holds for $P(s)$ in the sense that $P(s)$ has the same form when the size of the band b and the size of the matrix N are varied, keeping $\tilde{x}$ constant. This is also consistent with the result obtained for the kicked rotator on the torus.

The two distinct regimes in the scaling behaviour of β with $\tilde{x}$ (fig. 38) may have a counterpart in the so-called insulator and conductor regimes of solid state models with disorder. It is intriguing that, formally, the variable (4.5.3) is analogous to the electrical resistance, with β playing the role of the transmission coefficient.

5. Concluding remarks

As one can see from the above discussions, all the data presented in this review are dealing with a situation when in the classical limit the behaviour of the system is fully chaotic. In the kicked rotator model it corresponds to a relatively large value of the classical parameter K. Therefore, the deviation from maximal chaos in quantum models is entirely related to quantum interference effects only. It was

shown that the mechanism of such a "quantum suppression of classical chaos" is the localization of all eigenfunctions in the unperturbed momentum space, which is similar to the well-known Anderson localization. This situation turns out to be much easier to study, unlike the general case, when in the classical model (standard mapping) there are regions with quasiperiodic (stable) motion. In the latter case, the statistical properties are not maximal for two reasons, both of a classical and a quantum nature. In our model (2.2.1) this corresponds to a value $K \lesssim 1$, which, in this case, plays an essential role in determining the size of stable regions in phase space.

An attempt to relate the relative measure of stable motion to the spectrum statistics has led to the well-known Berry–Robnik distribution [BR84] for the spacings between neighbouring levels. However, in the above approach the influence of quantum effects, like the localization of EFs, is not taken into account. Therefore, this approach seems to be valid only in the deep semiclassical region. From this point of view, a very important problem arises, namely, the problem of a description of the statistical properties for the general situation when taking into account both the classical and quantum peculiarities of the model. This means that both the classical and the quantum parameter, K and k, are expected to determine the form of $P(s)$. The first question is: what are the changes in $P(s)$ when the classical parameter K changes, while the quantum parameter is constant? In some sense, this case is opposite to the one discussed in this paper. So far, no numerical experiments for the kicked rotator model with constant k, but changing K have been done.

Another question, which seems to be closely related to the above problem, is the structure of EFs as a function of the classical parameter K. As was mentioned in section 2.3, for $K \lesssim 1$ the localization length l_∞ is proportional to k, and not to k^2 as for $K \gg 1$. One may also assume that for $K \lesssim 1$ the degree of randomness in the length where the main probability of the EFs is concentrated, is strongly dependent on the value of K with a more and more regular structure when $K \to 0$. Indeed, this is qualitatively seen in numerical experiments; however, no systematic studies of this question have been made. One can say that the main influence of the classical parameter K on the structure of the EFs seems to determine the degree of chaos inside the EFs while the quantum parameter k is related to the degree of localization. This conjecture may be the main subject of further studies.

Acknowledgements

References

[A58]   Anderson, P.W., Phys. Rev. 109 (1958) 1492.
[A63]   Arnold, V.I., Usp. Mat. Nauk 18 (1963) No. 6, 91.
[A68]   Alekseev, V.M., Mat. Sbor. 76 (1968) 72.
[AA68]   Arnold, V.I. and A. Avez, Ergodic Problems of Classical Mechanics (Benjamin, New York, 1968).
[AJ81]   Alekseev, V.M. and M.V. Jakobson, Phys. Rep. 75 (1981) 287.
[AFIIK84] Abramson, F., R.W. Field, D. Imre, K.K. Innes and J.L. Kinsey, J. Chem. Phys. 80 (1984) 2298.
[B70]   Bogolyubov, N.N., Selected Works, Vol. 2 (Naukova Dumka, Kiev, 1970) p. 77 (in Russian).

[B73] Brody, T.A., Lett. Nuovo Cimento 7 (1973) 482.
[B74] Bunimovich, L.A., Funkt. Anal. Prilozh. 8 (1974) 73 [Funct. Anal. Appl. 8 (1974) 73].
[BK74] Bayfield, J.E. and P.M. Koch, Phys. Rev. Lett. 33 (1974) 258.
[B77] Berry, M., J. Phys. A 10 (1977) 2083.
[BGK77] Bayfield, J.E., L.D. Gardner and P.M. Koch, Phys. Rev. Lett. 39 (1977) 76.
[BT77] Berry, M.V. and M. Tabor, Proc. R. Soc. London Ser. A 356 (1977) 375.
[BZ78] Berman, G.P. and G.M. Zaslavsky, Dokl. Akad. Nauk SSSR 240 (1978) 1081.
[BZ78a] Berman, G.P. and G.M. Zaslavsky, Physica A 91 (1978) 450.
[B79] Bunimovich, L.A., Commun. Math. Phys. 65 (1979) 295.
[BB79] Berry, M.V. and N.L. Balazs, J. Phys. A 12 (1979) 625.
[BBTV79] Berry, M.V., N.L. Balazs, M. Tabor and A. Voros, Ann. Phys. 122 (1979) 26.
[B81] Berry, M.V., Ann. Phys. 131 (1981) 163.
[B81a] Bogolyubov, N.N., On some problems relating to the foundations of statistical mechanics, in: Proc. Second Intern. Symp. on Selected Problems of Statistical Mechanics (Dubna, 1981) p. 9.
[BFFMPW81] Brody, T.A., J. Flores, J.B. French, P.A. Mello, A. Pandey and S.S.M. Wong, Rev. Mod. Phys. 53 (1981) 385.
[BGR82] Buch, V., R.B. Gerber and M.A. Ratner, J. Chem. Phys. 76 (1982) 5397.
[BZ82] Berman, G.P. and G.M. Zaslavsky, Physica A 111 (1982) 17.
[BK83] Berman, G.P. and A.R. Kolovsky, Physica D 8 (1983) 117.
[BG84] Bohigas, O. and M.-J. Giannoni, Lect. Notes Phys. 209 (1984) 1.
[BGS84] Bohigas, O., M.-J. Giannoni and C. Schmit, Phys. Rev. Lett. 52 (1984) 1.
[BGS84a] Bohigas, O., M.-J. Giannoni and C. Schmit, J. Physique Lett. 45 (1984) 1015.
[BR84] Berry, M.V. and M. Robnik, J. Phys. A 17 (1984) 2413.
[BS84] Blumel, R. and U. Smilansky, Phys. Rev. Lett. 52 (1984) 137.
[BS84a] Blumel, R. and U. Smilansky, Phys. Rev. A 30 (1984) 1040.
[B85a] Berry, M.V., Proc. R. Soc. London Ser. A 400 (1985) 229.
[BFGS86] Blumel, R., S. Fishman, M. Griniasti and U. Smilansky, in: Quantum Chaos and Statistical Nuclear Physics, Proc. 2nd Intern. Conf. on Quantum Chaos (Cuernavaca, Mexico), eds T.H. Seligman and H. Nishioka (Springer, Heidelberg, 1986).
[BIKV86] Berman, G.P., F.M. Izrailev, A.R. Kolovsky and O.A. Vlasova, in: Proc. Conf. Renormalization Group 86 (Dubna, USSR, 1986), eds D.V. Shirkov, D.I. Kasakov and A.A. Vladimirov (World Scientific, Singapore, 1986) p. 290.
[BR86] Berry, M.V. and M. Robnik, J. Phys. A 19 (1986) 649.
[BIV87] Berman, G.P., F.M. Izrailev and O.F. Vlasova, Zh. Eksp. Teor. Fiz. 93 (1987) 470.
[BK87] Berman, G.P. and A.R. Kolovsky, Physica A 125 (1987) 188.
[BV87] Balazs, N.L. and A. Voros, Europhys. Lett. 4 (1987) 1089.
[BI88] Berman, G.P. and F.M. Izrailev, On the dynamics of correlation functions and suppression of diffusion in a region of quantum chaos, preprint 497F, Inst. of Phys., Krasnoyarsk, USSR (1988).
[BIK88] Berman, G.P., F.M. Izrailev and A.R. Kolovsky, Physica A 152 (1988) 273.
[BJ88] Breizman, B.N. and K. Jungwirth, Fiz. Plazmy 14 (1988) 1504.
[BS88] Bayfield, J. and D. Sokol, in: The Hydrogen Atom, Proc. Symp. (Pisa, 1988) p. 335.
[BW88] Bohigas, O. and H.A. Weidenmuller, Annu. Rev. Nucl. Part. Sci. 38 (1988) 421.
[BCGS89] Bayfield, J.E., G. Casati, I. Guarneri and D.W. Sokol, Phys. Rev. Lett. 63 (1989) 364.
[BV89] Balazs, N.L. and A. Voros, Ann. Phys. (NY) 190 (1989) 1.
[CI68] Chirikov, B.V. and F.M. Izrailev, Statistical trials of pseudo-random generators, Vychisl. Sistemy (Novosibirsk) 30 (1968) 77.
[CI73] Chirikov, B.V. and F.M. Izrailev, Colloques Internationaux du CNRS, No. 229 (Toulouse, 1973) (CNRS, Paris, 1976) p. 409.
[C79] Chirikov, B.V., Phys. Rep. 52 (1979) 263.
[CCFI79] Casati, G., B.V. Chirikov, J. Ford and F.M. Izrailev, Lect. Notes Phys. 93 (1979) 334.
[CVG80] Casati, G., F. Valz-Gris and I. Guarneri, Lett. Nuovo Cimento 28 (1980) 279.
[CIS81] Chirikov, B.V., F.M. Izrailev and D.L. Shepelyansky, Sov. Sci. Rev. C 2 (1981) 209.
[C83] Chirikov, B.V., Usp. Fiz. Nauk 139 (1983) 360.
[CG83] Camarda, H.S. and P.G. Georgopoulos, Phys. Rev. Lett. 50 (1983) 492.
[CG84] Casati, G. and I. Guarneri, Commun. Math. Phys. 95 (1984) 121.
[C85] Chirikov, B.V., Phys. Lett. A 108 (1985) 68.
[CB85] Christoffel, K.M. and P. Brumer, Phys. Rev. A 31 (1985) 3466.
[CCG85] Casati, G., B.V. Chirikov and I. Guarneri, Phys. Rev. Lett. 54 (1985) 1350.
[CS85] Chang, S.-J. and K.-J. Shi, Phys. Rev. Lett. 55 (1985) 269.
[C86] Chirikov, B.V., Found. Phys. 16 (1989) 39.
[CFGV86] Casati, G., J. Ford, I. Guarneri and F. Vivaldi, Phys. Rev. A 34 (1986) 1413.
[CS86] Chirikov, B.V. and D.L. Shepelyansky, Radiofiz. 29 (1986) 1041.
[CS86a] Chang, S.J. and K.-J. Shi, Phys. Rev. A 34 (1986) 7.

[CCSG87] Casati, G., B.V. Chirikov, D.L. Shepelyansky and I. Guarneri, Phys. Rep. 154 (1987) 78.
[CGI87] Casati, G., I. Guarneri and F.M. Izrailev, Phys. Lett. A 124 (1987) 263.
[CGS88] Casati, G., I. Guarneri and D.L. Shepelyansky, IEEE J. Quantum Electron. QE-24 (1988) 1420.
[CH88] O'Conner, P.V. and E.J. Heller, Phys. Rev. Lett. 61 (1988) 2288.
[CIS88] Chirikov, B.V., F.M. Izrailev and D.L. Shepelyansky, Physica D 33 (1988) 77.
[CM89] Casati, G. and L. Molinari, Suppl. Prog. Theor. Phys. 98 (1989) 287.
[CGIS90] Casati, G., I. Guarneri, F.M. Izrailev and R. Scharf, Phys. Rev. Lett. 63 (1990) 5.
[CIM90] Casati, G., F.M. Izrailev and L. Molinari, Phys. Rev. Lett. 64 (1990) 16.
[D62] Dyson, F.J., J. Math. Phys. 3 (1962) 140, 157, 166.
[DKS83] Delone, N.B., V.P. Krainov and D.L. Shepelyansky, Usp. Fiz. Nauk 140 (1983) 335 [Sov. Phys. – Usp. 26 (1983) 551].
[DGP84] Dorrizi, B., B. Grammaticos and Y. Pomeau, J. Stat. Phys. 37 (1984) 93.
[DF85] Dana, I. and S. Fishman, Physica D 17 (1985) 63.
[DG86] Delande, D. and J.C. Gay, Phys. Rev. Lett. 57 (1986) 2006.
[DH90] Dietz, B. and F. Haake, Z. Phys. B 80 (1990) 153.
[E88] Eckhardt, B., Phys. Rep. 163 (1988) 205.
[E88a] Elyutin, P.V., Usp. Fiz. Nauk 155 (1988) 397.
[F72] Froeschle, C., Astron. Astrophys. 9 (1972) 15.
[FGP82] Fishman, S., D.R. Grempel and R.E. Prange, Phys. Rev. Lett. 49 (1982) 508.
[FFGP85] Feingold, M., S. Fishman, D.R. Grempel and R.E. Prange, Phys. Rev. B 31 (1985) 6852.
[FM86] Frahm, H. and H.J. Mikeska, Z. Phys. B 65 (1986) 249.
[FF87] Feingold, M. and S. Fishman, Physica D 25 (1987) 181.
[FGP87] Fishman, S., D.R. Grempel and R.E. Prange, Phys. Rev. A 36 (1987) 289.
[FFGP88] Feingold, M., S. Fishman, D.R. Grempel and R.E. Prange, Phys. Rev. Lett. 61 (1988) 377.
[FM88] Frahm, H. and H.J. Mikeska, Phys. Rev. Lett. 60 (1988) 3.
[FM88a] Frahm, H. and H.J. Mikeska, Phys. Rev. Lett. 61 (1988) 378.
[FPG89] Fishman, S., R.E. Prange and M. Griniasti, Phys. Rev. A 39 (1989) 1628.
[FLP89] Feingold, M., D.M. Leitner and O. Piro, Phys. Rev. A 39 (1989) 6507.
[FMR89] Ford, J., G. Mantica and G.H. Ristov, The Arnol'd cat; failure of the correspondence principle (1989), unpublished.
[G39] Gurevich, I.I., Zh. Eksp. Teor. Fiz. 9 (1939) 1283.
[GP57] Gurevich, I.I. and M.I. Pevsner, Nucl. Phys. 2 (1957) 575.
[G79] Green, G., J. Math. Phys. 20 (1979) 1183.
[GSMKR88] Galvez, E.J., B.E. Sauer, L. Moorman, P.M. Koch and D. Richards, Phys. Rev. Lett. 61 (1988) 2011.
[G89] Gutzwiller, M.C., Lecture Notes at the Summer School (Les Houches, France, August 1989).
[HB80] Hannay, J.H. and M. Berry, Physica D 1 (1980) 267.
[HH82] Hogg, T. and B.A. Huberman, Phys. Rev. Lett. 48 (1982) 711.
[HPB82] Haq, R., A. Pandey and O. Bohigas, Phys. Rev. Lett. 48 (1982) 1086.
[HKC83] Haller, E., H. Koppel and L.S. Cederbaum, Chem. Phys. Lett. 101 (1983) 215.
[H84] Heller, E.J., Phys. Rev. Lett. 53 (1984) 1515.
[HOA84] Hanson, J.D., E. Ott and T.M. Antonsen Jr, Phys. Rev. A 29 (1984) 814.
[HKS86] Haake, F., M. Kus and R. Scharf, Z. Phys. B 65 (1986) 381.
[HKS87] Haake, F., M. Kus and R. Scharf, Lect. Notes Phys. 282 (1987) 3.
[IS79] Izrailev, F.M. and D.L. Shepelyansky, Dokl. Akad. Nauk SSSR 249 (1979) 1103 [Sov. Phys. – Dokl. 24 (1979) 996].
[IS80] Izrailev, F.M. and D.L. Shepelyansky, Teor. Mat. Fiz. 43 (1980) 417 [Theor. Math. Phys. 43 (1980) 553].
[I84] Izrailev, F.M., Distribution of Quasienergy Level Spacings for Classically Chaotic Quantum Systems, preprint 84-63, Inst. Nucl. Phys., Novosibirsk (1984).
[I86] Izrailev, F.M., Phys. Rev. Lett. 56 (1986) 541.
[I87] Izrailev, F.M., Phys. Lett. A 125 (1987) 250.
[I88] Izrailev, F.M., Phys. Lett. A 134 (1988) 13.
[IS88] Izrailev, F.M. and R. Scharf, Phys. Lett. A 142 (1989) 89.
[I89] Izrailev, F.M., J. Phys. A 22 (1989) 865.
[JLP80] Jones, D.A., J.G. Leopold and I.C. Percival, J. Phys. B 13 (1980) 31.
[K54] Kolmogorov, A.N., Dokl. Akad. Nauk SSSR 98 (1954) 527.
[K79] Krylov, N.S., Foundations of Statistical Mechanics (Princeton, 1979).
[KS80] Kheifets, S.A. and V.V. Sokolov, On the quantum corrections to the stochastic motion of a non-linear oscillator, preprint 80-133, Inst. Nucl. Phys. Novosibirsk (1980).
[KSH87] Kus, M., R. Scharf and F. Haake, Z. Phys. B 66 (1987) 129.
[KMH88] Kus, M., J. Mostowski and F. Haake, J. Phys. A 21 (1988) L1073.
[KPW88] Kamien, R.D., H.D. Politzer and M.B. Wise, Phys. Rev. Lett. 60 (1988) 1995.

[KMSGLR89] Koch, P.M., L. Moorman, B.E. Sauer, E.G. Galvez, K.A.H. van Leeuwen and D. Richards, Phys. Scr. T26 (1989) 51.
[LS55] Landau, L.D. and Ya.A. Smorodinsky, Lectures on the Theory of Nuclei (Nauka, Moscow, 1955) (in Russian).
[LP78] Leopold, J.G. and I.C. Percival, Phys. Rev. Lett. 41 (1978) 944.
[LGP82] Lifshits, L.M., S.A. Gredescul and L.A. Pastur, Introduction to the Theory of Disordered Systems (Nauka, Moscow, 1982) (in Russian).
[LL83] Lichtenberg, A.L. and M.A. Lieberman, Regular and Stochastic Motion (Springer, Berlin, 1983).
[LR85] Lee, P.A. and T.V. Ramakrishnan, Rev. Mod. Phys. 57 (1985) 287.
[MT61] Mott, N.F. and W.D. Twose, Adv. Phys. 10 (1961) 107.
[M62] Moser, J., Nachr. Akad. Wiss. Göttingen, Math. Phys. Kl. (1962) 1.
[M67] Mehta, M.L., Random Matrices (Academic Press, New York, 1967).
[MK79] MacDonald, S.W. and A.N. Kaufman, Phys. Rev. Lett. 52 (1979) 1189.
[M81] Molchanov, S.A., Commun. Math. Phys. 78 (1981) 429.
[MK81] MacKinnon, A. and B. Kramer, Phys. Rev. Lett. 47 (1981) 1546.
[MK83] MacKinnon, A. and B. Kramer, Z. Phys. B 53 (1983) 1.
[MMP84] Mackay, R.S., J.D. Meiss and I.C. Percival, Physica D 13 (1984) 55.
[MP87] Muttalib, K.A. and J.L. Pichard, Phys. Rev. Lett. 59 (1987) 2475.
[MK88] McDonald, S.W. and A.N. Kaufman, Phys. Rev. A 37 (1988) 3067.
[MKZ88] Meredit, D.C., S.E. Koonin and M.R. Zirnbauer, Phys. Rev. A 37 (1988) 3499.
[P65] Porter, C.E., ed., Statistical Theory of Spectra: Fluctuations (Academic Press, New York, 1965).
[P73] Percival, I.C., J. Phys. B 6 (1973) L229.
[PS81] Pichard, J.L. and G.J. Sarma, J. Phys. C 14 (1981) L127.
[P82] Peres, A., Phys. Rev. Lett. 49 (1982) 1118.
[P84] Pechukas, P., J. Chem. Phys. 88 (1984) 4823.
[PGF84] Prange, R.E., D.R. Grempel and S. Fishman, in: Proc. Conf. on Quantum Chaos (Como, 1983) (Springer, Berlin, 1984).
[P86] Pichard, J.L., J. Phys. C 19 (1986) 1519.
[P88] Pelegrinotti, A., J. Stat. Phys. 53 (1988) 1327.
[RP60] Rosenzweig, N. and C.E. Porter, Phys. Rev. 120 (1960) 1698.
[R66] Ritus, V.I., Zh. Eksp. Teor. Fiz. 51 (1966) 1544.
[RW80] Rechester, A.B. and R.B. White, Phys. Rev. Lett. 44 (1980) 1586.
[RRW81] Rechester, A.B., M.N. Rosenbluth and R.B. White, Phys. Rev. A 23 (1981) 2664.
[RB86] Robnik, M. and M. Berry, J. Phys. A 19 (1986) 669.
[R87] Robnik, M., J. Phys. A 20 (1987) L495.
[R87a] Ristov, G.H., A Quantum Mechanical Investigation of Arnold's Cat Map, MS Thesis (1987), unpublished.
[S70] Sinai, Y.G., Russ. Math. Surv. 25 (1970) 137.
[S74] Shnirelman, A.I., Usp. Mat. Nauk 29 (1974) No. 6, 181.
[S76] Shuryak, E.V., Zh. Eksp. Teor. Fiz. 71 (1976) 2039.
[S81] Shepelyansky, D.L., Teor. Mat. Fiz. 49 (1981) 117.
[S81a] Shepelyansky, D.L., Dokl. Akad. Nauk SSSR 256 (1981) 586.
[S83] Shepelyansky, D.L., Physica D 8 (1983) 208.
[S84] Sokolov, V.V., Teor. Mat. Fiz. 61 (1984) 128.
[S84a] Schuster, H.G., Deterministic Chaos: an Introduction (Physik-Verlag, Weinheim, 1984).
[SG84] Shapiro, M. and G. Goelman, Phys. Rev. Lett. 53 (1984) 1714.
[SH84] Stechel, E.B. and E.J. Heller, Annu. Rev. Phys. Chem. 35 (1984) 563.
[STB84] Shapiro, M., R.D. Taylor and R. Brumer, Chem. Phys. Lett. 106 (1984) 325.
[SV85] Seligman, T.H. and J.J.M. Verbaarschot, Phys. Lett. A 108 (1985) 183.
[SV85a] Seligman, T.H. and J.J.M. Verbaarschot, J. Phys. A 18 (1985) 2227.
[SVZ85] Seligman, T.H., J.J.M. Verbaarschot and M.R. Zirnbauer, J. Phys. A 18 (1985) 2751.
[S86] Shepelyansky, D.L., Phys. Rev. Lett. 56 (1986) 677.
[S87] Shepelyansky, D.L., Physica D 28 (1987) 103.
[S87a] Sinai, Ya.G. (1987), private communication.
[SS87] Shudo, A. and N. Saito, J. Phys. Soc. Jpn. 56 (1987) 2641.
[SDKHB88] Scharf, R., B. Dietz, M. Kus, F. Haake and M. Berry, Europhys. Lett. 5 (1988) 383.
[S89a] Scharf, R., J. Phys. A 22 (1989) 4223.
[SUZ89] Sagdeev, R.Z., D.A. Usikov and G.M. Zaslavsky, Nonlinear Physics: from the Pendulum to Turbulence and Chaos (Harwood, New York, 1989).
[SI90] Scharf, R. and F. Izrailev, J. Phys. A 23 (1990) 963.
[T69] Taylor, J.B., Culham Progress Report CLM-PR-12 (1969).
[T72] Thouless, D.J, J. Phys C 5 (1972) 77.

[TI87]   Toda, M. and K. Ikeda, J. Phys. A 20 (1987) 3833.
[TI87a] Toda, M. and K. Ikeda, Phys. Lett. A 124 (1987) 165.
 [V79]   Voros, A., Lect. Notes Phys. 93 (1979) 326.
 [W55]   Wigner, E., Ann. Math. 62 (1955) 548.
 [W57]   Wigner, E., Ann. Math. 65 (1957) 203.
[WF86]   Wintgen, D. and H. Friedrich, Phys. Rev. Lett. 57 (1986) 571.
[WF87]   Wintgen, D. and H. Friedrich, Phys. Rev. A 35 (1987) 1464.
 [Y80]   Yonezawa, F., J. Non-Cryst. Solids 35 & 36 (1980) 29.
 [Z66]   Zeldovich, Ya.B., Zh. Eksp. Teor. Fiz. 51 (1966) 1942.
[ZF73]   Zaslavsky, G.M. and N.N. Filonenko, Zh. Eksp. Teor. Fiz. 51 (1973) 643.
 [Z77]   Zaslavsky, G.M., Zh. Eksp. Teor. Fiz. 73 (1977) 2089.
 [Z81]   Zaslavsky, G.M., Phys. Rep. 80 (1981) 157.
 [Z85]   Zaslavsky, G.M., Chaos in Dynamical Systems (Harwood, New York, 1985).
[ZP88]   Zanon, N. and J.L. Pichard, J. Physique 49 (1988) 907.
[ZS88]   Zaslavsky, G.M. and R.Z. Sagdeev, Introduction in Nonlinear Physics (Nauka, Moscow, 1988) (in Russian).